CZECH TECHNICAL UNIVERSITY IN PRAGUE
Faculty of Civil Engineering
Thákurova 7, 166 29 Prague 6, Czech Republic

MASTER'S THESIS PROPOSAL

study programme: Civil Engineering

study branch: Advanced Masters in Structural Analysis of Monuments and Historical Constructions

academic year: 2017/2018

Student's name and surname: Bledian Nela

Department: Department of Mechanics

Thesis supervisor: Jiří Bláha

Thesis title: The analysis of the timber roofs of the Loreta in Prague

Thesis title in English see above

Framework content: Historical analysis of the timber roofs of Loreta in Prague.
Non-destructive testing of the timber frame in the southern part of West wing roof.
Structural analysis of a deformed timber frame in the West wing roof. The stability check and the efficiency of the current strengthening undertaken.
Safety evaluation of the frame and strengthening proposal to enforce the frame.

Assignment date: 9/04/2018 Submission date: 02/07/2018

If the student fails to submit the Master's thesis on time, they are obliged to justify this fact in advance in writing, if this request (submitted through the Student Registrar) is granted by the Dean, the Dean will assign the student a substitute date for holding the final graduation examination (2 attempts for FGE remain). If this fact is not appropriately excused or if the request is not granted by the Dean, the Dean will assign the student a date for retaking the final graduation examination, FGE can be retaken only once. (Study and Examination Code, Art 22, Par 3, 4.)

The student takes notice of the obligation of working out the Master's thesis on their own, without any outside help, except for consultation. The list of references, other sources and names of consultants must be included in the Master's thesis.

....
Master's thesis supervisor Head of department

Date of Master's thesis proposal take over: July 2018

.....
Student

This form must be completed in 3 copies – 1x department, 1x student, 1x Student Registrar (sent by department)

No later than by the end of the 2nd week of instruction in the semester, the department shall send one copy of BT Proposal to the Student Registrar and enter data into the faculty information system KOS.

DECLARATION

Name: Bledian Nela

Email: blediannela@gmail.com

Title of the Msc Dissertation: The analysis of the timber roofs of the Loreta in Prague

Supervisor(s): Jiří Bláha

Year: 2017/18

I hereby declare that all information in this document has been obtained and presented in accordance with academic rules and ethical conduct. I also declare that, as required by these rules and conduct, I have fully cited and referenced all material and results that are not original to this work.

I hereby declare that the MSc Consortium responsible for the Advanced Masters in Structural Analysis of Monuments and Historical Constructions is allowed to store and make available electronically the present MSc Dissertation.

University: Czech Technical University

Date: 02/07/2018

Signature: _____

This page is left blank on purpose.

To my family

This page is left blank on purpose.

ACKNOWLEDGEMENTS

The SAHC master is very intensive and quite challenging and without the help and support of some people would be impossible. Initially, I would like to thank my supervisor Prof. Jiří Bláha, for his guidance and his wise counselling throughout this thesis.

I am privileged to participate in SAHC master and therefore I would like to thank the SAHC consortium for giving me this opportunity. I would especially like to thank University of Minho, Czech Technical University and Institute of Theoretical and Applied Mechanics and all their staff. Many thanks go to Prof. Petr Kabele for his counselling in structural mechanics. Further thanks regarding structural modeling go to Jiří Kunecký and Hana Hasníková. With the help to draw the geometry I would like to thank Jaroslav Buzek. Many thanks go to Michal Kloiber and Jaroslav Hrivnák, with the help of whom were carried out the non-destructive tests.

Sincere thanks go to Ms Markéta Baštová and the menagement of Loreta, who provided access and many resources for this thesis. When it comes to resources lots of thanks go also to the Capuchin Order archives.

Additional thanks go to Sharrcem company, Kosovo CSR Network and the project leader of “Frozen Music” Senton Kaçaniku for the scholarship and guidance to carry out this master.

Some very special thanks go to my friends in SAHC for all the challenges, the many working hours and all the unforgettable moments we have been through. The most special thanks go to all the real Prague boys who will always be in my heart.

Finally, for all the support and the biggest patience I would like to thank my family and my beloved Sebi. Without their help and their sincere love, it would be impossible to be here.

This page is left blank on purpose.

ABSTRACT

The Loreto of Prague is a remarkable Baroque historic monument, a place of pilgrimage with a captivating history. Behind the main façade, which is the marvelous work of the famous Dientzenhofers, there is a courtyard with a copy of the St. Mary´s Holy House of Nazareth. Beside the St. Vitus Cathedral treasure, Loreto holds the most valuable treasury in Czech Republic whose main jewel is a monstrance called the Prague Sun created with the use of 6222 diamonds.

Since the placement of the first construction stone in 1626, the Loreto has faced many construction phases with many alterations. The majority of the works progressed between 1698 and 1748 under the supervision of Christoph and Kilian Ignaz Dientzenhofer. These alterations also generated some changes in the configuration of the roof structure and in some parts caused even damages. Some of interventions observed on timber frames are not documented and their purpose is not always obvious. To have a better understanding, a historical analysis of the Loreto complex was used recently refined by dendrochronological dating of timber roofs elements from different time periods, so the historical chronology of the building could be accomplished.

Non-destructive on-site tests were conducted on the timber frames to evaluate the condition of their individual elements and to obtain their mechanical properties. With these parameters, the structural analysis is executed of the timber frame section which suffers from the most significant deformation. A spatial model for the members affecting the frame was created. From the 3D model all the loads transferred to the frame of interest were regenerated in a more detailed 2D plane model.

Elements subjected to non-destructive testing proved relatively good condition with small qualitative differences between individual members. With the structural modeling, it was possible to evaluate their safety and stability and also to assess the effectiveness of their strengthening. The possible causes of their actual deformations were discussed and measures designed to eliminate future problems were proposed.

Keywords: Baroque, carpentry, dendrochronology, survey, timber

This page is left blank on purpose.

ABSTRAKT

Analýza dřevěných střech Lorety v Praze

Pražská Loreta je pozoruhodnou kulturní památkou, významným barokním poutním místem s podmanivou historií. Za hlavním průčelím, které je velkolepým dílem slavných Dientzenhoferů, je skryto nádvoří s kopii Svaté chýše, nazaretského domu Panny Marie. Po pokladnici katedrály sv. Víta vlastní muzeum Lorety druhou nejcennější klenotnici v České republice, jejímž hlavním skvostem je monstrance zvaná Pražské slunce zhotovená s použitím 6222 diamantů.

Od umístění základního kamene v roce 1626 zde postupně proběhla řada stavebních fází s mnoha většími, či menšími změnami. Většina prací proběhla v letech 1698 až 1748 pod vedením Kryštofa a Kiliána Ignáce Dientzenhoferů. Úpravy způsobovaly pochopitelně i změny v konfiguraci střech a střešních konstrukcí, v některých částech došlo i k jejich dílčímu poškození. Na krovových konstrukcích je možné vidět i mladší sanační zásahy, které nejsou zdokumentovány a ani jejich účel není vždy zcela zřejmý. Lepšímu porozumění napomohla zevrubná stavebněhistorická analýza komplexu Lorety, před nedávnem zpřesněná pomocí dendrochronologického datování.

Na vybraných úsecích krovů byly v rámci této práce provedeny nedestruktivní testy, a to s cílem přesně vyhodnotit stav dřevěných prvků a zjistit jejich mechanické vlastnosti. Zjištěné parametry posloužily ke strukturální analýze úseku s největšími zjištěnými deformacemi. Nejprve byl vytvořen komplexní prostorový model zahrnující všechny členy ovlivňující vyšetřovanou vazbu krovu. Z tohoto 3D modelu bylo následně zatížení převedeno na 2D (rovinný) model umožňující podrobnější vyhodnocení.

Prvky podrobené nedestruktivnímu testování vykazují celkově dobrý stav s nevýraznými kvalitativními rozdíly mezi jednotlivými členy. Díky konstrukčnímu modelování bylo možné vyhodnotit jejich bezpečnost a stabilitu a rovněž posoudit účinnost jejich dodatečně provedeného zpevnění. Diskutovány byly možné příčiny skutečných zjištěných deformací a byla navržena opatření směřující k vyloučení budoucích problémů.

Klíčová slova: Barokní, tesařství, dendrochronologie, přehled, rámování dřeva

This page is left blank on purpose.

ABSTRAKTI

Analiza e kulmeve prej druri të Loretës në Pragë

Loreta në Pragë është një monument i jashtëzakonshëm historik, një vend pelegrinazhi me një histori magjepsëse. Prapa fasadës kryesore, e cila është një kryevepër e arkitektëve të famshëm Dientzenhofer, në oborr gjendet kopja e "Shtëpisë së Shenjtë" të Shën Marisë së Nazaretit. Loreta poashtu ruan thesarin më të çmueshëm në Republikën Çeke, pas thesarit të Katedrales së Shën Vitus. Ky thesar quhet "Dielli i Pragës" dhe është një 'ostensorium' i përbërë nga 6222 diamantë.

Qysh nga vendosja e gur-themelit në vitin 1626, Loreta është ballafaquar me shumë faza ndërtimore dhe shumë modifikime. Shumica e punëve ndërtimore u zhvilluan gjatë viteve 1698 dhe 1748 nën mbikqyrjen e Kristof dhe Kilian Ignaz Dientzenhofer. Këto modifikime ndikuan në ndryshimin e strukturës së kulmeve dhe në disa pjesë shkaktuan dhe dëme. Në konstruksionet e drurit janë vërejtur disa intervenime të pa dokumentuara dhe qëllimi i tyre nuk është mjaft i qartë. Për të pasur një pasqyrë më të kjartë është bërë një analizë historike e kompleksit të Loretës. Kjo analizë është përmisuar me raportin dendrokronologjik të kulmeve prej druri nga periudha të ndryshme kohore, në mënyrë që arrihet deri tek kronologjia historike.

Testet jo-destruktive janë ekzekutuar në konstruksionet prej druri për të vlerësuar gjendjen e elementeve individuale dhe për të arritur deri tek parametrat mekanik. Me këta parametra është kryer analiza strukturale e ramës prej druri e cila ka deformimin më të shprehur. Një model strukturor hapësinorë është krijuar për elementet të cilat ndikojnë në ramën e deformuar. Nga modeli hapësinor janë bartur të gjitha ngarkesat ndikuese në një model planar më të detajuar.

Elementet e nënshtruara ndaj testeve jo-destruktive treguan ndryshime të vogëla kualitative ndërmjet tyre, mirëpo në gjendje të mirë në përgjithësi. Me modelimin struktural u arrit të vlerësohet siguria, stabiliteti dhe gjithashtu u arrit të vlerësohet efektshmëria e përforcimit. Shkaktarët e mundshëm të këtyre deformimeve janë diskutuar dhe janë propozuar masa për të eleminuar probleme të mundshme në të ardhmen.

Fjalët kyçe: Baroku, karpentieria, dendrokronologji, inspektim, konstruksione prej druri

This page is left blank on purpose.

TABLE OF CONTENTS

LIST OF FIGURES

LIST OF TABLES

Table 4.1 – Location of the loading jack performed in the church *27*
Table 4.2 – The mechanical parameters according to the Italian norms UNI 11035:2003 ..... *31*
Table 4.3 – Resistance measure (RM) for the microdrilling tests performed on Frame 1 ..... *35*
Table 4.4 – The average results for the resistance measures (RM) *36*
Table 4.5 – Correlation of RM to compressive strength (SC) and density (ρ) *36*
Table 4.6 – Data processing of loading jack results for the west wing roof; Conventional compressive strength (CSc) and Modulus of deformability (MOD) *42*
Table 4.7 – Correlation between the conventional strength (CSc) and modulus of deformability (MOD) with compressive strength (Sc), modulus of elasticity (MOE) and density (ρ) *44*
Table 4.8 – Mechanical parameters for C20 from ČSN EN-338 ..... *44*
Table 4.9 - Data processing of loading jack results for the church; Conventional compressive strength (CSc) and Modulus of deformability (MOD) *45*
Table 4.10 – Moisture content (MC) for the west wing roof *47*
Table 5.1 – Wind loads (w_e) for the both wind directions *59*
Table 5.2 – Partial safety coefficients from EN 1990:2002 ..... *59*

Table 5.3 – Load values in the plane configuration for the Frame 1 ..... *63*
Table 5.4 – Conversion factor for the axial loads on the lower rafter (Rafter_DO) from the upper one (Rafter_UP) *64*

Chapter 1

1. INTRODUCTION

In the Hradčany district of Prague is located the Loreta, a remarkable Baroque historic monument. The Prague Loreta is a place of pilgrimage with a captivating history. The expansive decorative frontal façade is a work of the prominent architects of the Czech Republic, the Dientzehofers. The clock tower in front carries on top the authentic Loreta carillon. The building on the inside hides the famous Loreta treasure, the Prague Sun, a 6222 diamonds monstrance. Beside the St.Vitus Cathedral treasure, it is the most valuable treasure in the Czech Republic. The surrounding cloisters conceal on the inside a copy of the St. Mary's Holy House of Nazareth, which also represents the first building in the Loreta complex.

The building of the monument, since the placement of the first stone in 1626, has faced many phases of construction. The majority of the works have progressed between 1698 and 1748, where the majority of them were supervised by Cristoph and Kilian Dientzenhofer. The changes in the cloisters levels and the extension in the buildings affected the timber roofs. In many areas of the roofs, the internal configuration of the structure is altered and lead to many damages. The southern part of the west wing roof contains many of these alterations in terms of historical changes, interventions and damages. Some of the interventions are not documented and their purpose is not quite understood. One of the timber frames is significantly deformed and a strengthening column is used as reinforcement. The cause of deformation is not straightforward and the strengthening efficiency purpose is not documented.

The scope of this thesis involves the historical analysis of the chronological construction of the monument. A historical background is developed with the available literature resources enriched by the dendrochronological dating of the timber roofs. The historical background is used to make the assumptions on the historical changes in the roof with the significant deformation. After the distinction of the interventions on that area, with the help of non-destructive tests a comparison between the original and new elements is accomplished. Mechanical parameters of the timber elements are obtained from the tests and are used in the structural analysis. Structural analysis of one frame suffering deformation is executed to demonstrate the historical assumptions. The stability of the current state of the frame is controlled to evaluate its safety. A strengthening proposal is given with the results obtained from the structural model.

This page is left blank on purpose.

Chapter 2

2. TIMBER MATERIAL IN CZECH REPUBLIC

Looking on timber's trunk can be seen the fibers which compose the internal structure. Since the fibers are in one direction, timber has anisotropy. Furthermore, timber is a hygroscopic material and moisture plays a key role in many aspects of timber elements. The moisture content of timber fluctuates according to the climatic conditions the element is exposed or even the place it is used. Even the protected timber elements can be in contact with moisture due to capillary rise of masonry walls, condensation or even leakage. High levels of moisture enable the fungal attack of timber elements. Another risk timber elements are exposed to is the insect attack. Moreover, it is a flammable material and catches easily fire, making timber a very delicate material for certain places. Timber with all these drawbacks is still used nowadays due to its durability. Its good behavior in tension and compression make it very appropriate for different structural systems. Strength to weight ratio is another advantage of timber for structural use, especially in large spans. In addition, the ability of creating different shapes with timber makes it a very useful material in construction. Although the cross-sectional dimensions of timber elements are limited to the tree size, with new technology timber elements can go to tremendous spans with transport as the only limitation.

2.1 History of timber as a construction material

Timber is a building material which was used in construction since ancient times. The abundance of timber and its properties made it the most suitable material for buildings. High strength to weight ratio, workability and the easiness to create various shapes made it possible for it to be used for a long time and even in modern days. Timber was used to build a vast variety of structures such as buildings, boats and ships, bridges and so forth. At first (40 000 until 10 000 BC) the shelters were made out of tree branches and later (4 500 until 3 000 BC) to be continued with the timber-framed houses (Kuklík, 2008). Furthermore, as Kuklík (2008) explains the structural detailing was difficult, and the connections together with joints were not easy. Nevertheless, longhouses were constructed with dimensions ranging from a width of 5.5 m to 7 m and with large lengths of up to 45 m and a gable roofs on top (Figure 2.1).

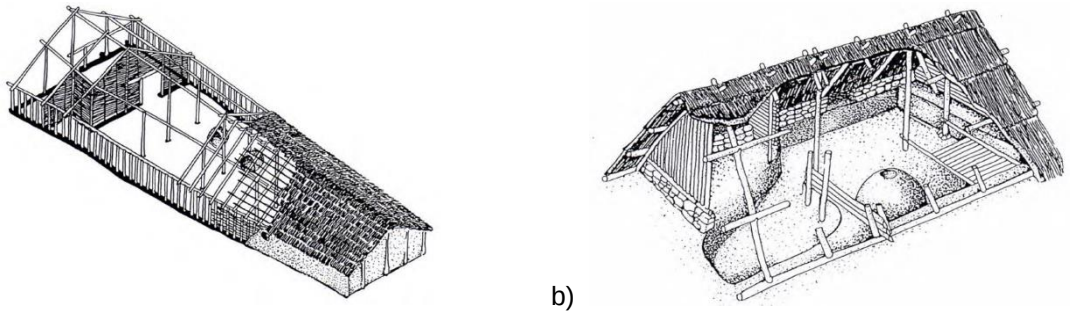

a) b)

Figure 2.1- a) Longhouse with linear increase in height 3,000 BC; b) House construction by Celts 400 BC (Kuklík, 2008)

When the Celts inhabited the territory of Central Europe, they started a new construction of light houses with stone pedestal (Figure 2.1-b). One of these tribes named that region Boiohaemum, which is the western region of Czech Republic known as Bohemia in recent days. Afterwards, during the 400-550 AD the Slavic tribes inhabited these regions and their house construction was similar to the Celts. Later on, with the invasion of different tribes and the diversity of many cultures, the typology of houses changed and from the 13th century houses from countryside differentiated from the townhouses. Moreover, from the 18th century timber was prohibited to be used in buildings except for floors, partition walls and roofs (which continues to be used in the present days) (Kuklík, 2008).

2.2 Roof typology in the Czech Republic

The roof typology gradually changed over time. In some countries many of the same roof systems are seen on same periods of time. Nevertheless, in the Bohemian and Moravian region of Czech Republic the roof typology progressed gradually with time. This makes it easier to date some of the roof systems in the region, observing the typology of the roof. The majority of the historical roofs surviving from the Middle Ages are the group of historic roofs known as common rafter roofs with collars (Bláha, 2006). The term *Common Rafter Roofs* (in Czech: Hambalkové Krovy) refers to the roof consisting of coupled rafters joined at the apex and connected on their ends by a tie beam. If reinforcement elements are used in certain levels to tie the rafters, such as collars, then these systems are known as *Common Rafter Roofs with Collars*. This basic principle of triangles can be arranged differently in both directions to create various roofing systems. Bigger spans can be covered with the use of stiffening timber elements such as struts and posts, which play an important role in the stability of the system. They can also be used in the longitudinal direction as stiffening frames or also known as wind-braces. The longitudinal frames usually consist of king-struts or queen-posts combined with collar plates, purlins and short-spanning pieces. The tie-beams can be replaced with hammer-beams as a more economical solution or for open ceilings (galleries). In Czech Republic the roof systems without the tie beams are also called “empty” or “barren” trusses. In common rafter roofs with collars often can be seen some elements connected to the outer side of the rafters, called sprockets, which enable the extension of the wings of

the roof as far away from the façade. This typology of roofs can be clearly seen in the Czech Republic in locations with historic values.

With the help of dendrochronological dating of timber, some of the roof structures are dated and represent the preserved state of roofing systems typology. Bláha (2006) describes these typologies and the dated examples of each one. One of the oldest timber roof dated is the roof of the Church of Annunciation of Our Lady in the Bohemian town called Cheb. The roof dates back to 1318 and represents a common rafter roof with collar and struts (Figure 2.2-a). An example of a typical common roof with collars is the roof of Church of All Saints in Slivenec near Prague, which is the oldest of its type and dates back to 1322/23 (Figure 2.2-b). Another typology commonly found in Czech Republic is the common rafter roof with collar and scissor braces. The truss of the Dominican Church of St. Anne in Prague serves as the best example of this type, which dates to 1324/25 (Figure 2.2-c). A very steep pitch roof is made possible by the construction of roofs with collars and king struts. This system consists of rafters connected with horizontal beam linked to the king struts. This typology enabled the roof construction of the Old Town Bridge Tower in Prague, as the oldest example (Figure 2.2-d). Whereas, if the king strut is joined with rafters at the apex the typology is known as the common rafter roof with collar and the upper king strut. The king strut in the upper part allows for a free space on the lower part. A good example of this typology is the Church of St. Peter and Paul in Petrovice, dated to 1616/17 (Figure 2.2-e). Another simple but efficient typology is the common rafter roofs with collars and crown posts. A typical example with the post attached upward is the House no. 50 in Telč (Figure 2.2-f). Common rafter roofs with collars and queen posts are a roof typology which enable the load reduction on the tie beam and enable a spacious roof. This can be seen in the Church of St. Kundegunda by Jihlava, which has been dated to 1803/04 (Figure 2.2-g). A simple solution of a roof is always the common rafter roof with collars which covers considerable spans and presents a less complicated distribution of loads. This typology is seen also in the roofs of Loreta in Prague (Figure 2.2-h).

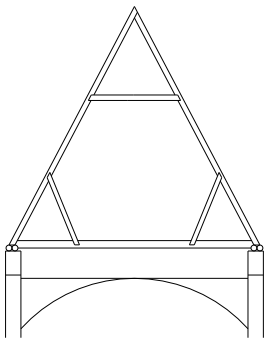

a)

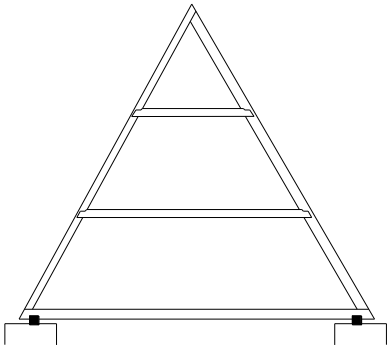

b)

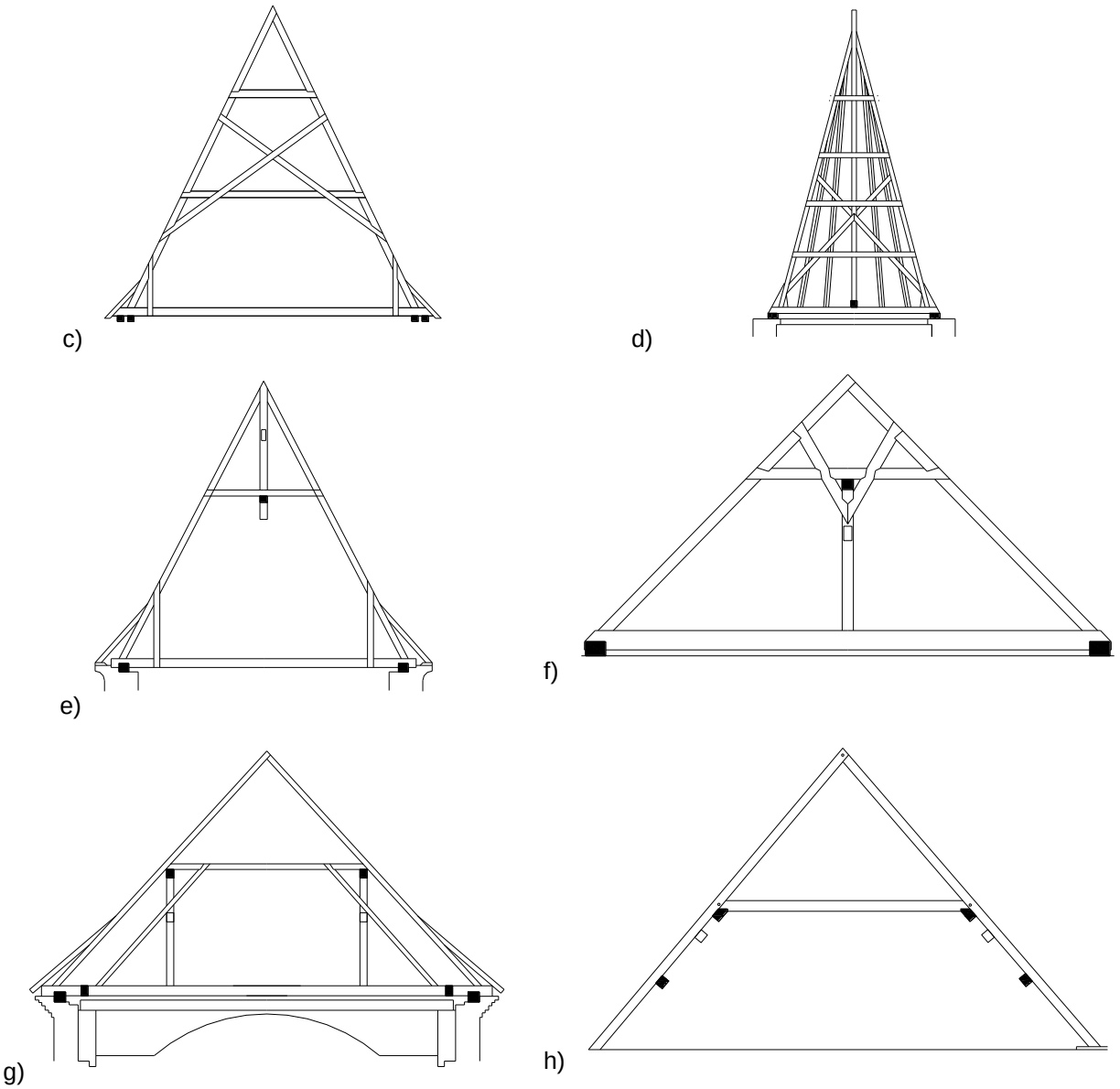

Figure 2.2- Different roof types in the Czech Republic; a) Church of Annunciation of Our Lady in Cheb; b) Church of All Saints in Slivenec near Prague; c) Dominican Church of St. Anne in Prague; d) Old Town Bridge Tower in Prague; e) Church of St. Peter and Paul in Petrovice; f) House no. 50 in Telč; g) Church of St. Kundegunda; h) Timber truss in the roofs of Loreta in Prague; (Bláha, 2006)

Chapter 3

3. THE LORETA IN PRAGUE

Serving as a place of pilgrimage is the Loreta in Prague with a Baroque architecture. It is called "The Loreta in Prague" because it is a copy of the original Loreta in Italy. The front façade is a remarkable work of the Dientzenhofers, the famous son and father architects. In the center of the façade is the tower where the authentic carillon still remains. The monument is composed of perpendicular closed cloisters of two stories high. The cloisters surround on the inside the most significant building of the complex which is the Santa Casa. Moreover, on the center of the eastern cloister is the Church of Nativity of our Lord with the sacristy on the northern side and with the crypt underneath. On the four corners of the cloisters and on the middle of the northern and southern cloisters, are six chapels. The Loreta complex labelled can be seen in Figure 3.1.

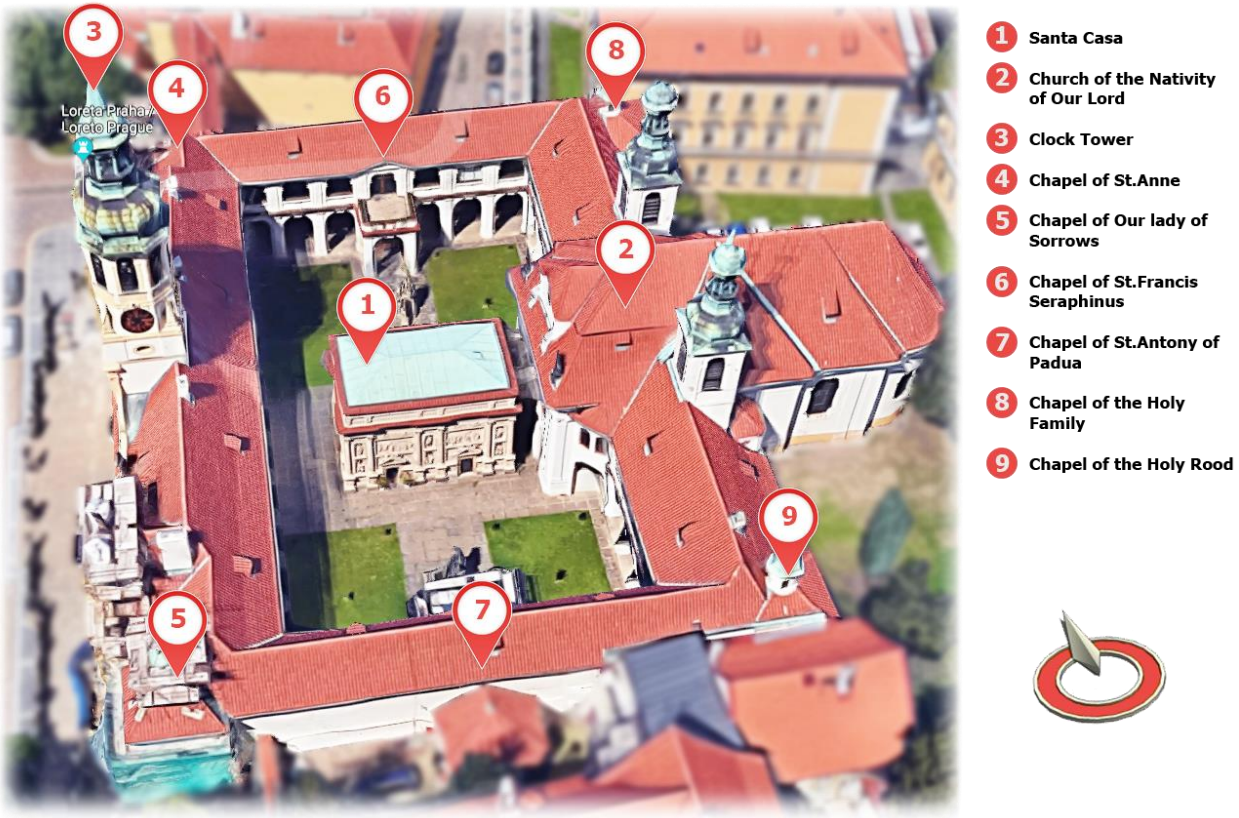

Figure 3.1 – The Loreta in Prague monument

3.1 Site location

The Loreta site is located in Loretánské square in the Hradčany district of Prague. In front of Loreta is the Czernin Palace and on the side is Bohemia's first monastery of the Capuchin Order. Prague is the capital of the Czech Republic located northwest of the country in the Vltava river, with a population of around 1.3 million inhabitants. Hradčany is also known as the castle district of Prague and part of the historical center. The Loreta site is at an altitude of about 277m, in an urban area with good connection to the city center. The exact coordinates that localize the Loreta site are 50°05'21" North and 14°23'29" East (Figure 3.2).

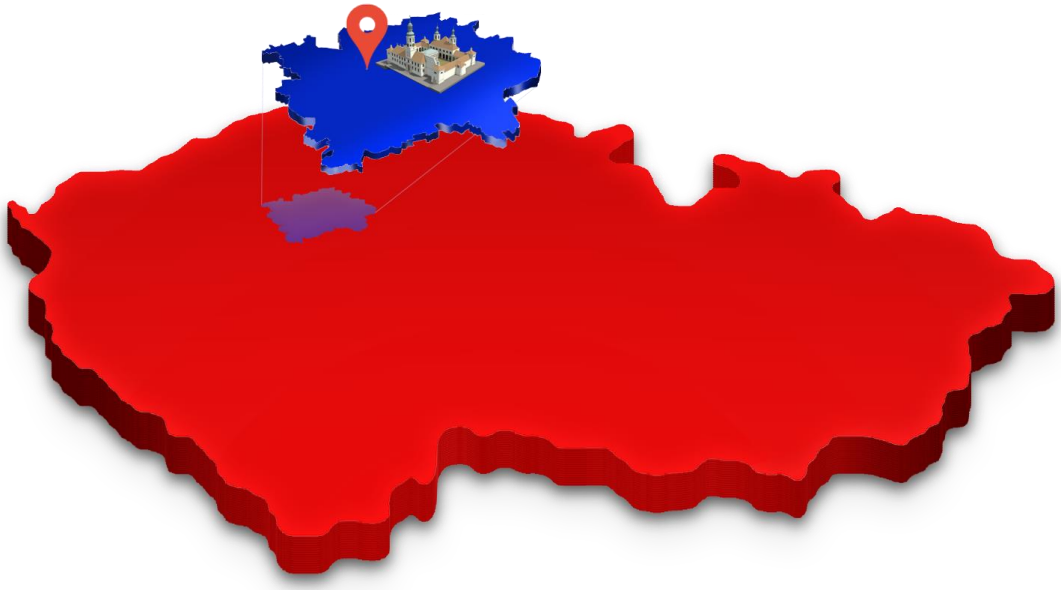

Figure 3.2 – Loreta location in Prague, Czech Republic

3.2 Climatic conditions

According to the Köppen–Geiger climate classification system, Prague has an Oceanic climate with cold winters and relatively warm summers. From the data retrieved for the years 1981 to 2010, it can be seen that the temperatures have a large variation. The average temperature is around 10°C with the highest temperature recorded in this period in July which was 37.8°C. Whereas, the lowest temperature recorded is in March and it was -27.6°C. From the graph of this data in Figure 3.3, can also be observed that the average temperatures vary between 0°C and 20°C.

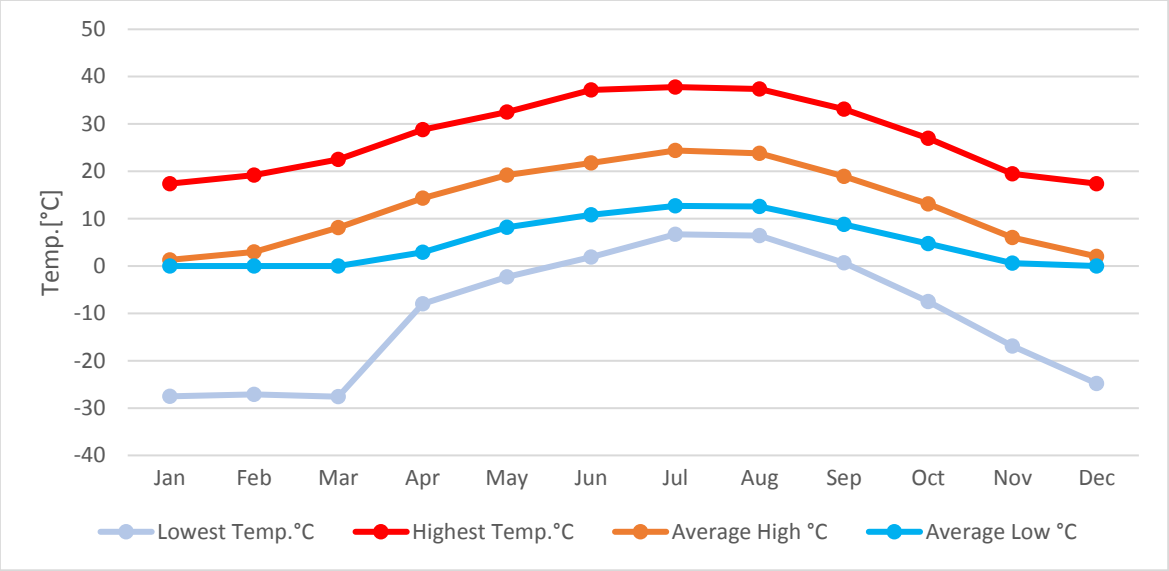

Figure 3.3 – Temperature variation between the years 1981-2010 (Weather and Climate, Pogoda.ru.net)

The average precipitation is observed to be the highest during May until August as can be seen in Figure 3.4 (a). The average precipitation during the year is around 7.5 mm. Observing from the graph of relative humidity in Figure 3.4 (b), it is seen that the values are almost constant at an average relative humidity of about 77%. During winter the precipitation is less but snowfall increases and it is highest during January, around 17.9 cm. The snow stops by the beginning of April as it can be seen in Figure 3.4 (c), and it starts around November.

a)

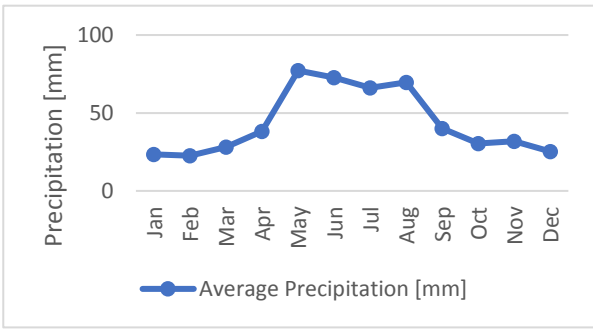

b)

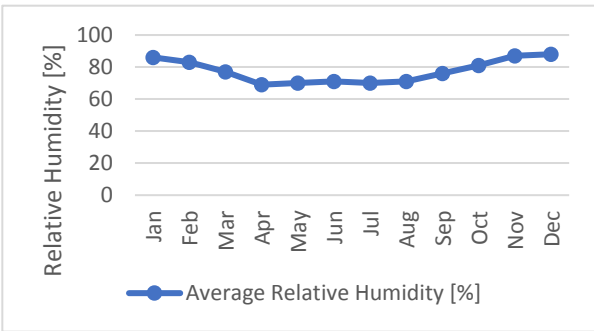

c)

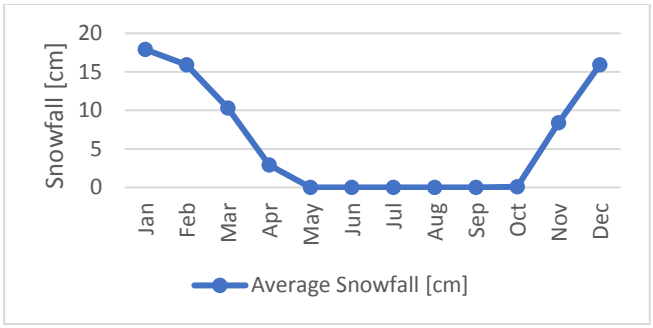

Figure 3.4 - Data retrieved for the years 1981-2010, a) Average Precipitation (National Oceanic and Atmospheric Administration, NOAA); b) Average Humidity (Weather and Climate, Pogoda.ru.net); c) Average Snowfall (National Oceanic and Atmospheric Administration, NOAA);

The sun path during the year is shown in Figure 3.5, and it can be seen that most sun is obtained from the South direction and the longest daylight is during summer. From this can be understood that the highest temperature change in Loreta is in the southern roof and the two roofs in the southern wings of the western and eastern parts.

a) b) c) d)

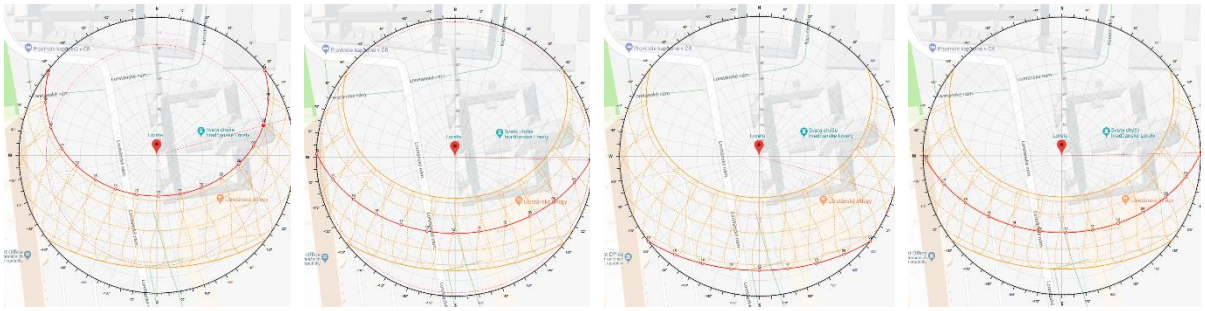

Figure 3.5 - Sun path during the year, a) Summer; b) Autumn; c) Winter; d) Spring; (Dr. Andrew J. Marsh, 2014)

3.3 Architectural features

3.3.1. The Santa Casa

The Santa Casa or “The Holy House” is a copy of the Nazareth Santa Casa located also in the Italian Loreto. The Santa Casa is the building where according to the legend the archangel Gabriel announced to the Virgin Mary that she will conceive the Son of God. The legends explain that it had been transported from the Holy Land by angels to Italy. It is the first building in the monument and the most significant. The walls on the outside are decorated with sculptures and the inside is covered with bricks following the original Santa Casa, to be covered on top with a flat roof and an attic. On the inside is located the statue of Our Lady of Loreto which is made out of linden wood, whereas the original is out of cedar wood. A picture of the Santa Casa is shown below in Figure 3.6 (Loreto Prague, 2015).

Figure 3.6 – The Holy House

3.3.2. The Church of Nativity of Our Lord

In the middle of the eastern cloister is located The Church of Nativity of Our Lord with extensions to the east and west. The church consists of one big nave with the main altar in front (eastern side as seen in Figure 3.7-left) and a choir on the back (western side as seen in Figure 3.7-right) with an authentic organ. Under the church is located the crypt with numerous frescoes with motives of Death and Resurrection. On top of the church are featured two polyhedral towers with truncated polyhedron roofs and finish with spires out of an onion dome.

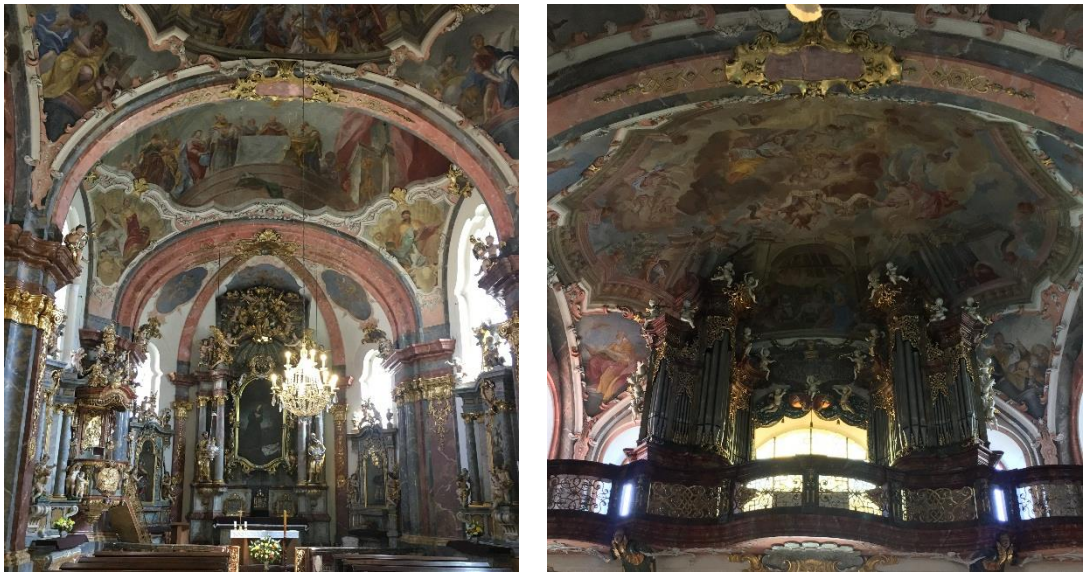

Figure 3.7 – The main altar (left) and the authentic organ (right)

3.3.3. The Chapels and Cloisters

Four chapels are located in the four corners of the complex and two more are in the middle of the northern and southern cloisters. On the eastern side, in the north and south corner are the Chapel of the Holy Family and the Chapel of the Holy Rood respectively. On the western side, in the other corners are the Chapel of St. Anne and Chapel of Our Lady of Sorrows, north and south respectively. On the middle of the northern cloister is the Chapel of the St. Francis Seraphinus, while on the opposite side on the southern cloister is the Chapel of St. Antony of Padua. The corner chapels are constructed on a rectangular base plan and with a dome on top which ends with a truncate polyhedron roof and a spire above on top. The chapels are connected through two-story cloisters. On the ground floor they are open in the form of arcades. On the second level they are closed by windows with a view to the garden of the complex and closed to the outside. The two-story cloisters are shown in Figure 3.8.

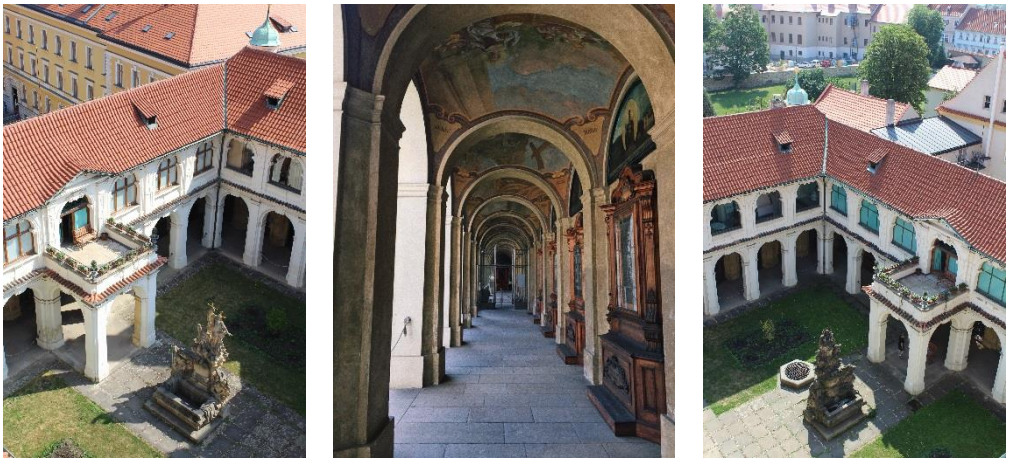

Figure 3.8 – The cloisters on the northern side (left), the arcades in the cloisters (center) and the cloisters on the southern side (right)

3.3.4. Front Façade and the Tower

On the west is the main entrance with the significant façade from the Dientzenhofers and the clock tower with famous Loreta carillon. The front façade with a Baroque style is symmetrical and it is divided by pilasters rising two stories up. The entrance building is a two-story building with a hipped roof. In the center of the façade, above the entrance stands the clock tower with the carillon on top. The tower starts with a square base and is followed by an octagonal one up to the roof which finishes with a truncated polyhedron roof and a spire on top of an onion dome. The last level of the tower is lit through semicircular openings on each side of the octagonal. On top of the tower stands the carillon of Loreta which still carries the authentic bells and mechanism from the date of order. The front façade and the carillon with the bells and mechanism are presented in the Figure 3.9 below.

Figure 3.9 – Front façade and the main tower (left), the carillon mechanism (top) and the authentic carillon bells (bottom)

3.4. Construction development through history

The construction of the Loreta in Prague started in 1626. During its years of service it underwent many historical changes throughout different eras. The construction process itself was not continuous and was performed throughout different years and affected the appearance together with the purpose it served. The construction development of the Loreta complex is explained chronologically by Líčeníková (2017), from the beginning of construction until the Dientzenhofers last touch.

-1626

On June 3rd, 1626 the Santa Casa foundation stone was laid with the financing of the Lobkowicz family. The next year in the statue of Our Lady of Loreto was brought to the Prague and four years later the building was consecrated by the Cardinal Ernst Adalbert von Harrach.

-1634

This year marks the construction of the cloisters in a type of fortification, which was very typical at the times of Thirty Years' War. The architect contracted by Katerina Benigna of Lobkowicz to construct the cloisters was Giovanni Battista Orsi. Due to the Thirty Years' War the construction was interrupted quite often. With the death of Battista the work is continued by Andrea Allio.

-1646

During these years the tower was finished and the cloisters were without plaster by the Italian architect Silvestro Carlone who carried on the work after the death of Allio.

-1664

With these data and archival reports, a hypothesis of the construction phase of Loreta in the year 1664 is shown in Figure 3.10. It can be seen in the picture that the complex was of one story cloisters perpendicularly closed, connecting the buildings of the complex. According to archive reports the Santa Casa was covered only in black and white murals. The front building in the western part was a two-story building with a saddle roof and with the tower in the center. The tower was polyhedral with windows on the last level in the form of a three-part Serlian windows. On the eastern side can be seen the Church of Nativity, which at the time it was without the extensions. The cloisters on the outside were closed, representing a typical pilgrimage building for the time of Thirty Years' War in the form of fortification.

Figure 3.10 – The architectural model for the year 1664 (Líčeníková, 2017)

-1685

During the years 1685-1687, there were two additions to the front façade. Jiří Mayer added the chapel of Our Lady of Sorrows in the south-west corner and the chapel of St.Anne in the north-west corner.

-1699

During 1694 the upper part of the main tower was taken down to be replaced by an octagonal base tower. The change was done in order to fit the installation of the bells by the bellfounder Claude Fremy from Amsterdam. During 1691, two more chapels were added on the two other corners. On the north-east corner was added the chapel of the Holy Family, while in the south-east the chapel of the Holy Rood. The model of the construction phase of Loreta of the year 1699 is presented in Figure 3.11. In the model is clearly shown the different base of the tower and the addition of the chapels in all the four corners. The addition of the corner chapel emphasizes the fortification character of the complex. The front building's roof is also changed from a saddle roof to a hipped one.

Figure 3.11 – The architectural model for the year 1699 (Líčeníková, 2017)

-1712

On the northern and southern sides, the middle part of the cloisters was extended to leave place for two more chapels. In the southern side in the year 1712 was added the chapel of St. Antony of Padua, while in the year 1716 the chapel of St. Francis of Seraphinus. These extensions present the valuable work of the prominent architect Christoph Dientzenhofer, which still survived to today. During 1717, the Church of the Nativity was extended to the East. Another major development during these years was the elevation of the treasury in the northern part of the west wing, which yielded in a two-story unification of the front façade. Nevertheless, the southern part of the façade was not elevated and a wall can be seen as the intention of this construction.

-1720

The model which represents the construction phase until that time is shown in Figure 3.12. It the model are represented the changes from the previous model. The extensions of the two chapels in the north and south and also the extension to the east of the church. The unification of the front façade is lost, but the attic wall in the southern side presents the intention of this unification.

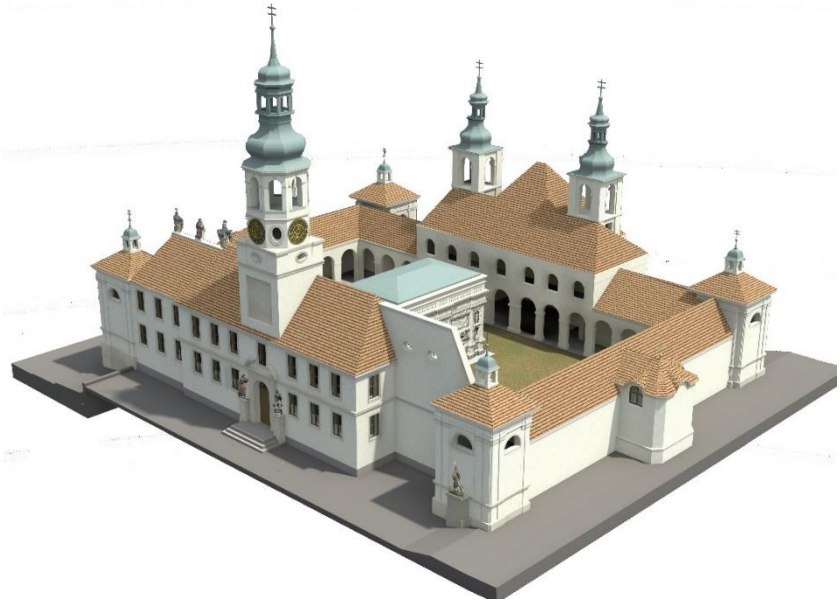

Figure 3.12 – The architectural model for the year 1720 (Líčeníková, 2017)

-1722

During this year Cristoph Dientzenhofer was contracted for the enlargement of the Church of Nativity to the west. In the same year later Cristoph dies and the work is continued by his son Kilian Ignaz Dientzenhofer. The appearance of the Loreta complex of present days is the merit of Kilian. Kilian unified the front façade by elevating the roof to the same height. In the two lateral sides of the façade two big dormer windows were placed. The façade was divided by pilasters which go up two stories and in the center the tower is left exposed to view. The Church of Nativity was extended to the western direction during 1722 and to the East direction during 1734.

-1747

The cloisters were elevated by Kilian on the entire perimeter of the second floor. Facing the courtyard were opened semicircular windows. With the completion of his works in Loreta, Kilian managed to finally diminish the fortification character of the complex.

The construction phases of the Loreta complex through different periods present valuable information about the actual appearance and configuration of Loreta. The stratigraphic configuration of Loreta complex is presented below in Figure 3.13, in order to have a better understanding of the historical development.

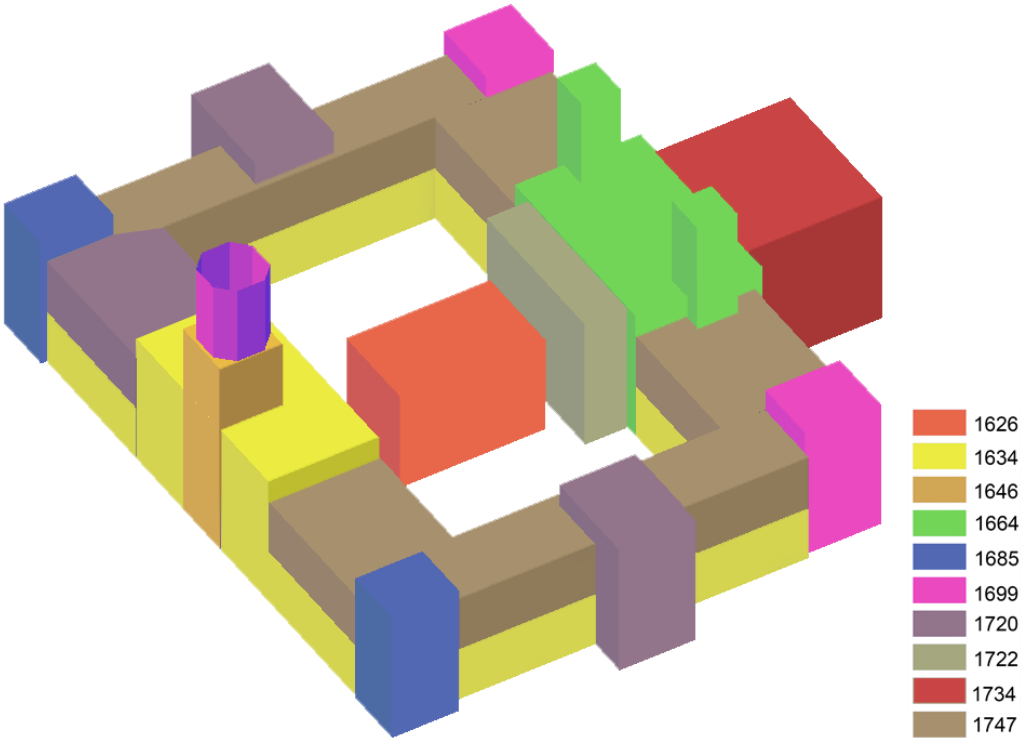

Figure 3.13 – Stratigraphy model of the Loreta

3.4 Roofs of Loreta

Timber roofs provide information about the construction technology and history of the structure. Wood as a material during its lifecycle develops annual rings which are called tree rings. These rings during the formation create the earlywood and latewood layer. The earlywood layer shows the beginning of the formation of the ring while the latewood shows the completion of one ring. In the center of the wood section which indicates the juvenile wood the earlywood is thicker, while in the outer parts which indicate the mature wood there are more latewood. The formation of the tree layers start from the top in the form of cones stacked to each other, rather than around the center (Ferguson, 1970). Dendrochronological dating is a discipline which enables the dating of the tree by analyzing the annual rings. A profile of the annual rings of the tree can be obtained by boring into the tree and taking samples. Since the timber elements used in roofs of structures are already cut, then the samples taken from these elements represent the felling date of the member.

As mentioned before, the Loreta complex underwent many construction developments and this affected the roof construction of the complex. A dendrochronological dating survey was performed in the roofs of Loreta and Bláha,J (2017) presents the information obtained. The erection of the second-floor of cloisters in the northern wing by Kilian Dientzenhofer was done by using the same timber elements which were supporting the old roof of the first-floor cloisters. This is also supported by the dating, where the elements in that area belong to a felling date of 1629/30 and 1630/31, while the erection of the

second-floor was done during 1740 as previously mentioned. The southern part of the East wing shows combined dating, where some of the older rafters were used to build the lower pitched roof. These two rafters are the oldest samples dated with a felling date of 1628/29 and 1629/30. The other rafters used to build the upper part date from 1716/17.

The samples from the middle part of the West wing have a felling date of 1632/33. The roof of that area presents an authentic timber material since construction. The previously hipped end roof in the middle part of the West wing is visible in the present days and traces of the frames supporting it can be seen in the Figure 3.14.

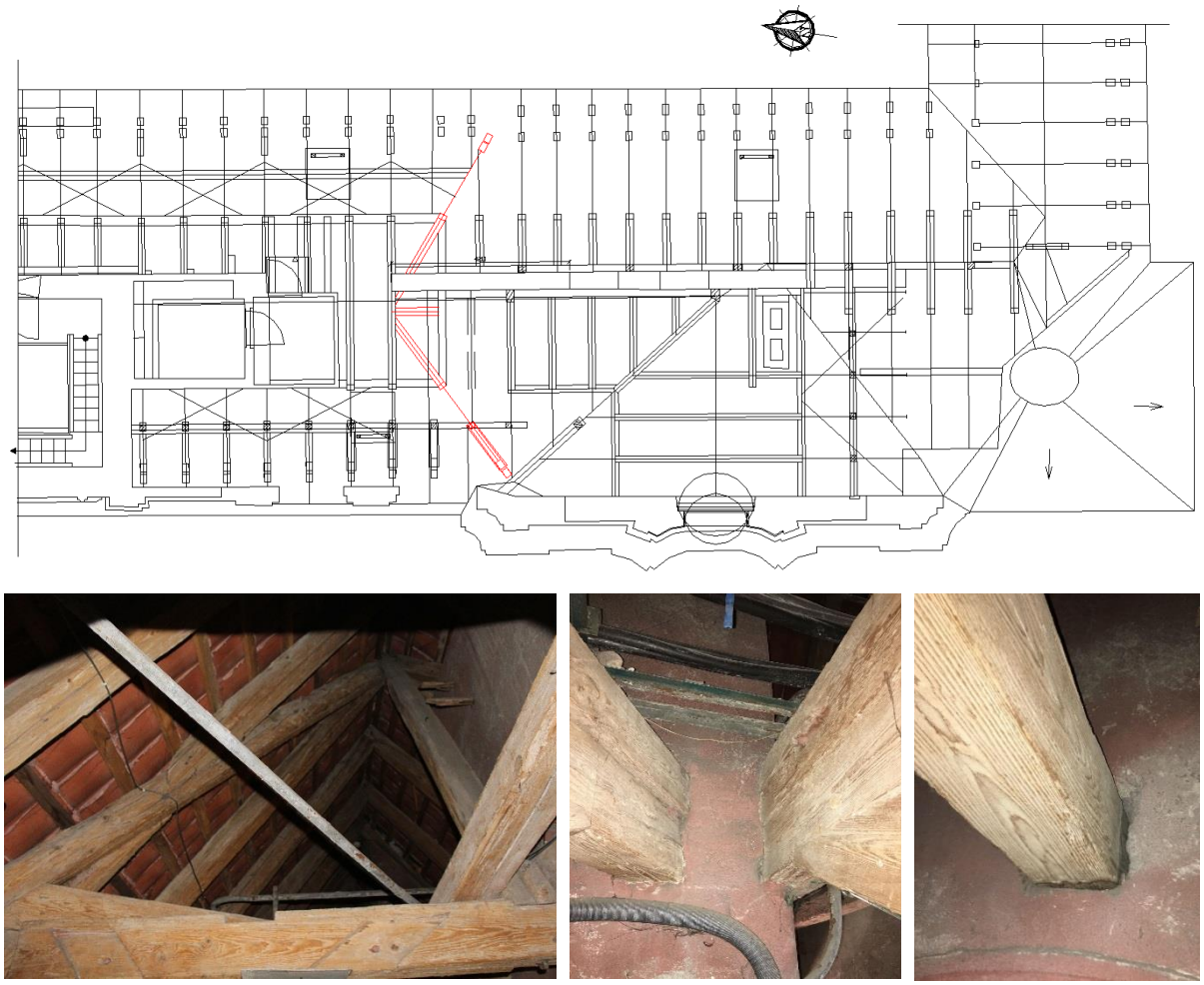

Figure 3.14 – The base plan of the southern part of the west wing roof (top), the traces of the original roof (left), the original tie beam (center) and the new tie beam (right)

From the Figure 3.14 (top) are visible the frames of the hipped roof and the cut rafter in the middle from later developments. The ridge of the previous hipped roof is seen in Figure 3.14 (left), while in Figure 3.14 (center) is shown the tie beam which connects the two rafters. From the figure it is visible that the attic wall added later was built around the frame. However, with the unification of the front façade the cloisters as mentioned before were elevated to a second level and the roof was attached to the wall. It

is also visible in the Figure 3.14 (right) the chipping of the wall to insert the new members to support the new roof. Bláha (2017) presents the felling dates of the members of the eastern side of the West wing roof which correspond to the elevation of that part by Kilian Dientzenhofer. The felling date of those members is 1744-48, whereas the members in the western side have a felling date of 1720/21. On the northern side of the West wing during 1717 was built the treasury and from the dendrochronological dating the members in that area show a felling date of 1697/98 and 1698/99.

The Church of Nativity of Our Lord underwent many extensions to the East and West. The initial part of the church is the center section which has a felling date of1716/17. The second large extension was to the West during 1722 and the last extension was to the East during 1734. The dendrochronological data correspond exactly to these years where for the western extension the felling date is 1720/23 and for the eastern extension 1733/34. These data are also supported by the current configuration of the roof in the church (Figure 3.15).

Figure 3.15 – The western part of the church's roof (top-left), the wall openings of the older church (top-right), the central roof of the church (bottom-left) and the eastern part of the roof (bottom-right)

From the Figure 3.15 (top-left) can be seen the hipped roof rafters that used to be in the central section where now continues to the West the choir's roof. Furthermore, in the Figure 3.15 (top-right) can be seen the openings which used to be before the extensions. In the Figure 3.15 (bottom-left) from the western extension is shown the central section of the church's roof. The two slopes of the previous roof are visible and also in the further back can be seen the roof of the eastern extension, also shown in Figure 3.15 (lower-right). The dendrochronological dating of the roofs of Loreta can be seen in Figure 3.16 below.

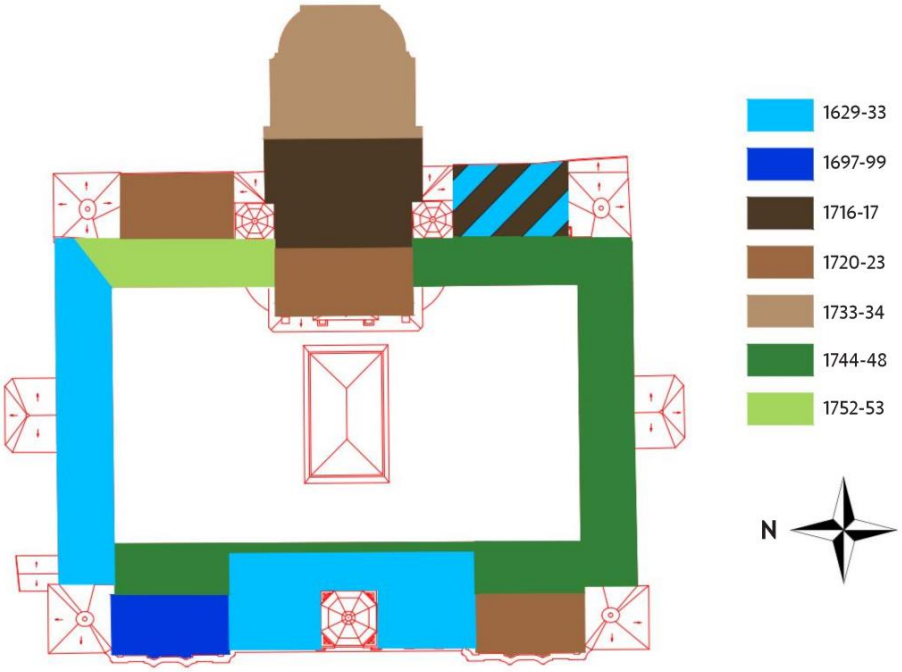

Figure 3.16 – Dendrochronological dating of the timber roofs (Bláha, 2017)

3.5 South part of the West wing roof

The main focus of this thesis is the southern part of the West wing roof. In this part of the roof occurred many alterations. The saddled roof of the front building was changed to the hipped one. In the mid part of the west cloisters was added the wall, which was not covered on the southern side until the unification of the façade. With the alterations in the façade from Kilian Dientzenhofer, also the roof slopes experienced many changes. The addition of the massive window on the level of the roof on two lateral sides of the front façade caused the elevation of another slope in the both sides. To support this slope there is a timber frame holding the two different planes of inclination. From the configuration of the loading or from the alterations during the construction, this frame was highly deformed. A column has been added to it on the lower end as a matter of strengthening. For this reason, the focus of the analysis will be on that frame. The area of focus can be seen in the drawing presented in Figure 3.17, with the frame of interest highlighted in red. More detailed drawings are presented in Appendix A.

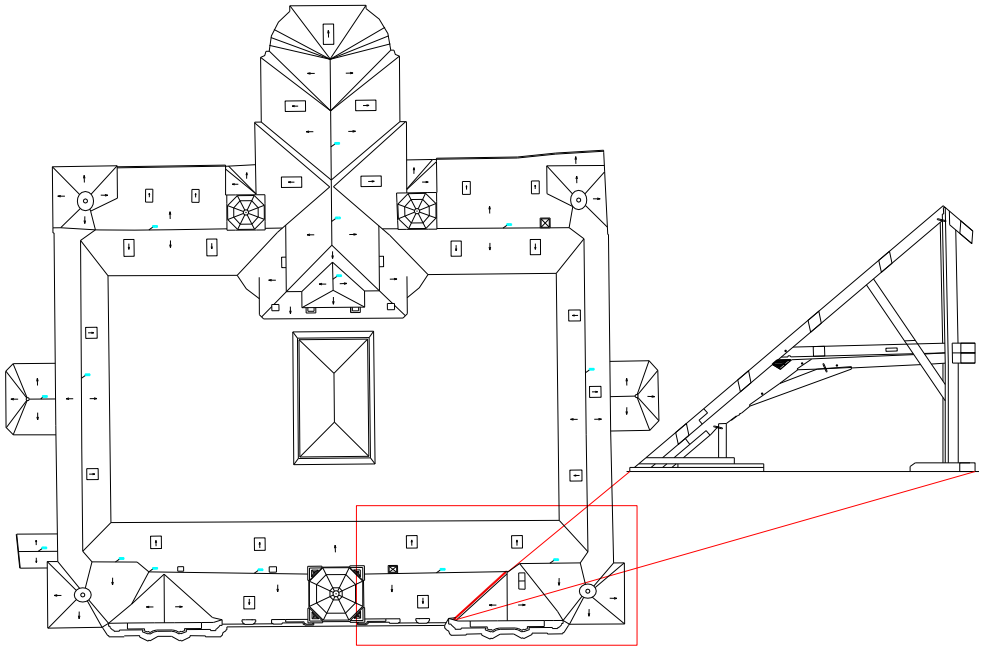

Figure 3.17 – The location of the frame of interest

3.4.1. Connections

Although there are seen some metallic elements in the joints, the original connections of the elements are timber carpentry joints. From alterations through time some of the members are removed and used in other areas and thereupon some gaps from previous connections are visible where the type of connections can be observed. Some of these examples can be seen in the Figure 3.18 below.

Figure 3.18 – Examples of the carpentry joint connections in the southern part of the west wing roof

3.4.2. Past Interventions

The interventions in the different construction phases caused many changes in the load path. Additionally, with the change of use, the structure was exposed to many other damages which lead to many deteriorations. Henceforth, in the roof are observed many interventions. After reviewing the archives from the Capuchin Order, not so much information was found. Concerning the restoration works carried out in the Loreta complex, the majority of the documents present in the archives were about the restoration works of the paintings and sculptures which are not in the scope of this thesis. Therefore, the information about the past interventions on the roof is found only on the roof itself.

The first intervention measure which can be observed are the strengthening short columns on the timber frames. These columns are on the sides, near the end of the rafters connected directly to them. The columns are supported on a timber beam which is embedded in the concrete floor. Moreover, the end of the rafter is connected with two timber planks to the column as seen in Figure 3.19.

Figure 3.19 – The short columns connected to the rafters

The current floor is of concrete and the presence of the previous tie beams of the roof are not visible. The construction date of the concrete floor is not known. However, seen from the current configuration of the beams embedded in the concrete floor it can be assumed that the floor was added together with the strengthening columns.

On the timber elements can be observed a considerable number of small diameter holes. The number of these holes per area are too many as can be seen in Figure 3.20 (left). This can be an injection to the timber elements as a measure of protection against the insects. Moreover, layers of fireproofing can be observed in certain elements as can be seen in the Figure 3.20 (right).

Figure 3.20 – The injection holes (left) and the fireproofing (right)

Something else which can be observed on the roof are the metallic elements. These elements are located usually near the connections to strengthen them, as can be seen in the Figure 3.21. Furthermore, a strengthening measure carried out in the roof are the end rafter repairs. The cause may have been the decay of the rafter on the ends due to the contact with moisture. Therefore, prosthesis have been used as a strengthening measure which can be seen in the Figure 3.21 (right).

Figure 3.21 – The metallic element in the diagonal strut (left) and the prosthesis (right)

This page is left blank on purpose.

Chapter 4

4. NON-DESTRUCTIVE TESTS

Especially when dealing with historical constructions is very important to maintain the integrity of the structure. Since in historical times the design procedure most of the time was performed by experience, few data and technical reports are available for the materials used. Furthermore, there is few information on the mechanical parameters used in the elements of constructions. The first step to evaluating a structure is knowing the historical background of the structure and the past interventions in order to continue with the appropriate visual inspection. Visual inspection is a crucial step in the evaluation of the structure. Through visual inspection qualitative information can be collected about the condition of the elements. Especially in the timber constructions it is a preliminary step on determining the locations of interest for further investigation. In timber constructions with the help of visual inspection it is possible to locate the majority of decays in the structure and measure the deformations, cracks and the superficial damage. Afterwards, in order to evaluate properly the condition of the construction and obtain information about the members some tests are needed to be carried out. The tests need to be less intrusive and not cause too much damage in the construction. The commonly known non-destructive tests (NDT), are able to provide information with few intrusions in the construction. NDTs also provide information about the inner condition of the elements without the need of taking samples or causing damage to the structure. With the help of these tests it is possible to have mostly an exact idea of the structural state of the members which can be used for further analyses, strengthening purposes or to evaluate the safety of the construction.

4.1 Location of the tests

The area of interest on this thesis as previously mentioned is the south wing of the western roof. Due to the different construction periods and the changes in the construction, this part of the roof consists of timber elements of different historical timelines. With the non-destructive techniques it is possible to differentiate the parameters from these various periods. The chosen locations to perform the tests are two different frames which represent two different historical states of construction. One frame is an original timber truss with a felling year 1629-33 shown in Figure 4.1 (center) as frame number 2, and represents the roof construction period during those years. The other frame is the one which is deformed and will be used for further structural evaluation. This frame felling in the year 1720-23 with some

additions during the later strengthening and it is shown as frame number 1 in Figure 4.1 (left). On another frame, frame number 3 shown in Figure 4.1 (right), only the moisture meter is used to evaluate the moisture content of the timber elements. This because the frame is embedded in the masonry wall and is constantly in contact with it.

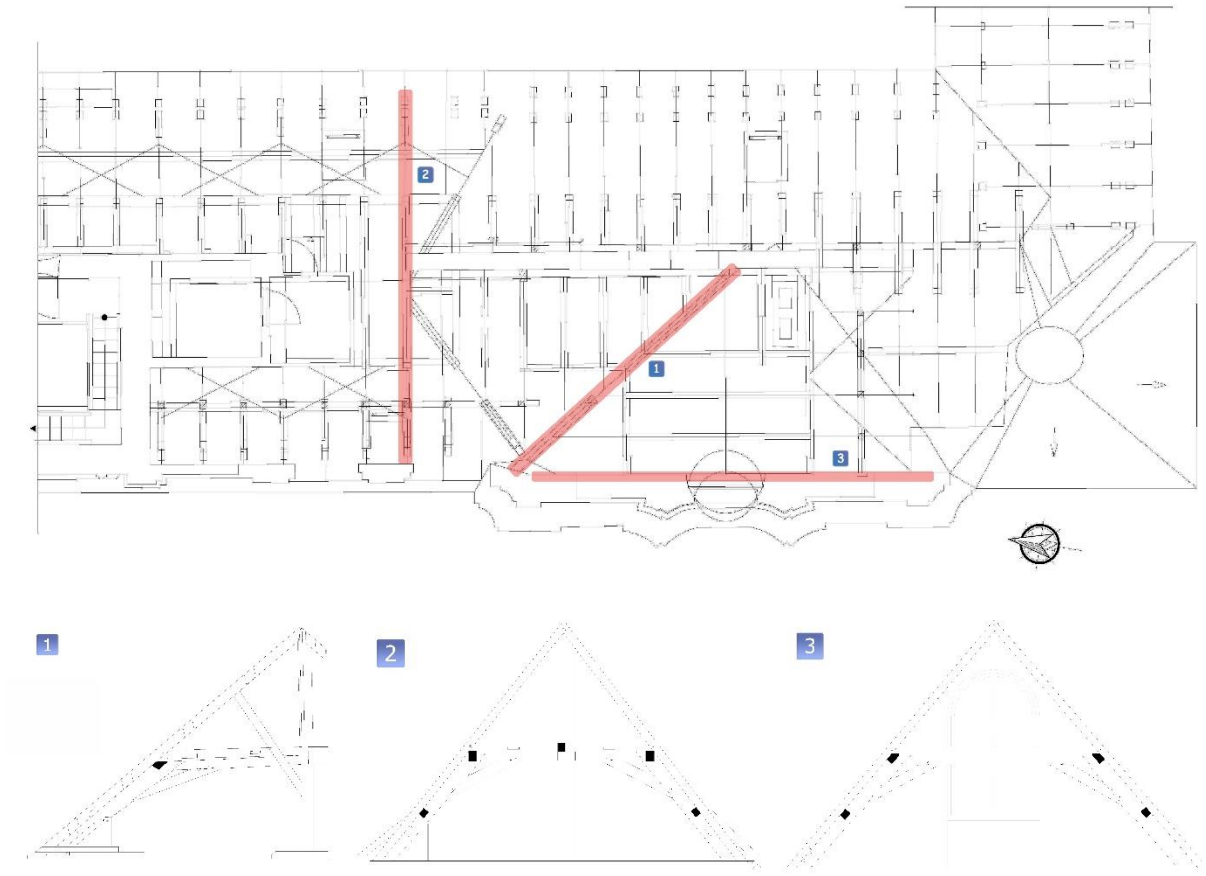

Figure 4.1 – Base plan drawing of the southern part of the west wing roof (top), Frame 1 (left), Frame 2 (center) and Frame 3 (right)

On frame number 1 is performed the resistance microdrilling test, the loading jack test and the moisture content. On the other frame, frame number 2, was performed the loading jack and the moisture content in order to compare it with frame number 1. Whereas, in frame number 3 only the moisture content was measured since it is embedded inside the masonry wall and presents valuable information about the degradation state of timber.

However, to observe the differences between other parts of the Loreta complex, the loading jack test was carried out also in the Church of the Nativity of Our Lord. Afterwards, the moisture content was measured in the drilled holes. The location of the tests performed in the church are described in the Table 4.1 below.

Table 4.1 – Location of the loading jack performed in the church

Test	Location	Dimension	Description
CLJ-1	Loc 1 Roof of the choir	(28 x 30) cm	Sill beam (header beam) on the southern side (drilled from the upper side between 3rd and 4th truss counted from the west)
CLJ-2	Loc 2 Roof of the choir	(16 x 34) cm	Truncated principal on the southern side (drilled from the NE side 180 cm from the bottom end)
CLJ-3	Loc 3 Roof of the choir	(16 x 24) cm	Cross bar of the second main transversal truss from the west (drilled from the western side 40 cm from the south end)
CLJ-4	Loc 4 Roof of the nave	(32 x 31) cm	Upper beam of the coupled girder supporting the roof frame (drilled from the upper side 150 cm from the northern wall)
CLJ-5	Loc 5 Roof of the nave	(30 x 30) cm	Lower beam of coupled girder supporting the roof frame (drilled from the western side 100 cm from the southern wall)

4.2 Visual Inspection

Visual inspection is a reliable method of grading the overall quality of the elements. This method of inspection is to be carried out by a skillful inspector with experience. The experience of the inspector is very important because of the judgment of each of the qualitative parameters which can grade a timber element. After each parameter is graded appropriately with an objective qualification the timber element can be categorized into three different classes. According to UNI 11035:2003, there are three different classes which categorize the timber element, namely S1, S2 and S3. The features which are examined in order to achieve a category are:

- wane and growth rate
- knots
- slope of grains
- fissures
- geometric features

Nevertheless, since the part of the roof in interest is a large area with many timber elements, the focus of the visual inspection and the grading is focused only on one frame. The frame of focus is the deformed frame, namely Frame 1. To carry on with the visual inspection of the frame, each element should be inspected separately and a classification of each element should be done. Regardless, the frame is inspected as a whole in order to achieve a unified class for the entire frame.

The growth rate is measured as the ratio of the tree rings in a distance of z, which is taken as 75 mm where possible. Since there are no cross sections visible to measure this parameter, the rings are drawn by using the data from the microdrilling which will be presented in the following paragraphs. Ring trees are drawn from three different locations R5, R7 and R15, which represent the original rafter, prothesis and the beam respectively. The tree rings drawn are shown below in Figure 4.2.

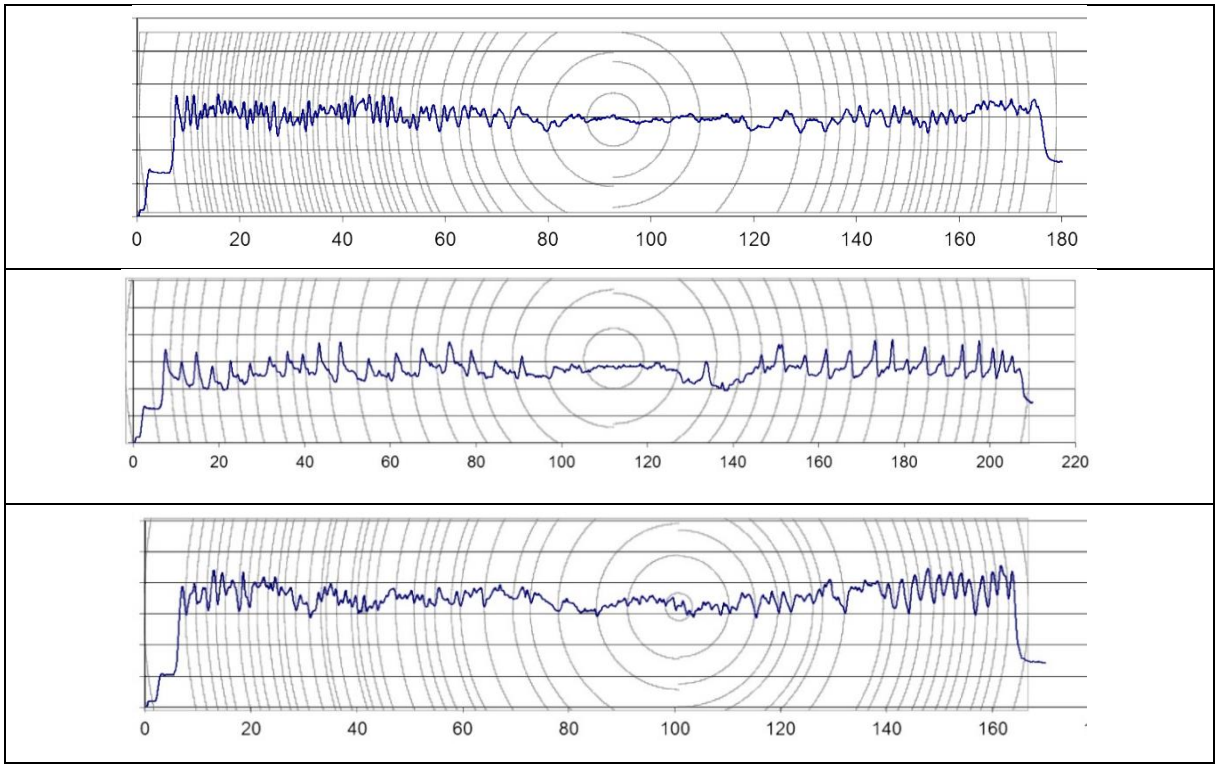

Figure 4.2 – Tree rings drawn according to the microdrilling measurements; R5 (top), R7 (center) and R15 (bottom)

As can be concluded from the Figure 4.2 above, the tree rings vary between the mature wood and the juvenile wood. Nevertheless, the number of rings in a distance of 75 mm varies between 12 to 35. The width of the rings varies from 2 to 4 mm for the mature wood rings and from 5 to 7 mm for the juvenile wood rings. According to UNI 11035:2003 table for Coniferous 1, for the parameter of distance between rings the frame is classified as S1, since the majority of the rings is from mature wood.

Wane is the rounded chamfering of the corners of the cross section of the elements. The elements of Frame 1 are roughly all with perpendicular edges and there are no chamfered edges. An exception is the column which has a cross section with many non-perpendicular edges. Therefore, the frame for the wane parameter can be classified between S1 and S2.

Concerning the knots in the elements, the entire frame has few single knots with small diameter as can be seen in Figure 4.3. In Figure 4.3 (right) can be seen grouped knots as the only example of grouped knots. Therefore, for the parameter of knots the frame can be classified as S1.

Figure 4.3 – The highlighted knots on Frame 1

The slope of the grains is measured in different locations, where the deviation of the straight grains can be observed. The places where the slopes are measured can be seen in the Figure 4.4 below. The values obtained vary from 1:16 to 1:8 with a majority of values bigger than 1:14. According to this parameter the frame is classified as S2.

Figure 4.4 – The direction of the grains on Frame 1

In the frame can be seen a majority of fissures on the outside. They are mainly longitudinal and follow the direction of the fibers as can be seen in Figure 4.4. The widths of fissures vary from 5 mm to 20 mm. As for the internal fissures they are not assessed and no categorization can be done. Moreover, as can be seen in the Figure 4.5 below, there is a big deformation of about 56 mm on one end of the lower beam. This deformation caused the separation of the two beams and its safety will be further evaluated in the other chapter.

Figure 4.5 – Measurement of cracks and deformations on Frame 1

Another parameter which is required for the categorization of the timber class is the insect attack and the degradation from fungus. As previously mentioned in the past interventions, injections are performed as a protective measure from the insect attack and fungus attack. Therefore, for this parameter the frame can be categorized in the S1 class.

It can be concluded from the visual inspection that the timber element is in a good condition with the issue of large deformation at one point. Nonetheless, the mechanical condition observed from the inspection can be stated in a good state. As for the visual grading of the timber according to the UNI 11035:2003, the frame can be classified in the S1 class, leaning towards S2. The mechanical parameters which this code provides are mainly for the Italian wood species. Therefore, only an approximation can be made for the current frame. The species which corresponds to the frame of interest is the fir in the North of Italy. The mechanical parameters of this category for classes S1 and S2 are shown in Table 4.2.

Table 4.2 – The mechanical parameters according to the Italian norms UNI 11035:2003

Mechanical Parameter		S1	S2
Bending	$f_{m,k}$ *[MPa]*	29	23
Tension parallel to grain	$f_{t,0,k}$ *[MPa]*	17	14
Tension perpendicular to grain	$f_{t,90,k}$ *[MPa]*	0.4	0.4
Compression parallel to grain	$f_{c,0,k}$ *[MPa]*	23	20
Compression perpendicular to grain	$f_{c,90,k}$ *[MPa]*	2.9	2.9
Shear	$f_{v,k}$ *[MPa]*	3	2.5
Mean value of modulus of elasticity parallel to grain	$E_{o,mean}$ *[GPa]*	12	10.5
Mean value of density	ρ_{mean} *[kg/m³]*	415	415

4.3 Resistance Microdrilling

4.3.1 Test Description

A small diameter drill is driven into the timber profiles to obtain the condition of the timber element. By this method it is possible to determine the damage, the decay rate, cracks and also hidden parts of the timber element. The drilling needle needs to be very small in order to minimize the damage in the member. However, if the needle is too small the hardness of the wood can cause deviations in the needle and that is why a diameter of 1.5mm with a tip of 3 mm is suggested (Figure 4.6-a). For many machines the needle tends to incline with depth for wood densities higher than 600 kg/m³ (Tannert, et al., 2013). The needle is driven into the member at a constant speed to obtain the difference in resistance of drilling. To obtain more sensitivity the drilling machine can be operated at a higher speed, with the condition that the needle does not break. While interpreting the results the species of the wood plays a crucial role. In some woods like coniferous the center is less dense and the resistance is lower. Moreover, the latewood is much denser than the earlywood and it can be seen in the resistance profile by the microdrilling device. The microdrilling devices record the energy needed to keep the constant drilling at a certain speed. The output of this device is a graph with the penetration depth in one axis and the profile of energy consumption or relative resistance on the other. The variation of the energy on the graph indicates the different phenomena inside the timber element. A commercial instrument that is widely used for microdrilling is Resistograph® and the one used for these tests is Resistograph® 4453-P shown in Figure 4.6-b.

a) b)

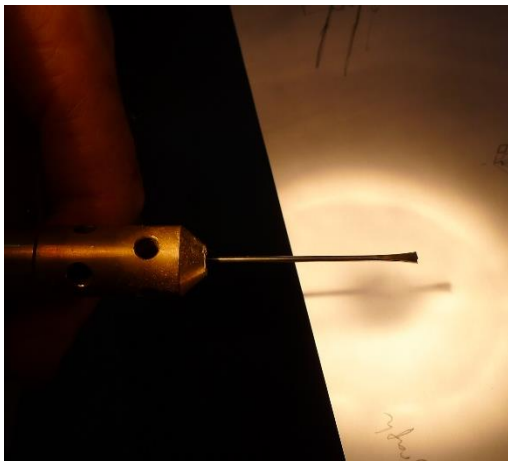

c) d)

Figure 4.6 – a) The drilling needle; b) the microdrilling device Resistograph®; c) microdrilling on the prosthesis; d) microdrilling on the original beam

4.3.2 Procedure and Results

Microdrilling with the Resistograph® was carried on Frame 1. It was performed in many locations with a concentration of testing in the area where the frame is supported in the wall, shown in Figure 4.6 (c) and (d). This area is chosen due to the presence of the prostheses as strengthening. The previous part of the frame was probably replaced due to moisture and the assessment of the placed timber prostheses is done with the microdrilling. While comparing the original timber with the replaced one it is possible to assess the efficiency and the condition state of the strengthening. The location of the tests and the test number are shown in Figure 4.7, with their reference points where the respective distances are measured and presented in the Table 4.3.

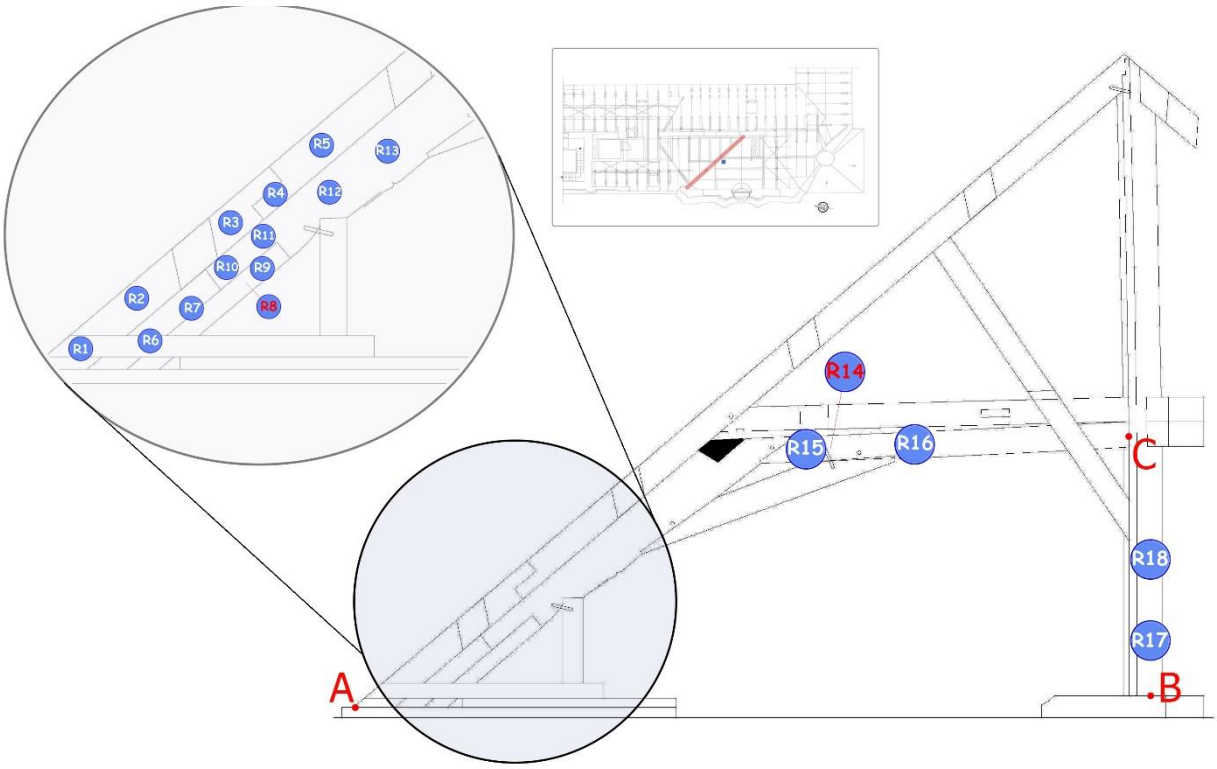

Figure 4.7 – Location of the microdrilling tests performed on Frame 1

As can be observed in the Figure 4.7, 18 tests are performed on the frame. During the test R8, which was performed near R9, the needle broke because it ended in a metal element and it can be clearly seen in the graph in Figure 4.8 (top). From the graph can be observed how the resistance experiences an immediate jump and then stops. This was peculiar since the connections in the roof are mainly timber connections and from this can be stated that there are some strengthening works which are not visible. Furthermore, during the drilling of R14 the needle ended in a crack and the test was carried on with R15 on the other side of the element. It can be observed from the graph in Figure 4.8 (bottom), that the resistance amplitude decreases drastically until the test was stopped.

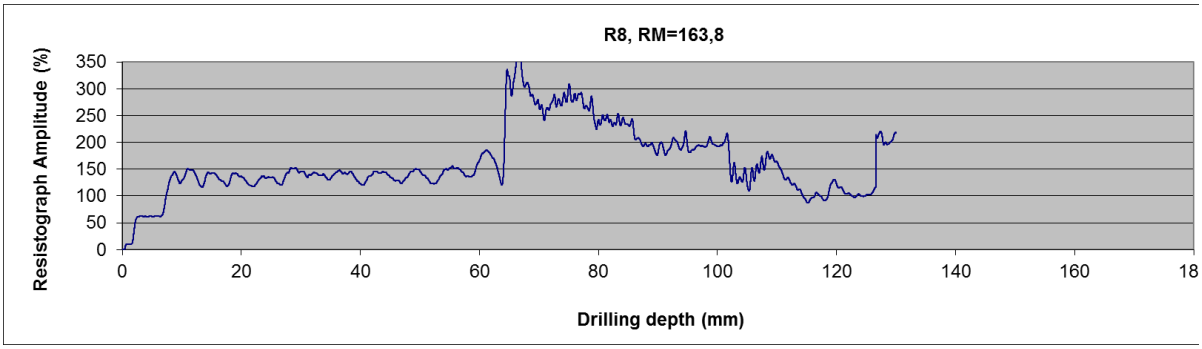

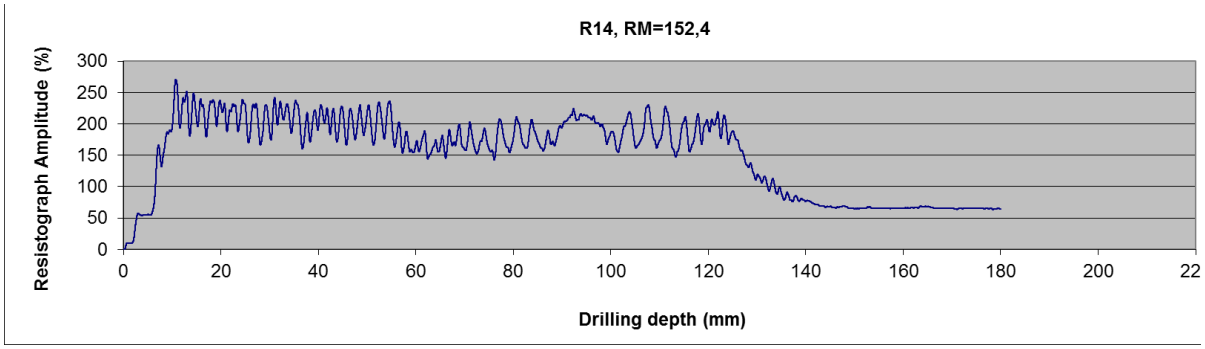

Figure 4.8 – Microdrilling resistance graph for R8 (top) and R14 (bottom)

From the test R10 which is plotted and shown in Figure 4.9, can be seen a variation in resistance. The testing point in on the connection joint which is a wooden joint. If the joint is supposed to be a twin mortice and tenon then the sudden reduction in resistance can be due to a gap in the connection between the first tenon. According, to the test the width is about If the second tenon is placed symmetrically on the opposite side the last drop in reduction can be expected as a small gap between the two members. The two reductions in the middle of the section can be due to cracks in the section. A schematic illustration is shown below in the Figure 4.9, where on top is shown the possible top view of the joint and below is the graph of R10.

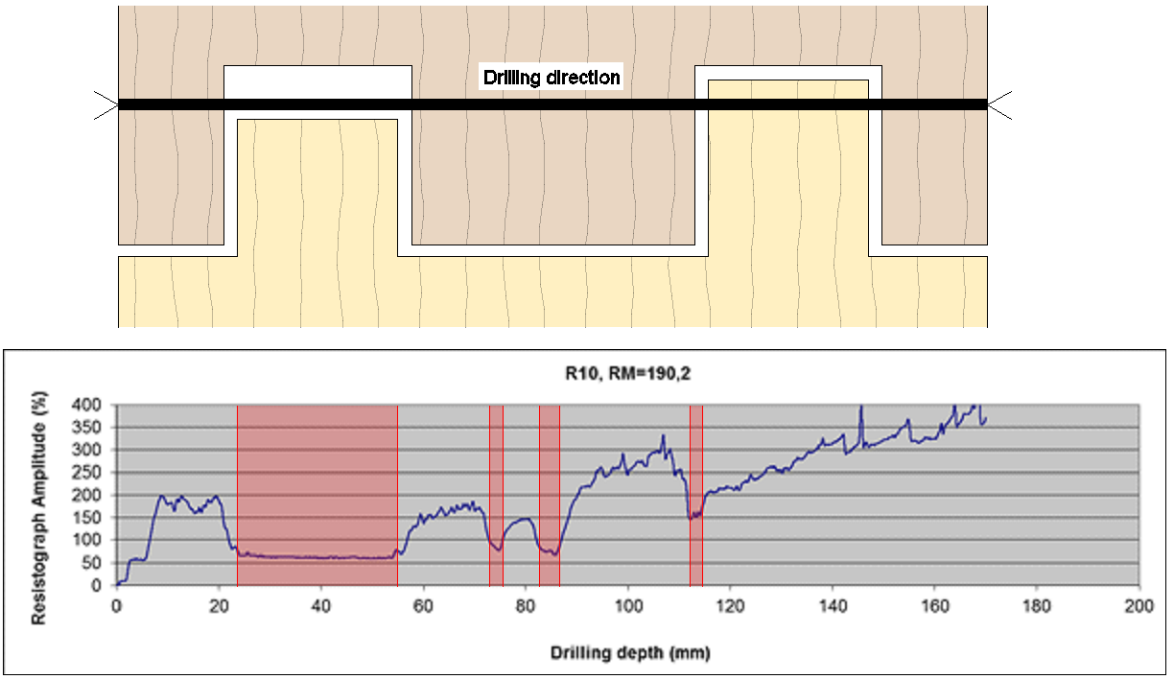

Figure 4.9 -Hypothetical drawing of the internal structure of the carpentry joint according to microdrilling measurement R10

On the contrary in the test R11 a reduction of resistance is seen in the middle of the graph. Since R11 is also in the connection joint, the reduction can be due to a single tenon and mortice connection. The graph can be seen below in Figure 4.10.

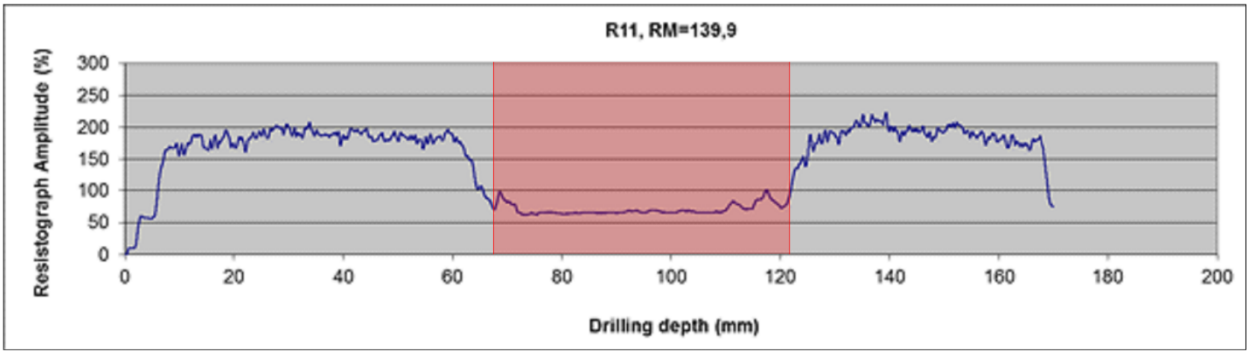

Figure 4.10 – Reduction of the resistance in the microdrilling measurement R11

Further, the other results show good condition of the timber with relatively constant resistance. The graphs for all the tests performed with the Resistograph® are presented in Appendix B. The graphs give a qualitative idea of the timber elements. However, it is needed to compute the resistance measure (RM) to obtain a quantitative value to compare with other parameters. The resistance measure is the ratio between the area under the graph (A), which presents the energy consumption, and the width of the measured section (L). The results of each test and the computed RM are shown in Table 4.3.

Table 4.3 – Resistance measure (RM) for the microdrilling tests performed on Frame 1

Test no.	Ref. point	Radial length [cm]	Area under graph	Section width [mm]	RM
R1	A	30	33973.7	210	161.8
R2	A	90	30672.48	210	146.1
R3	A	138	29012.075	200	145.1
R4	A	163	30146.525	200	150.7
R5	A	205	26324.61	180	146.2
R6	A	67	26785.76	200	133.9
R7	A	94	27594.235	210	131.4
R8	A	140	21050.23	130	161.9
R9	A	146	31163.08	200	155.8
R10	A	116	32333.97	170	190.2
R11	A	136	23791.385	170	139.9
R12	A	165	30648.74	170	180.3
R13	A	215	31371.35	180	174.3
R14	C	250	27440.04	180	152.4
R15	C	250	28695.7	170	168.8
R16	C	150	31178.535	180	173.2
R17	B	55	28686.245	200	143.4
R18	B	120	28414.505	200	142.1

As can be observed in the Table 4.3, the overall average of RM is 155. Nevertheless, by removing R8 and R14, the computed average of RM for different members is shown in Table 4.4. It can be clearly seen how the rafter is in a better condition than the prosthesis. Even though the rafter is an older element, the direct contact of the prosthesis with the wall has caused more damage to it. The beam shows the highest value while the column shows even a lower value than the prosthesis.

Table 4.4 – The average results for the resistance measures (RM)

Prosthesis	Rafter	Beam	Column
145.7	163.6	171.5	142.8

The RM values can also be related to the compressive strength and the density. According to (Kloiber, et al., 2014), the relation between RM and compressive strength of wood (S_C) is expressed with the equation:

$$RM = (-343.83) + (22.296) * S_C \quad (4.1)$$

The correlation factor is R^2=0.746. The relation between RM and the density (ρ) with a correlation factor of R^2=0.807 is expressed with the equation:

$$RM = (-137.67) + (1.665) * \rho \quad (4.2)$$

According to these relations with the RM, the values obtained are shown in Table 4.5.

Table 4.5 – Correlation of RM to compressive strength (SC) and density (ρ)

Test no.	RM	SC [Mpa]	ρ [kg/m³]
R1	161.8	22.68	179.85
R2	146.1	21.97	170.41
R3	145.1	21.93	169.81
R4	150.7	22.18	173.21
R5	146.2	21.98	170.52
R6	133.9	21.43	163.12
R7	131.4	21.31	161.60
R8	161.9	22.68	179.94
R9	155.8	22.41	176.27
R10	190.2	23.95	196.92
R11	139.9	21.70	166.74
R12	180.3	23.51	190.96
R13	174.3	23.24	187.36
R14	152.4	22.26	174.24
R15	168.8	22.99	184.07
R16	173.2	23.19	186.72
R17	143.4	21.85	168.83
R18	142.1	21.79	168.01

The average value of the compressive strength is 22.4 MPa, whereas the average value of the density is 176 kg/m³. According to (Kloiber, et al., 2014) the wood species used to obtain the relation equations is silver fir, which is one of the most frequently used species in historical trusses in Czech Republic. Furthermore, according to the dendrochronological data the frame tested is made from fir also and therefore the tests should correlate well. Nevertheless, the density value seems to be very small for a fir species, which according to (The Wood Database, 2018) is around 415 kg/m³.

From the Resistograph® it also possible to assess the rings of the cross section. The latewood is much denser than the earlywood and that is expressed also in the resistance measure as the beginning of a ring. Usually if the middle of the section experiences a reduction of resistance with a smaller variation of amplitude, indicates the presence of the juvenile wood rings. Whereas, in the parts of the graph with bigger variation of amplitude and higher resistance indicates the presence of mature wood rings. To obtain the exact profile of the tree rings, a cross section is required. However, observing the measures from the test a hypothesis of the rings is possible to be made. The test R5 presents a clearer resistance profile where the mature wood can be distinguished from the juvenile wood. The tree rings of the rafter according to R5 resistance measures are shown in the Figure 4.11. On the both sides of the graph are similar high variations in amplitude and small variations in the middle. Therefore, the juvenile wood rings can be seen in the middle of the section, while the mature wood ones are on the sides.

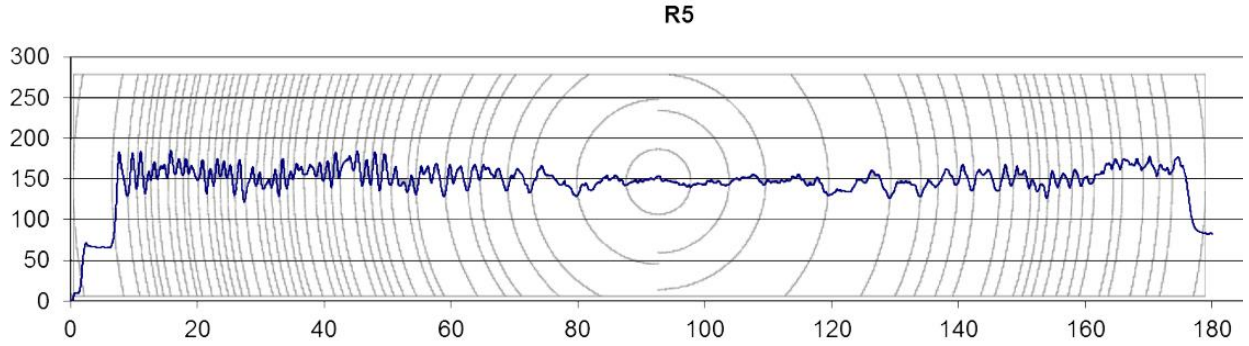

Figure 4.11 - Tree rings drawn according to the R5 microdrilling measurement

From the R7 test, the tree rings of the strengthening prosthesis can be observed. It can be clearly seen in the Figure 4.12 the distribution of the juvenile wood and mature wood rings. Again, the mature wood rings are on the sides, while the juvenile wood is on the middle.

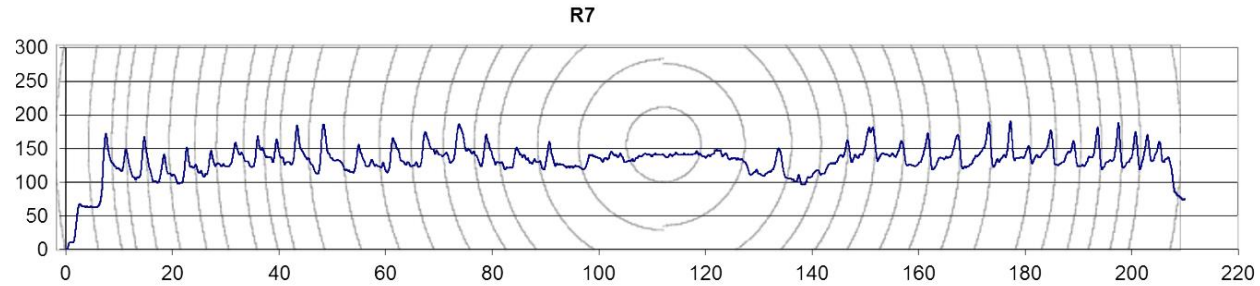

Figure 4.12 - Tree rings drawn according to the R7 microdrilling measurement

The R15 presents the tree rings of the beam in the frame as seen in Figure 4.13. In contrast to the other tests, the juvenile wood rings in R15 are a bit shifted to the right side of the section. Nevertheless, the mature wood rings are again on the sides of the section.

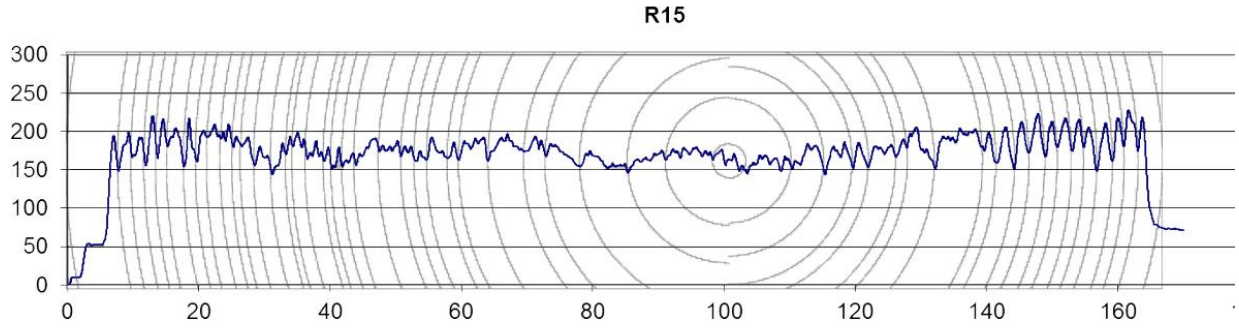

Figure 4.13 - Tree rings drawn according to the R15 microdrilling measurement

4.4 Loading Jack

4.4.1 Test Description

The loading jack is a device which is used to evaluate the mechanical parameters of timber elements. It is a portable device which can be used in situ and in laboratory. It consists of a jack with two jaws in opposite directions. The jack is inserted in a small pre-drilled hole of 12 mm wide, and the jaws are opened apart by pushing laterally to the surface. The loading on both sides goes up to 1.5 mm and it records both the displacement and the force. The jaws are 5 mm wide and 20 mm long and are rounded as shown in Figure 4.14.

Figure 4.14 - The loading jack jaws

The output is a graph of force-displacement where the ultimate load can be read and used to compute the maximum compressive force. The ultimate force is read by joining the elastic part with the plastic and the intersection gives the ultimate force. Furthermore, from the graph can be also computed the

modulus of deformability. The ability of this device to record the force and the displacement at different depths of the element, is a big advantage to the other devices (Kloiber, et al., 2014). The inaccuracy in drilling has no influence on the results and the device is very sensitive to the natural differences of the elements tested (Kloiber, et al.).

4.4.2 Procedure and Results

The first step during the loading jack test is the drilling of the hole of 12 mm wide. To drill the hole the drill machine has been used as shown in Figure 4.15. The machine is fixed to the member in order to drill the hole perpendicularly and without deviations. Since timber is a combustible material also the drilling speed should be controlled to avoid eventual heating. The holes have been drilled in a depth of about 120 mm in order to carry on with four loading jack tests on the elements.

Figure 4.15 - The drilling machine (left) and a close-view of the intrusiveness on the member (right)

The holes have been opened in two frames of the roof, namely Frame 1 and Frame 2. The locations of the performed tests are shown in Figure 4.16, where up is Frame 1 and down is Frame 2.

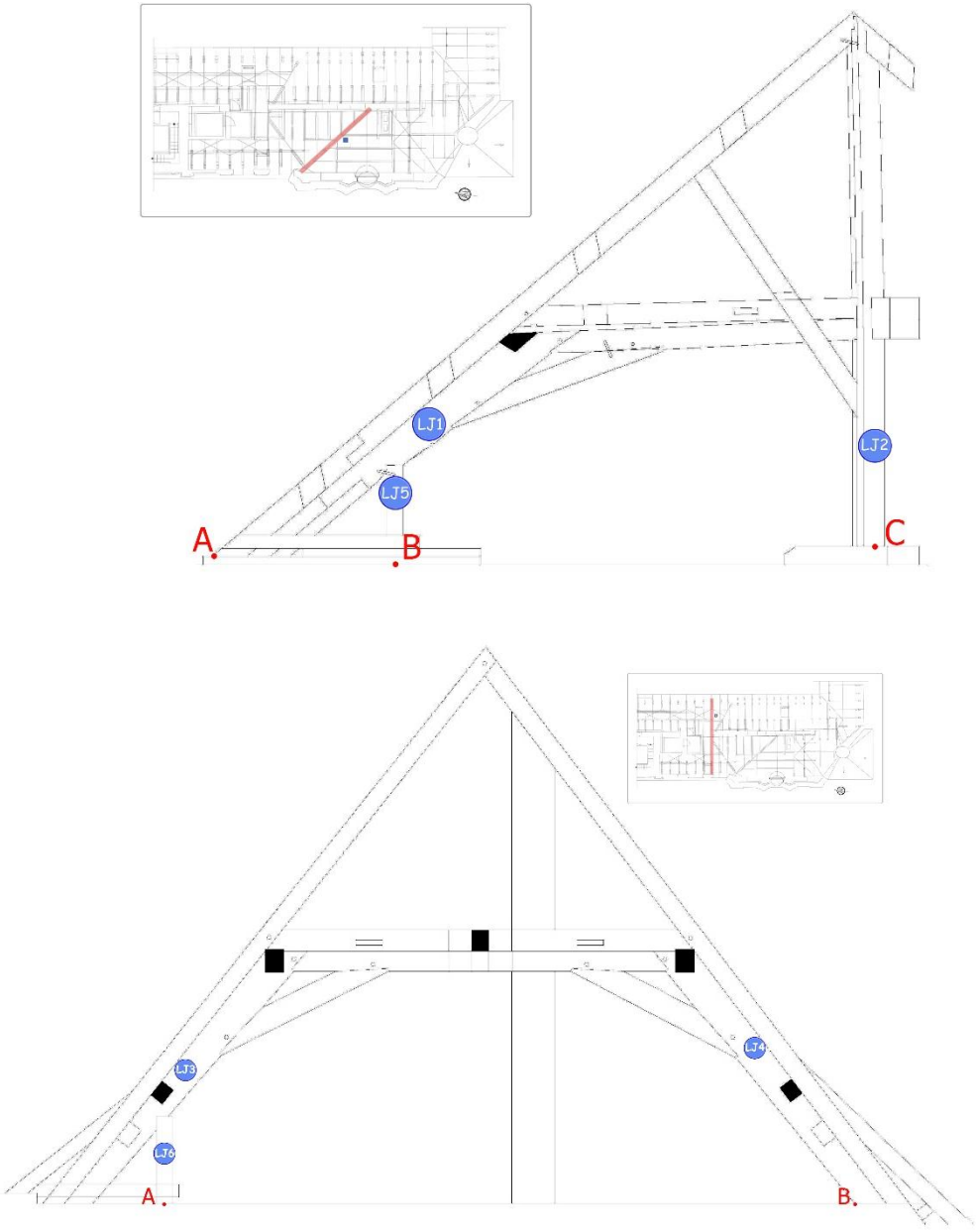

Figure 4.16 - Loading jack loactions performed on Frame 1 (top) and Frame 2 (bottom)

Afterwards, the test is carried on with the loading jack device in the six locations presented in the figure. In each point the tests are done in four core depths; (5-25) mm, (35-55) mm, (65-85) mm and (95-115) mm (Figure 4.17-right). According to the depth of the measurement the tests are named with numbers from 1 to 4, where the third depth of the first test will be named LJ-3 and so forth. An important factor before continuing with the test is the direction of the grains of the timber element. The device is designed to measure the force parallel the direction of the grains and if done differently gives wrong results. To control the direction of the force of the device help the arresting screws. They are on the sides of the device and their direction indicates the direction of force. The loading jack device is shown in Figure

4.17 (top). The device is wirelessly connected to a laptop and the software “SigVis” records the force and the displacement of the jaws, as shown in Figure 4.17 (bottom).

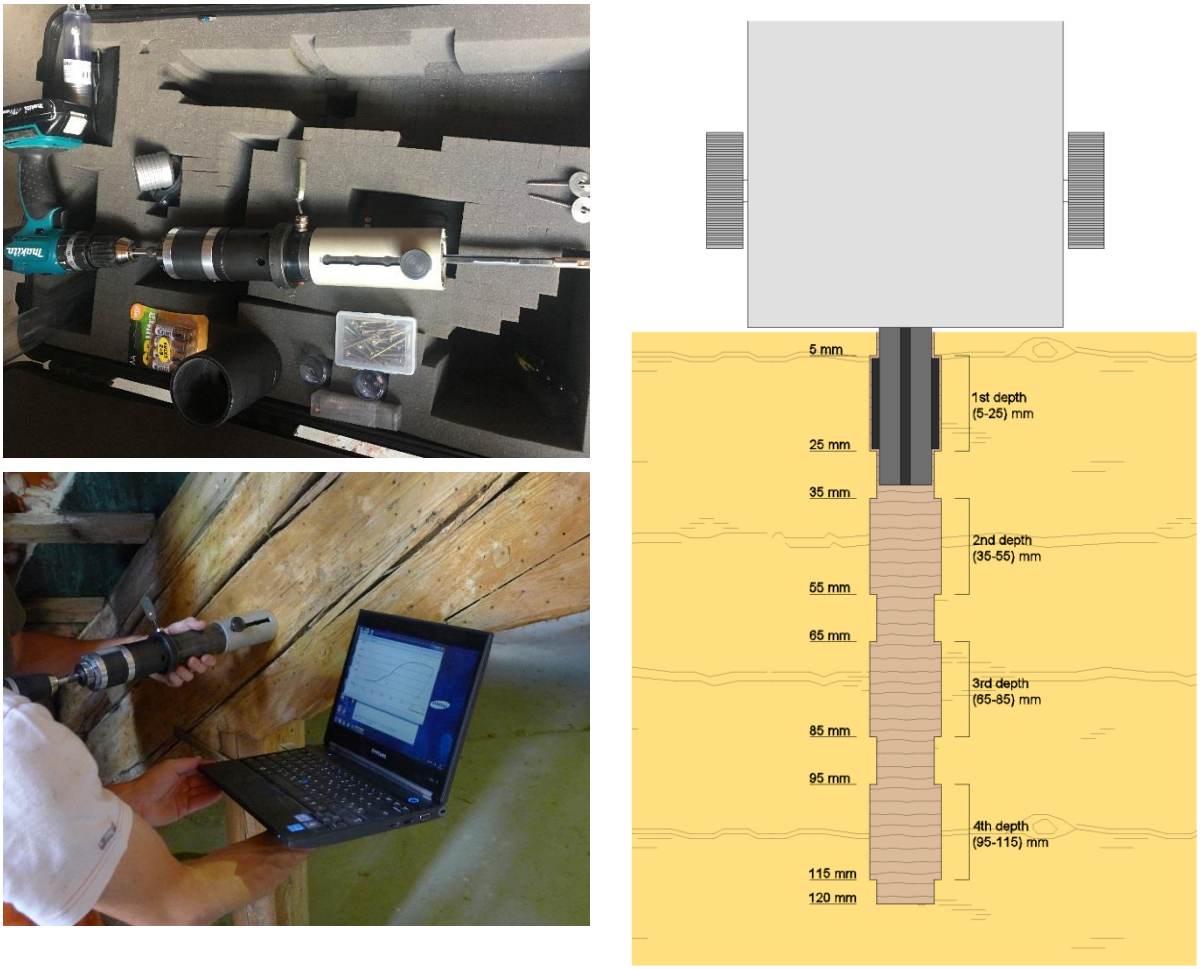

Figure 4.17 – The loading jack device (up), the measurement of the loding jack test with the SigVis software (bottom) and the detail of the measurement depths (right)

The software records the force required to push away the jaws in the element. Furthermore, it records the drawback force required to return the jaws to their initial position and therefore calibrates the force and the displacement. The graph goes from the elastic zone to the plastic zone. By connecting the elastic part of the graph with the plastic is obtained the ultimate force. The ratio of the ultimate force to the area of the jaw (5*20 mm) gives the conventional compressive strength (CS_C). Additionally, the ratio of the ultimate force to the displacement in that point gives the modulus of deformability (MOD). The recording of a test from the loading jack in “SigVis” is shown in Figure 4.18 (left). The elastic zone and the plastic one are distinguished with a red line. In the bottom part are shown the conventional strength from the ultimate load and the modulus of deformability. Furthermore, for each of the test performed a picture is taken with the endoscopic camera. The pictures are taken in order to have a visual image of the state of the wood where the test is taken. If some anomalies are obtained in the results than the

picture can help understand them better. An example of the picture is shown in Figure 4.18 (right), while for each of the tests together with the graphs of the loading jack are presented in the Appendix C.

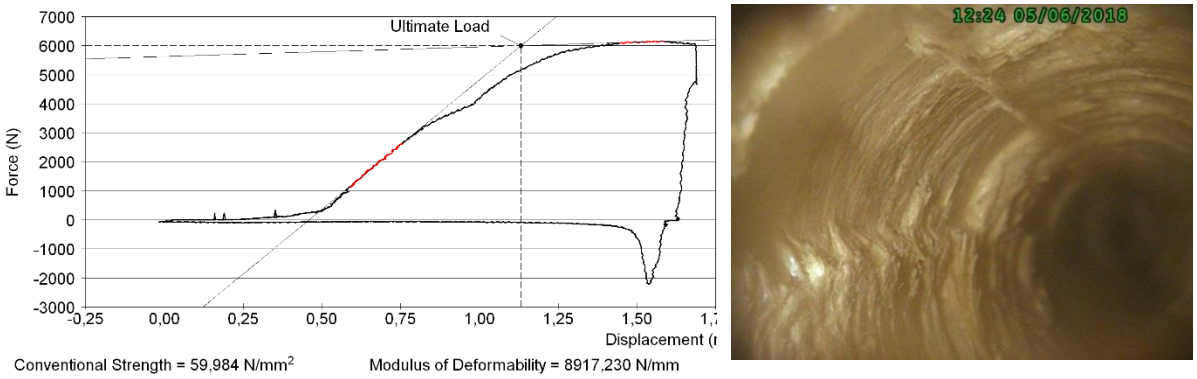

Figure 4.18 – Example of the graph Force-Displacement plotted in SigVis (left) and an endoscopic picture of the test on the internal

Table 4.6 – Data processing of loading jack results for the west wing roof; Conventional compressive strength (CSc) and Modulus of deformability (MOD)

Test No.	Depth No.	CSc (L) [MPa]	Average CSc(L) [Mpa]	MOD (L) [Mpa]	Average MOD(L) [Mpa]
LJ-1	1-1	82.31	67.29	23924.03	16099.02
	1-2	60.14		16362.99	
	1-3	65.16		13712.65	
	1-4	61.53		10396.43	
LJ-2	2-1	60.90	58.42	10508.49	9120.12
	2-2	59.98		8917.23	
	2-3	56.59		10150.96	
	2-4	56.19		6903.81	
LJ-3	3-1	67.87	62.87	16125.31	13127.82
	3-2	59.06		10958.52	
	3-3	61.16		16052.95	
	3-4	63.40		9374.49	
LJ-4	4-1	79.10	68.36	22508.41	16348.06
	4-2	63.75		10908.83	
	4-3	67.31		17179.17	
	4-4	63.29		14795.85	
LJ-5	5-1	73.33	64.89	19898.19	14050.92
	5-2	62.08		14320.81	
	5-3	59.27		10263.63	
	5-4	64.88		11721.06	
LJ-6	6-1	72.76	60.93	16730.32	12982.91
	6-2	59.60		12480.46	
	6-3	55.60		10179.87	
	6-4	55.74		12540.99	

The results of the conventional strengths and the modulus of deformation are shown in the Table 4.6. From the results can be observed that usually the highest values are obtained from the first depth of the test which is from (5-25) mm. As mentioned previously, the density of the mature wood is higher than the juvenile wood and since the compressive strength correlates to the compressive strength the first layers provide higher compressive strengths.

The CS_C and the MOD of the first test which represent the original rafter of Frame 1 show higher values than the newly added column (LJ5) and the original column (LJ2). The mechanical condition of the rafter is in good compared to the above mentioned. Nevertheless, the mechanical property of the added column and the rafter are similar and therefore the mechanical compatibility is roughly achieved. The modulus of deformability of the column of the frame is considerably low. Regardless, the column works mostly in axial forces and the axial deformations are usually lower. Correspondingly, the deformability is measured in the axial direction and will not highly influence the column. In contrast the values from Frame 2 of CS_C and MOD are similar with small variation in-between. Compared to Frame 1 the values are similar overall. The average values are shown in the Figure 4.19.

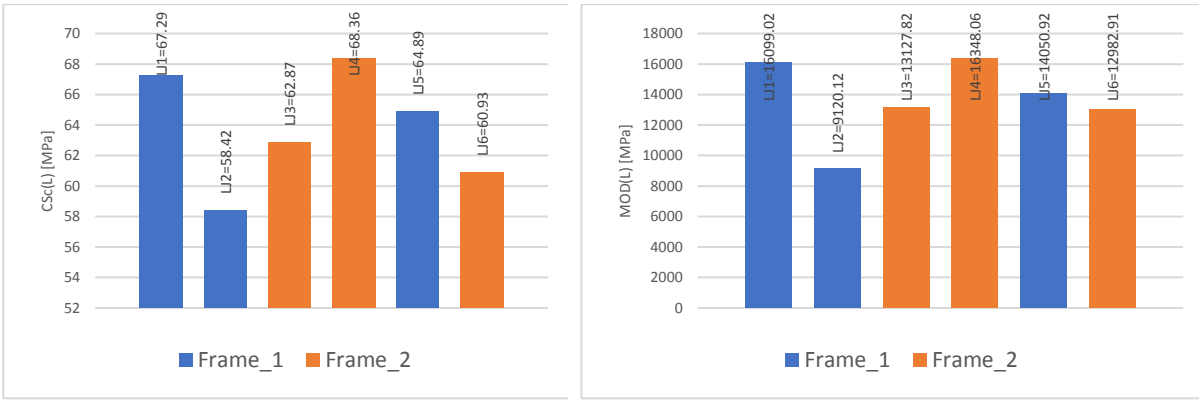

Figure 4.19 – Comparison of results between Frame 1 and Frame 2 for conventional strength (left) and modulus of deformability (right)

The conventional strength and the modulus of deformability can be related to other parameters such as density, compressive strength and modulus of elasticity. After performing some experiments, Kloiber, et al. (2016) have obtained some correlation equations with good results. These equations relate the loading jack results with density, compressive strength and modulus of elasticity, and they will be used to relate the loading jack test performed on the frames. The tests include the comparison of results from the parameters measured with the loading jack and the standard samples parallel to the grain. The measurements have been done for samples at moisture contents of 12, 18 and 24%. Only the equations for 12% will be used since the moisture content of the elements tested does not exceed 12%.

The correlation of conventional strength ($CS_{C\,(L)}$) with the compressive strength ($S_{C\,(L)}$) with a correlation coefficient of R^2=0.8876 is expressed with the equation:

$$S_{C\,(L)} = 0.5661 * CS_{C\,(L)} - 3.3584 \quad (4.3)$$

The correlation of modulus of deformability ($MOD_{(L)}$) with the modulus of elasticity ($MOE_{(L)}$) with a correlation coefficient of R^2=0.6794 is expressed with the equation:

$$MOE_{(L)} = 0.4934 * MOD_{(L)} - 1901.7 \quad (4.4)$$

Lastly the correlation of conventional strength ($CS_{C\,(L)}$) with the density (ρ) with a correlation coefficient of R^2=0.8402 is expressed with the equation:

$$\rho = 5.1214 * CS_{C\,(L)} + 27.265 \quad (4.5)$$

Table 4.7 – Correlation between the conventional strength (CSc) and modulus of deformability (MOD) with compressive strength (Sc), modulus of elasticity (MOE) and density (ρ)

Test No.	Average CSc(L) [Mpa]	Average MOD(L) [Mpa]	Sc(L) [Mpa]	MOE(L) [Mpa]	ρ [kg/m³]
LJ-1	67.29	16099.02	34.73	6041.56	371.86
LJ-2	58.42	9120.12	29.71	2598.17	326.44
LJ-3	62.87	13127.82	32.23	4575.56	349.26
LJ-4	68.36	16348.06	35.34	6164.43	377.38
LJ-5	64.89	14050.92	33.37	5031.02	359.58
LJ-6	60.93	12982.91	31.13	4504.07	339.29

The obtained results can be seen in the Table 4.7. From these results can be seen that the average compressive strength is $S_{C\,(L)}$= 32.75 [Mpa], the average modulus of elasticity is $MOE_{(L)}$= 4819.14 [Mpa] and the average density is ρ= 353.97 [kg/m³]. From the Czech annex ČSN EN-338, the elements can be classified as C20. In the code the values of the compressive strengths are the characteristic values and therefore the average value of $S_{C\,(L)}$= 32.75 [Mpa] correlates to the characteristic value of compressive strength parallel to the grains $f_{c,0,k}$= 19 [Mpa]. The parameters for C20 according to ČSN EN-338 are presented in the Table 4.8.

Table 4.8 – Mechanical parameters for C20 from ČSN EN-338

Mechanical Parameter		C20
Bending	$f_{m,k}$ *[MPa]*	20
Tension parallel to grain	$f_{t,0,k}$ *[MPa]*	12
Tension perpendicular to grain	$f_{t,90,k}$ *[MPa]*	0.5
Compression parallel to grain	$f_{c,0,k}$ *[MPa]*	19
Compression perpendicular to grain	$f_{c,90,k}$ *[MPa]*	2.3
Shear	$f_{v,k}$ *[MPa]*	2.2

Mean value of modulus of elasticity parallel to grain	$E_{o,mean}$ *[GPa]*	9.5
Mean value of density	ρ_{mean} *[kg/m³]*	390

The other location where the loading jack was carried out is the Church of Nativity of Our Lord. The results are presented in the Table 4.9. Again, it can be seen that the mature wood shows higher values in the first depth than in the inner layers.

Table 4.9 - Data processing of loading jack results for the church; Conventional compressive strength (CSc) and Modulus of deformability (MOD)

Test No.	Depth No.	CSc (L) [MPa]	Average CSc(L) [Mpa]	MOD (L) [Mpa]	Average MOD(L) [Mpa]
CLJ-1	1-1	89.23	75.19	22083.11	15286.63
	1-2	79.86		16464.80	
	1-3	72.15		14334.30	
	1-4	59.54		8264.30	
CLJ-2	2-1	65.36	59.33	12510.26	10079.09
	2-2	56.29		7422.50	
	2-3	56.12		10940.92	
	2-4	59.56		9442.67	
CLJ-3	3-1	77.64	76.03	20992.23	16291.21
	3-2	75.35		17571.03	
	3-3	74.10		14335.44	
	3-4	77.02		12266.15	
CLJ-4	4-1	63.34	54.11	11070.02	9064.14
	4-2	58.67		10865.83	
	4-3	58.36		7672.63	
	4-4	36.09		6648.08	
CLJ-5	5-1	68.98	67.18	20133.51	26513.00
	5-2	61.35		14029.22	
	5-3	72.39		63675.03	
	5-4	66.02		8214.24	

CLJ-1, CLJ-2 and CLJ-3 represent the tests performed in the Choir and the average values for it are CS_C=70.2 [MPa] and MOD=13885 [MPa]. On the other hand, CLJ-4 and CLJ-5 represent the tests from the Nave and the average values are CS_C=60.6 [MPa] and MOD=17788 [MPa]. The average values of each test are shown in the Figure 4.20.

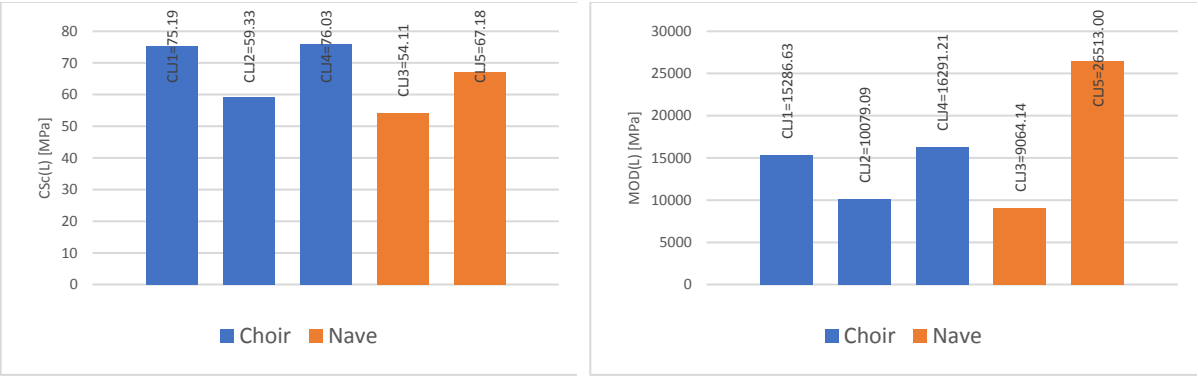

Figure 4.20 – Comparison of results between Choir roof and Nave roof for conventional strength (left) and modulus of deformability (right)

As mentioned before the roof of the nave is older than the choir, but with the felling date not so much different from each other. Nevertheless, the roof of the choir shows a better mechanical state than the roof in the nave. Possibly that also justifies the restoration works being carried out in the roof of the nave.

The average conventional strength from the west roof is CS_C=63.8 [MPa], whereas from the church is CS_C=66.4 [MPa]. In addition, the average modulus of deformability from the west roof is MOD=13621 [MPa], while from church is MOD=15446 [MPa]. Even though, the choir roof and the part of Frame 1 have the same felling date, the conventional compressive strengths show different values. The average CS_C of Frame 1 is CS_C=63.5 [MPa], while the choir CS_C=70.2 [MPa]. Nevertheless, their modulus of deformability are similar.

4.5 Moisture Content

4.5.1 Test Description

Wood is a hygroscopic material. Water exists in timber elements in the form of free water within cell cavities and the water absorbed by the cell walls. The fiber saturation point is reached when the free water in the cell cavities is dried. The fiber saturation point usually occurs at e moisture content of 25 to 30 %. If the moisture content in the timber elements is higher than the fiber saturation, the elements swell and the strength and elasticity are reduced. Furthermore, the durability of wood decreases and the elements are more susceptible to biological decay. On the other hand, if the timber elements are dried and the moisture content is under the fiber saturation point the elements shrink and cause cracking. These cracks beside their mechanical effects are another cause of insect attack and fungal decay. The highest dimension change occurs in the tangential and radial directions, whereas in the longitudinal it is less. The instrument used to measure the moisture content in the timber elements is the Hygrometer. Two instruments have been used where one is the surface moisture meter (Figure 4.21-right), and the other one in the form of a pistol which was used to measure the moisture inside the predrilled holes (Figure 4.21-left).

Figure 4.21 – Internal moisture meter (left) and surface moisture meter (right)

4.5.2 Procedure and Results

To measure the temperature are used the predrilled holes used for the loading jack. The moisture content is measured with the help of the hygrometer which measures the moisture inside the timber as seen in Figure 4.21 (left). Moreover, the moisture is measured in the different levels of depth similar to the depths where the loading jack test is performed. That is why the naming of the moisture levels correspond to the loading jack naming, where the moisture content of test 1 in level 2 (MC2-2) corresponds to the loading jack test LJ2-2. The results of the moisture measures are presented in the Table 4.10 below.

Table 4.10 – Moisture content (MC) for the west wing roof

Test No.	Depth No.	MC [%]	Average MC [%]
MC-1	1-1	12.3	10.2
	1-2	9.8	
	1-3	9.3	
	1-4	9.3	
MC-2	2-1	12.5	10.7
	2-2	10.8	
	2-3	10.6	
	2-4	8.8	
MC-3	3-1	11.2	11.4
	3-2	11.3	
	3-3	11.3	
	3-4	11.9	
MC-4	4-1	11.3	9.5
	4-2	9.0	
	4-3	8.9	
	4-4	8.8	

MC-5	5-1	12.1	8.2
	5-2	7.1	
	5-3	7.1	
	5-4	6.4	
MC-6	6-1	11.5	9.2
	6-2	8.8	
	6-3	8.6	
	6-4	7.8	

The higher values of moisture in the first depth of measurement are due to the contact of the outer layers with change of relative humidity of air. From the measurements it can be concluded that the frame is not susceptible to any decay or any fungus attack since the moisture level is low.

The moisture was also measured on the surface of Frame 1 and 3. To have a clear idea of the moisture content of the frames the measurements are presented on the drawings in Figure 4.22 and Figure 4.23 below.

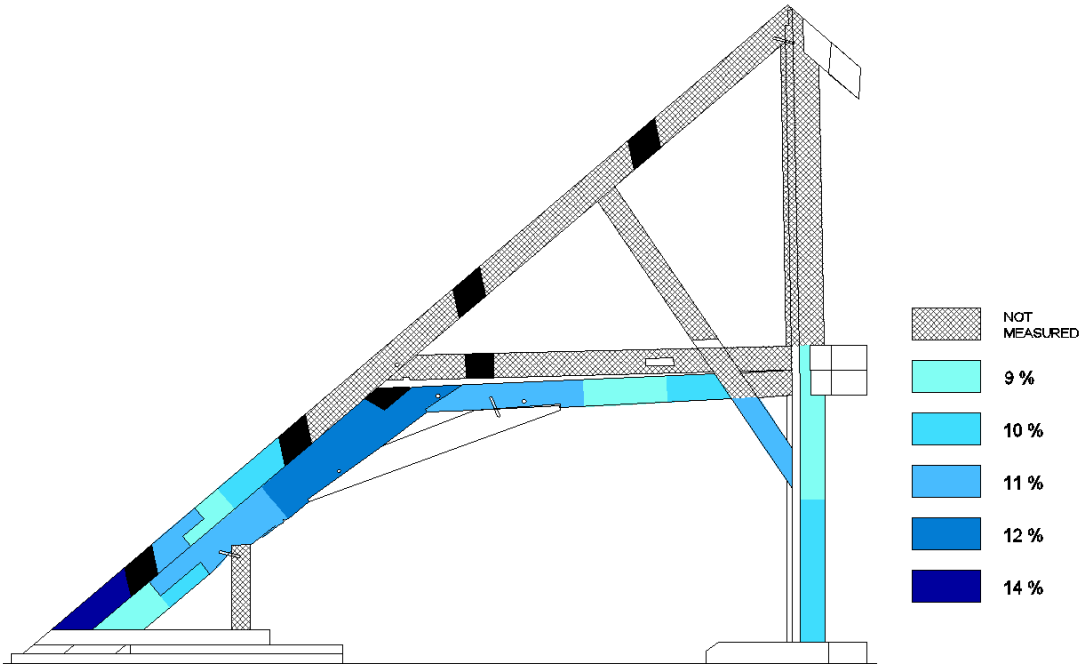

Figure 4.22 – Surface moisture content measurement on Frame 1

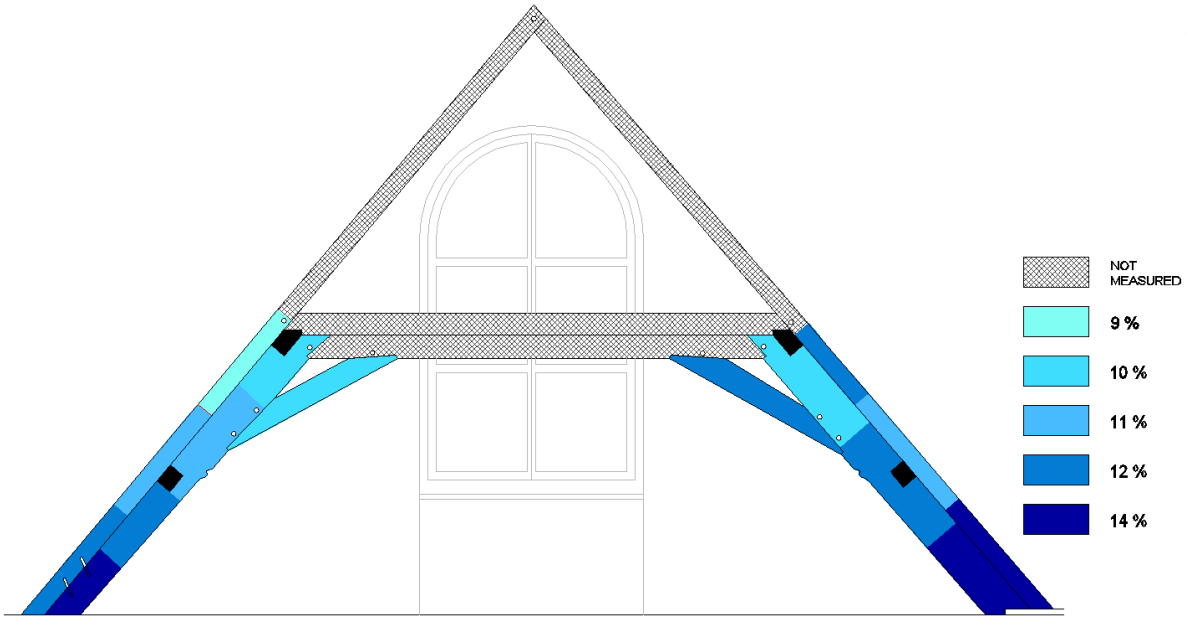

Figure 4.23 - Surface moisture content measurements on Frame 3

Similarly, the levels of moisture are relatively low and do not present any threat of decay to the frames. On the lower end of the rafter in Frame 1 (Figure 4.22), the value is larger than the rest of the frame. The value is naturally higher due to the location of the measurement, which is in the contact of rafter to the wall and in that part of roof is mostly in shadow. As for the Frame 3 (Figure 4.23) it is clear that the right side, which is located in the northern side, shows larger values of moisture. The left side located in the southern side shows lower values of moisture with an increase on the lower ends of the rafter where they contact the wall. Nevertheless, the actual moisture levels do not present any threat to the timber or any signs of decay.

This page is left blank on purpose.

Chapter 5

5. STRUCTURAL ANALYSIS

Buildings like Loreta that are constructed in different phases and have underwent many alterations during its service present many changes in the load path. Therefore, the structure suffers many problems and damages. As previously shown, the frame in the southern part of the West wing has big deformations. A column has been added but due to no technical reports the purpose is not known and not quite understood. In order to analyze the behavior of the frame with the strengthening column a finite element model is to be executed. From the model the stability should also be checked and the safety evaluation must be made.

5.1 Roof Simplification

The loads on the frame of interest are transferred through complex configuration of the roof. The modeling of the entire roof requires a lot of geometrical information and due to the lack of time some simplifications have been done to represent the real structure. To unify the front façade Kilian Dientzenhofer elevated the entire front building to the same height. Therefore, he made the fortification effect vanish by covering the corner chapels. This created some complex variations in the slopes of the roof and the internal timber structure. The current slopes of the roof can be seen in the Figure 5.1 below.

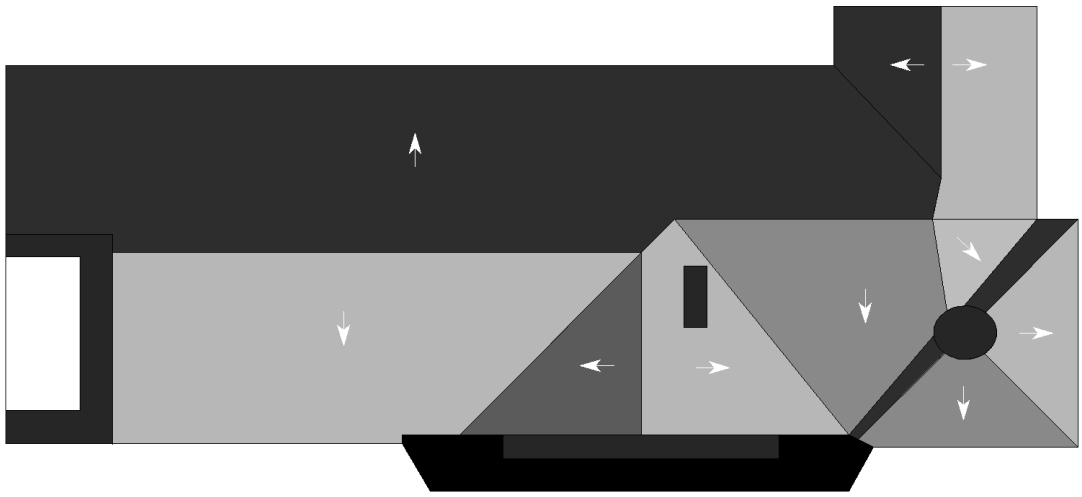

Figure 5.1 – Slopes of the southern part of the west wing roof

The loads on the roof currently are transferred through the roof tiles to the internal members. The pressure values from the wind cannot be analyzed simply because many factors have to be taken into account considering the actual roof configuration. The effect of the tower on the wind direction from North to South and the other way will be neglected. Furthermore, the main window in the façade will be neglected. This will simplify the wind load analysis but also disregard some effects these neglections have on the wind fluctuation. The corner chapel also will be disregarded and the roof will be divided into two different configurations. The entire roof is divided in two gable roofs in the two principal directions as it is shown in Figure 5.2.

Figure 5.2 – Simplification of the roof; East-West direction (left) and South-North (right)

5.2 Loads

5.2.1 Self-weight

The load from the self-weight in the timber roof in this case includes the weight of the timber elements and the weight of the roof tiles. The roof tiles are directly supported on battens which are placed every 32 cm between each other. The battens are supported on the rafters which are placed as can be seen in the drawings from the Appendix A.

The self-weight of the timber elements is generated automatically by the software for analysis. The density of the members used in the software is the one corresponding to the C20 class obtained from the results.

The weight of the roof tiles cannot be generated automatically in the software and therefore is calculated differently. The weight of the roof tiles is taken from a technical paper from the archives of the Loreta, which explains the parameters of the tiles they installed on the roof. The technical paper is presented in the Figure 5.3.

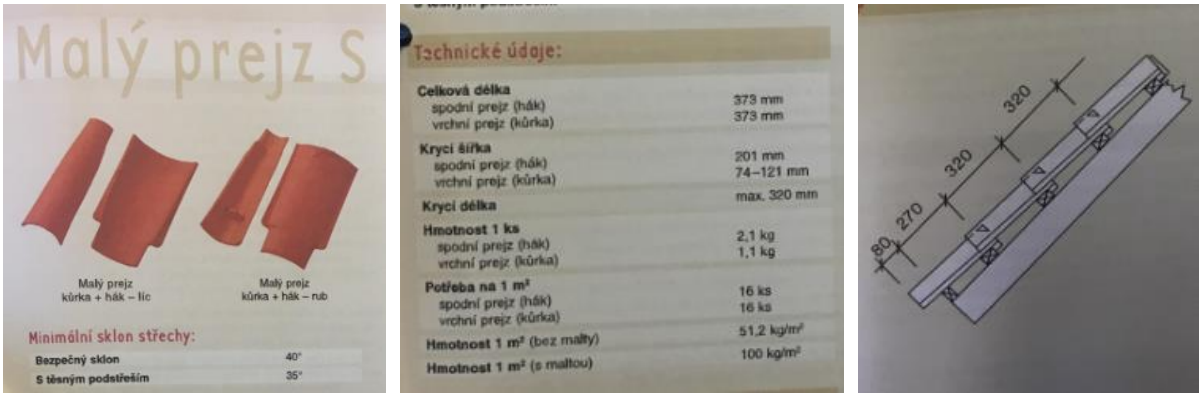

Figure 5.3 – Technical sheet for the roof tiles retrieved from the archives

The weight of the tiles is about 51.2 [kg/m²] and in a m² can be places 6 tiles. To input this load in the software, the weight of the roof tiles is converted into a 2 cm concrete slab. The weight of the 2 cm concrete slab is 0.5 kN/m², which is the equivalent weight of the tiles per square meter.

5.2.2 Live load

The roof of Loreta is not accessible to the public or to special services. It can be accessible only for the normal maintenance and repair. According to the Table 6.9 in EN 1991-1-1:2002, which categorizes the roofs according to their use, this roof is categorized as H.

From the same norms in the Table 6.10 can be obtained the intensity of live load for category H, which is q_k = 0.4 [kN/m²].

5.2.3 Snow load

The load from the snow according to EN 1991-1-3:2003 is calculated using the following equation:

$$s = \mu_i \, C_e \, C_t \, s_k \tag{5.1}$$

where:

μ_i	the snow load shape coefficient
C_e	exposure coefficient
C_t	thermal coefficient
s_k	characteristic value of snow on the ground

The characteristic value of snow on the ground is obtained from ČSN EN 1991-1-3:2005/Z1:2006 according to the snow map shown in Figure 5.4. From the snow map the value of the snow load on the ground is sk = 0.7 [kN/m²].

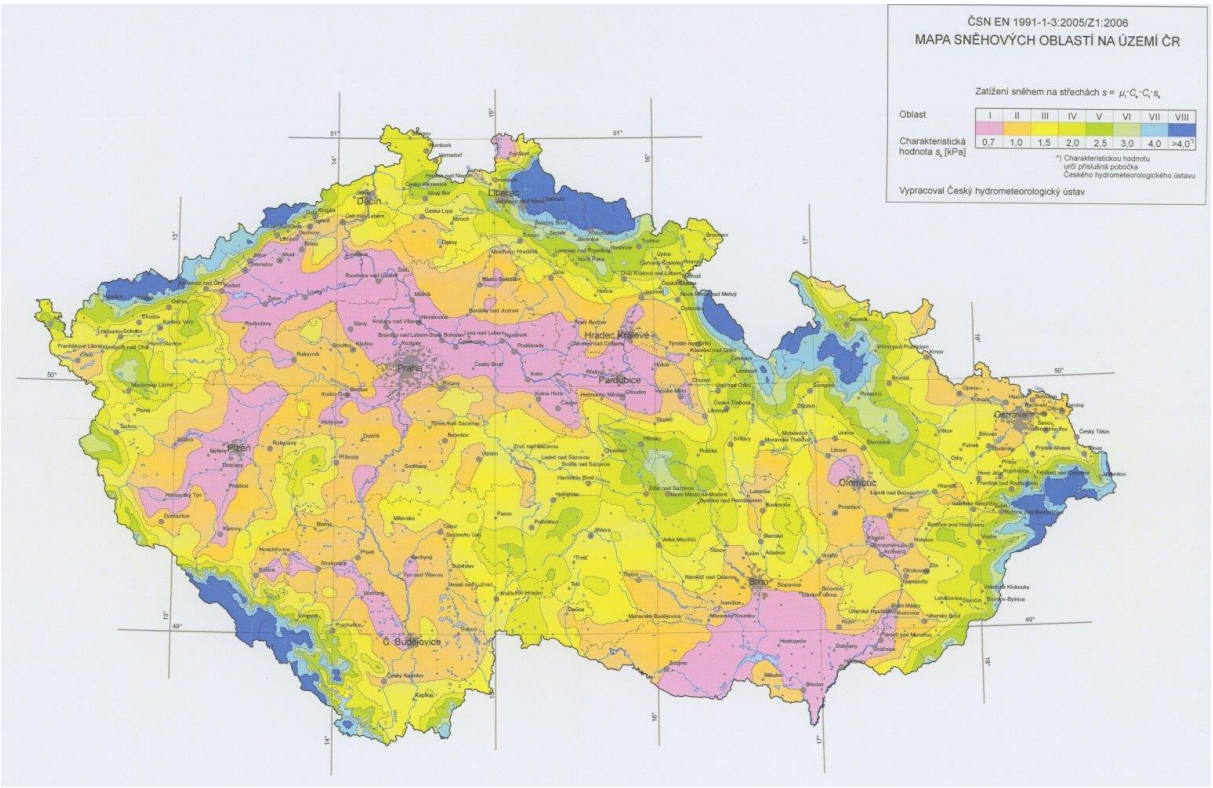

Figure 5.4 – Map of characteristic values of the snow load on the ground for the Czech Republic (ČSN EN 1991-1-3:2005/Z1:2006)

The snow load also is dependent on the slope of the roof. From EN 1991-1-3:2003 in Table 5.2 the shape coefficient for the shape of the roof is given according to the angle of the roof. In the case of the analyzed roofs the angle is around 50° and the shape coefficient is computed as $\mu_i = 0.27$. The thermal coefficient and the exposure coefficient are taken as 1.0. With these parameters the snow load on roof is calculated as s = 0.187 [kN/m²] but for the analyses will be used as 0.2 [kN/m²].

5.2.4 Wind load

In the case of the complex geometry for the wind analyses is used the simplified roof. The load is calculated for the two principal wind directions, South-North (SN) and East-West (EW).

Initially the basic wind velocity has to be computed which is given by EN 1991-1-4:2005 by this equation:

$$v_b = c_{dir}\, c_{season}\, v_{b,0} \tag{5.2}$$

where:

c_{dir} the directional factor

c_{season} the season factor

$v_{b,0}$ the fundamental value of wind velocity

Both the season and the directional factor for the Czech Republic have a value of 1.0. The fundamental value of wind velocity is read from the wind velocity map of the Czech Republic. As can be seen in the Figure 5.5, Prague is in the first category and the velocity is $v_{b,0}$ = 22.5 [m/s].

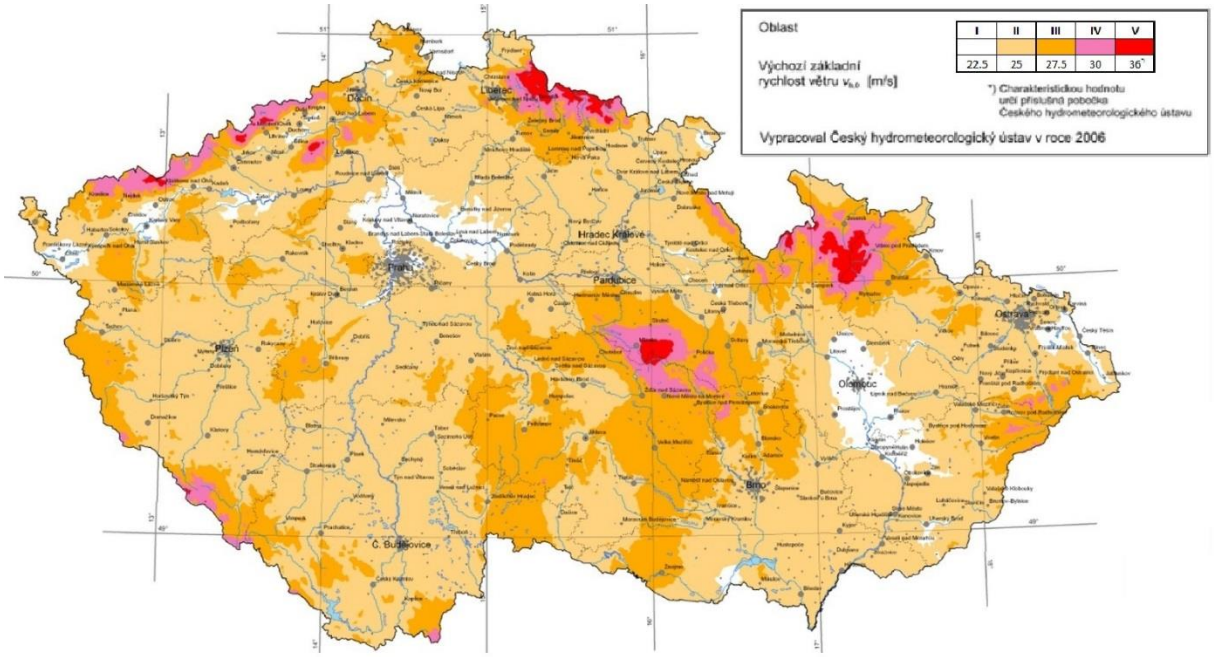

Figure 5.5 – Map of the fundamental wind velocity for the Czech Republic (ČSN EN 1991-1-4:2007)

Therefore, from the equation the basic wind velocity basically equals the fundamental wind velocity and v_b = 22.5 [m/s]. With the basic velocity is computed the mean wind velocity ($v_{m(z)}$) which depends on the terrain roughness and the orography. The mean wind velocity is given by EN 1991-1-4:2005 with the equation:

$$v_{m(z)} = c_{r(z)}\, c_{o(z)}\, v_b \tag{5.3}$$

where:

$c_{r(z)}$ the roughness factor

$c_{o(z)}$ the orography factor

In the case of hills and cliffs the orography coefficient varies, whereas in other cases this factor is taken as c_0 = 1.0. The roughness factor for a height of z = 15m is calculated with the given equation:

$$c_{r(z)} = k_r \ln\left(\frac{z}{z_0}\right) \tag{5.4}$$

where:

k_r terrain factor

z_0 roughness length

z height above ground

From Table 4.1 in EN 1991-1-4:2005 the building is classified in the fourth category where z_0 = 1 m and the z_{min} = 10 m. The terrain factor is computed from equation (4.5) in EN 1991-1-4:2005 and the value is k_r = 0.234. With these parameters the value of roughness factor is $c_{r(z)}$ = 0.634. Finally, the mean velocity comes to be $v_{m(z)}$ = 14.28 [m/s].

The following parameter to be computed is the peak velocity pressure of wind which is given by the equation:

$$q_{p(z)} = \left[1 + 7\, I_{v(z)}\right] \frac{1}{2}\, \rho\, V_{m(z)}^2 \tag{5.5}$$

where:

ρ the air density (1.25 [kg/m³])

$I_{v(z)}$ the turbulence intensity

The turbulence intensity for z = 15m is given by the equation:

$$I_{v(z)} = \frac{k_I}{c_{0(z)}\, \ln(z/z_0)} \tag{5.6}$$

where:

k_I the turbulence factor which can be taken as 1.0 as recommended

With these parameters the turbulence intensity is $I_{v(z)}$ = 0.37. The peak velocity pressure with the values obtained comes to be $q_{p(z)}$ = 456.8 [N/m²].

Lastly, the wind pressure on the surfaces of the roof is calculated with the equation:

$$w_e = q_{p(z)}\, c_{pe} \tag{5.7}$$

where:

c_{pe} pressure coefficient for the external pressure

The pressure coefficients are given in the code for different shapes of the roof. Since the simplified roof shape consists of two duo pitch roofs, the pressure coefficients are taken from the Table 7.4a (wind direction Θ = 0°) and from Table 7.4b (wind direction Θ = 90°) from EN 1991-1-4:2005. The code divides the roof in different zones and different coefficients are used for each zone correspondingly. However, since the roof surfaces are small some modifications are made to obtain one single value for pressure coefficient on the roof.

For each direction of the wind the roofs are divided into zones. For each zone is given a pressure coefficient. To see whether the differential coefficients affect the overall one, an equivalent pressure coefficient is taken according to the percentage of area each zone takes. The equivalent pressure coefficient is taken as:

$$c_{pe,eq} = \frac{\sum A_{\%,i}\, c_{pe,i}}{100} \tag{5.8}$$

where:

A%,i the percentage of each zonation area

cpe,i the pressure coefficient of each zone

From these assumptions the equivalent pressure coefficients are obtained for each side of the roof as a single value. The division of the areas and the values obtained for the roof facing West and East are shown in the following Figure 5.6.

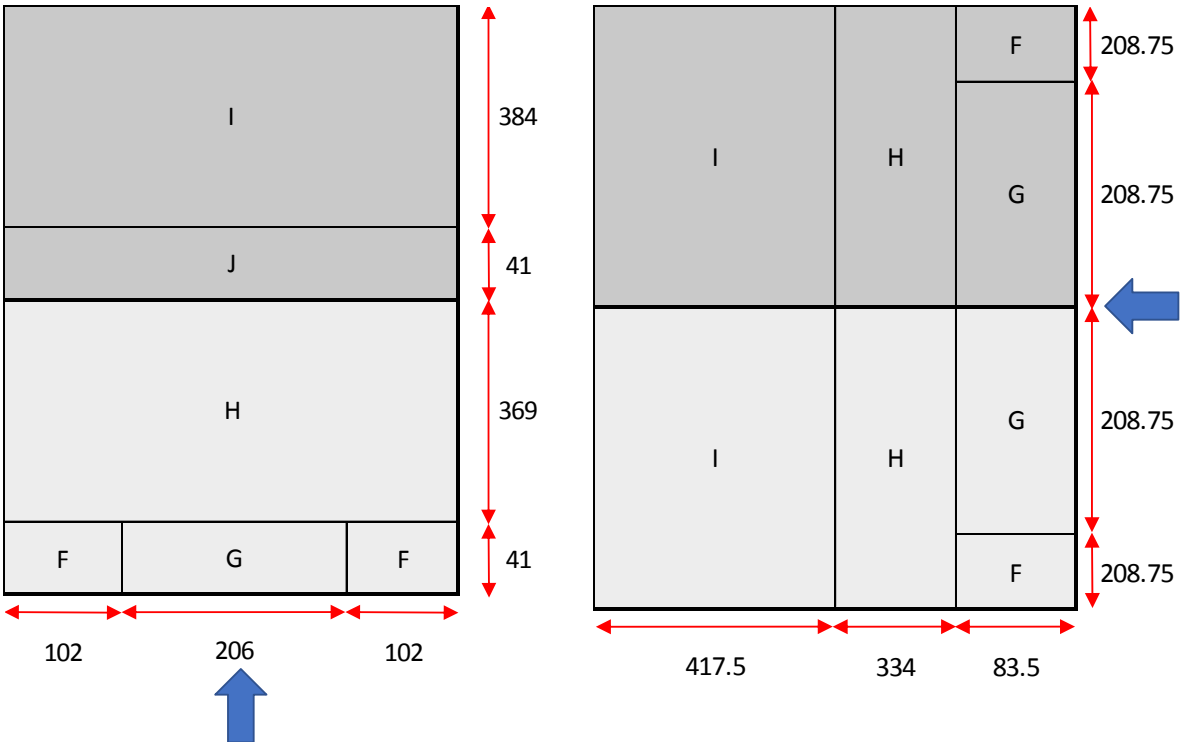

Zone	A%,i	Cpe,i	Cpe,eq
F	4.97561	0.7	0.6397
G	5.02439	0.7	
H	90	0.633	
I	90.35294	-0.066	-0.06928
J	9.647059	-0.1	

Zone	A%,i	Cpe,i	Cpe,eq
F	5	-1.1	-0.7179
G	5	-1.33	
H	40	-0.866	
I	50	-0.5	

Figure 5.6 – Zonation of the West-East roof (up) and the equivalent pressure coefficients (bottom); wind direction Θ=0° (left) and wind direction Θ=90° (right)

For the roof facing South and North, the equivalent pressure coefficients are shown in the Figure 5.7.

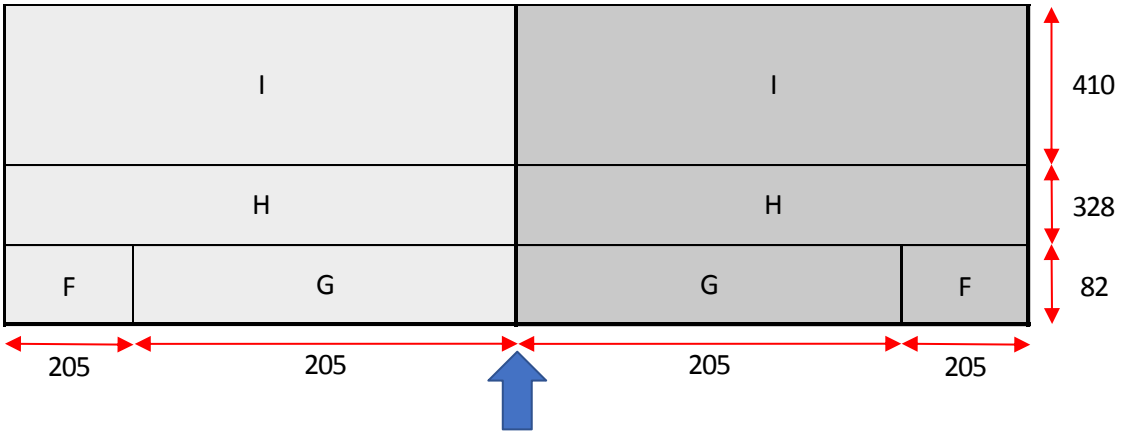

Zone	A%,i	Cpe,i	Cpe,eq
F	5	-1.1	-0.7179
G	5	-1.33	
H	40	-0.866	
I	50	-0.5	

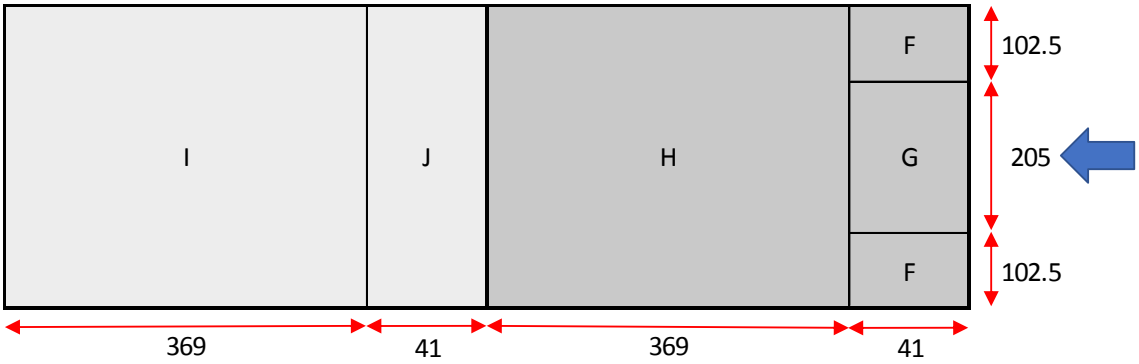

Zone	A%,i	Cpe,i	Cpe,eq
F	5	0.7	0.6397
G	5	0.7	
H	90	0.633	
I	90	-0.066	-0.0694
J	10	-0.1	

Figure 5.7 - Zonation of the South-North roof and the equivalent pressure coefficients; wind direction Θ=0° (top) and wind direction Θ=90° (bottom)

It can be seen how the values do not variate so much from their respective pressure coefficient. To obtain the wind loads these coefficients are multiplied with the peak velocity pressure. The values obtained can be seen in the Table 5.1 below.

Table 5.1 – Wind loads (w_e) for the both wind directions

Wind direction	**Θ = 0°**		**Θ = 90°**	
Roof face	downwind	upwind	left	right
w_e [kN/m²]	0.0	0.3	-0.35	-0.35

5.2.5 Load Combinations

The load combinations were done according to EN 1990:2002 for the ultimate limit states. The fundamental combination in the code is given as:

$$\sum_{j\geq 1} \gamma_{G,j}\, G_{k,j}\, " + " \, \gamma_{Q,1}\;\, Q_{k,1} " + " \sum_{i>1} \gamma_{Q,i}\, \psi_{0,i}\, Q_{k,i} \tag{5.9}$$

For the values of ψ are used the values given in the Table A1.1 in the code. According to the code, the load from the Category H for roofs is not combined with the other live loads. The design values for the loads are taken from the Table A1.2 from the code and the safety coefficients are shown in the Table 5.2.

Table 5.2 – Partial safety coefficients from EN 1990:2002

Permanent Actions (G)		Variable Actions (Q)	
Unfavorable ($\gamma_{G,sup}$)	Favorable ($\gamma_{G,inf}$)	Unfavorable ($\gamma_{Q,sup}$)	Favorable ($\gamma_{Q,inf}$)
1.35	1.00	1.50	0.00

5.3 FEM Model

5.3.1 3D Model

The load path on the frame which will be analyzed (Frame 1) is challenging and not straightforward. In order to obtain the loads on the frame from all the loads and the load combinations a 3D model is generated. Firstly, the load path and the effective members transferring loads on the frame are identified, in order to achieve a realistic 3D model without many complications. The 3D model is simplified into a model which captivates all the possible loads transferred to the frame. To achieve this model from the eastern side of the roof is taken only the side which contributes to the frame as a wind load in the asymmetrical loading. The western side of the roof is taken as a duo pitch roof, again for the asymmetrical loading. The area which is considered for the modelling is highlighted in the Figure 5.8

(a). The 3D modelling is executed using the finite element software SCIA Engineer and the model is shown in Figure 5.8 (b), (c), (d) and (e).

a)

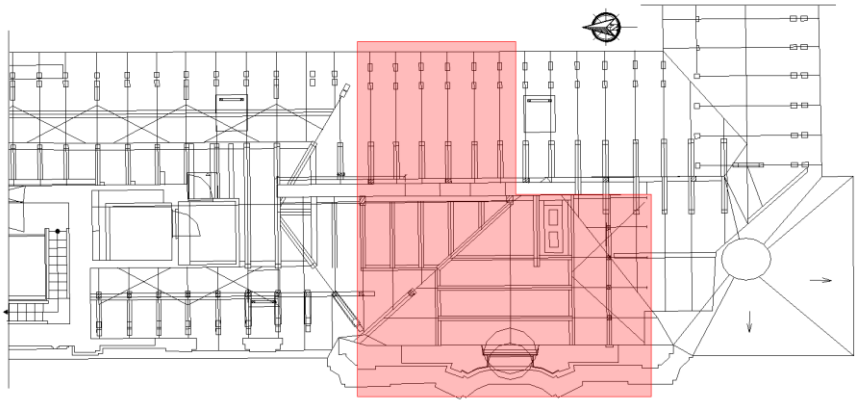

b)

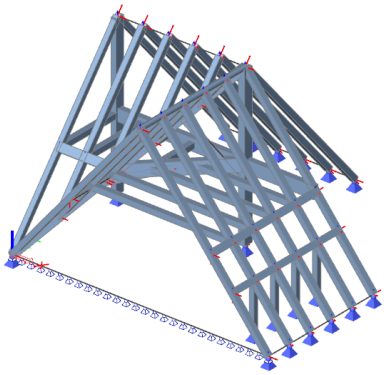

c)

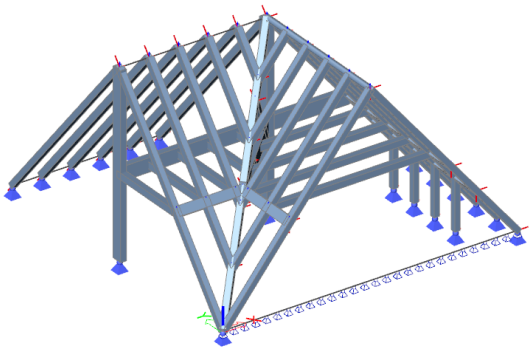

d)

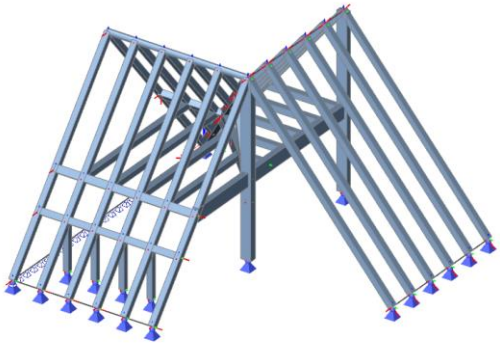

e)

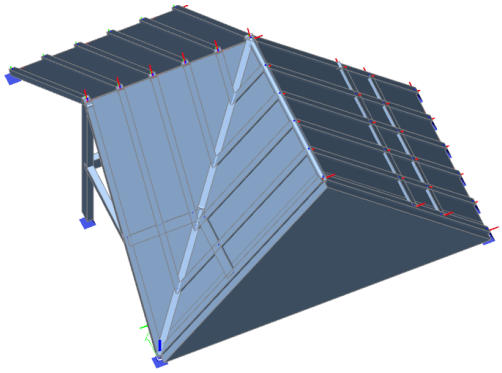

Figure 5.8 – a) Highlighted area of the model; b) timber frames (south-west view); c) timber frames (north-west view); d) timber frames (south-east view); e) roof covering (north-west view)

As described previously, the self-weight is taken into account by the software and the load from the roof tiles is considered by a concrete slab as the equivalent load. The self-weight, live load and the snow

load act perpendicular to the global z-axis. In contrast, the wind acts perpendicular to the surface of the roof in the local axis of the roof. The loading conditions are presented in the Figure 5.9 below.

a)

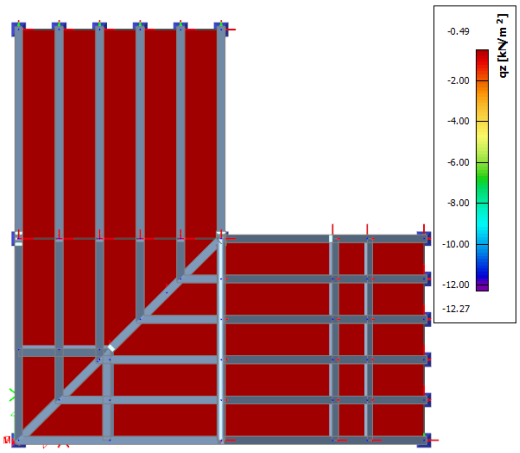

b)

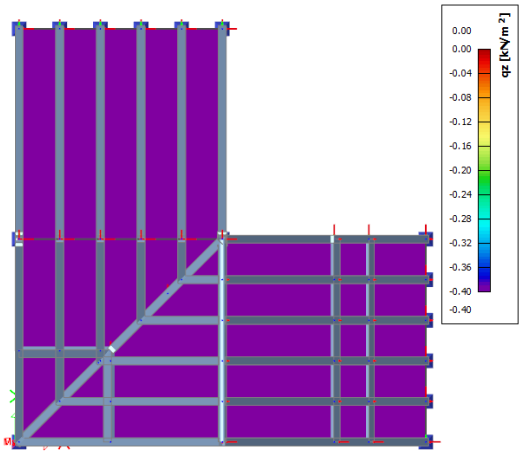

c)

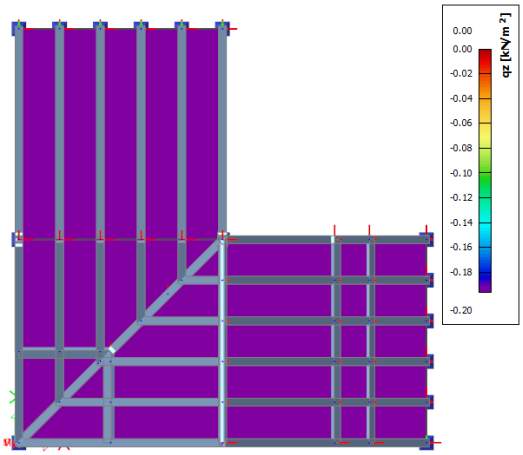

d)

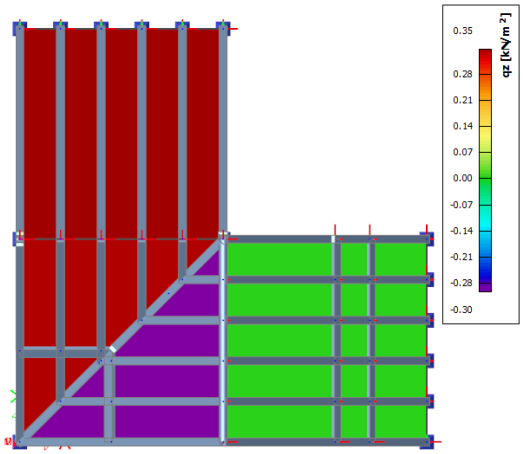

e)

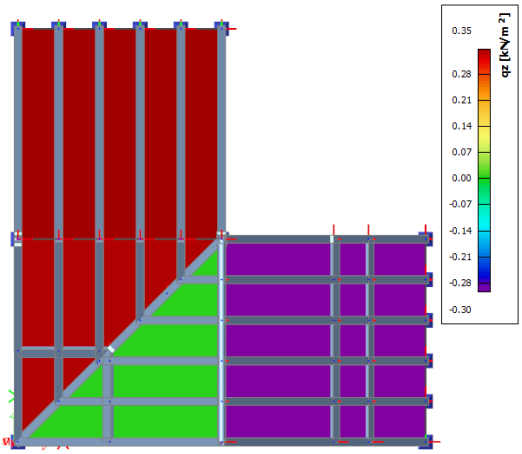

f)

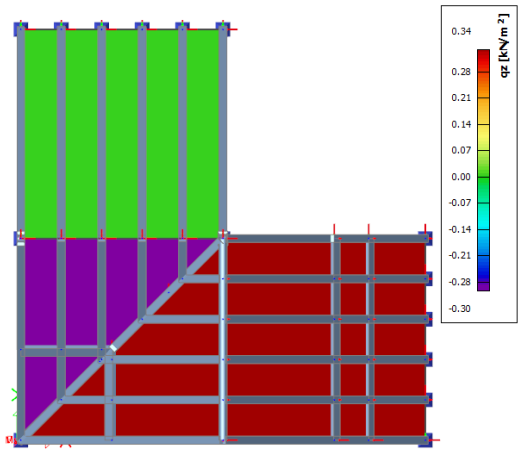

g)

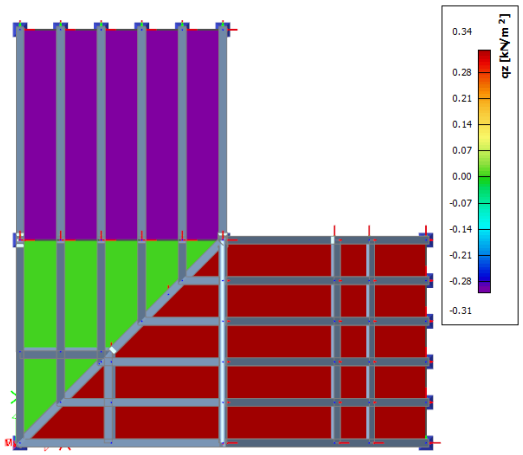

Figure 5.9 – Loading conditions; a) dead load (G); b) live load (Q); c) snow load (S); d) north to south wind load (WX+); e) south to north (WX-); f) west to east (WY+); g) east to west (WY-);

From the 3D model all the loads affecting the frame of interest are noted and will be used to load the frame in the 2D model.

5.3.2 2D Model

The 2D model is more detailed in terms of modelling and analysis. Radimpex Tower 6 software has been used to model the frame. This software has an option of constraining a member to work only in compression or tension. This option will be helpful in understanding the behavior of some of the members and also to model the contact between two rafters, which will be discussed in the next paragraph. The loads from the 3D model are taken as concentric loads on certain nodes, noted in the Figure 5.10 below, and as distributed loads.

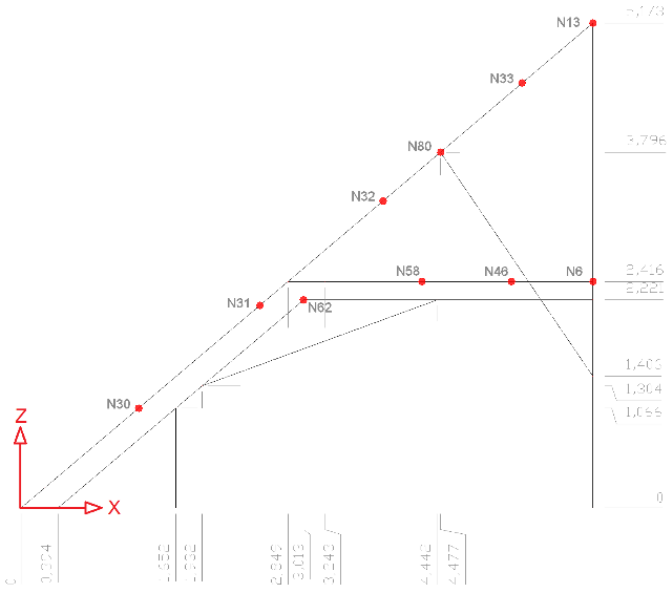

Figure 5.10 – Nodes of Frame 1

The loads are divided into dead loads and the positive and negative loads from the envelope obtinained in the 3D model. In the spatial configuration the loads are read from the local axis of each element. Afterwards to input them in a plane configuration the loads are converted into a global system by summing them as vectors. The resultant concentric loads are presented in Table 5.3.

Table 5.3 – Load values in the plane configuration for the Frame 1

Node	Global Axis	Dead Load [kN]	Envelope	
			P [kN]	N [kN]
N30	X	1.5	2.9	0.7
	Z	1.6	3.1	1.2
N31	X	2.2	4.2	1.0
	Z	1.0	2.0	0.7
N62	X	-0.7	0.7	-2.5
	Z	1.2	2.3	0.7
N32	X	1.3	2.9	0.4
	Z	1.0	2.0	0.5
N80	X	0.1	0.2	0.0
	Z	0.2	0.3	0.1
N33	X	-0.1	0.5	-0.4
	Z	1.1	2.3	0.8
N13	X	-2.6	1.3	-7.0
	Z	6.9	14.2	5.1
N58	X	1.4	2.9	0.3
	Z	0.4	0.5	0.3
N46	X	1.1	2.6	0.0
	Z	0.4	0.5	0.3
N6	X	0.6	1.6	-0.3
	Z	1.6	2.1	1.5

As can be seen in the drawings of the deformed frame (Appendix A), the principal rafter and the truncated rafter are in contact with each other. In the finite element software, the contact modeling is a complex task and requires a more powerful software. In order to take the contact into account, a simplification model is done. The simplification is made possible through the option the software contains to restrict a member to work only in compression. Therefore, the two rafters are connected between each other with rigid links which are restricted to work only under compression. With this restriction the rafters can transfer normal forces to the other but not receive tension. The rigid connections are with dimensions of 10 x 10 cm and an infinite rigidity in order to not deform in the axial direction. They are hinged on both ends and are weightless so that there is no additional dead load. This modelling simplifies the transferring of deformation from a rafter to the other. Nevertheless, the friction between the rafters presents another problem for this type of modelling. Friction from the upper rafter to the lower one is transferred as an axial load. To consider this effect, the axial force in the rigid links can be transferred

as a normal stress. The normal stress through the friction coefficient of timber to timber elements can be converted into shear stress and after into axial load (Figure 5.11).

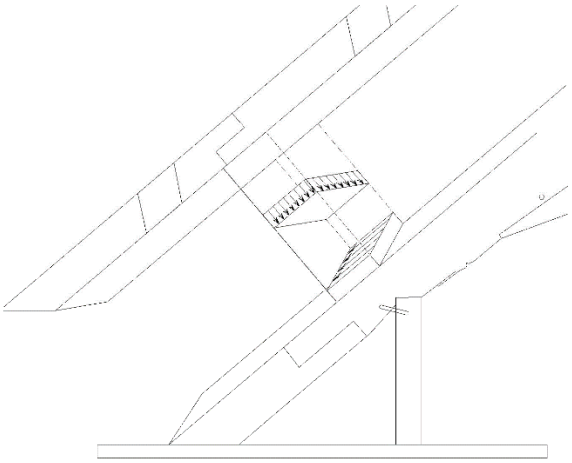

Figure 5.11 – The contact stress distribution; deformations transferred as normal stress and friction transferred as shear stress

To obtain the load factor which converts the load from the upper rafter to the lower one as an axial load, a simulation with the rigid links has be conducted. Different loads are applied on the upper beam and the axial forces in the links are noted. The normal stress from these loads is converted into a shear stress with the help of the timber-timber friction coefficient. This coefficient of friction for timber elements with specific gravity of 0.38, have a coefficient of friction of $\mu = 0.27$ (Hirai et al.). From different loads the difference in the axial load is linear and the converting coefficient therefore can be easily obtained. As can be seen in the Table 5.4, which includes the loads for the simulation, the conversion factor from the load in the upper rafter (Rafter_UP) to the lower one (Rafter_DO) is 0.262.

Table 5.4 – Conversion factor for the axial loads on the lower rafter (Rafter_DO) from the upper one (Rafter_UP)

Load on Rafter_UP	Axial Force	Normal Stress	Shear Stress	Load on Rafter_DO	Percentage
[kN/m]	[kN]	[kPa]	[kPa]	[kN/m]	[%]
5.00	1.31	131.00	35.37	1.31	0.262
10.00	2.62	262.00	70.74	2.62	0.262
15.00	3.93	393.00	106.11	3.93	0.262

With this factor all the linearly distributed loads from the upper rafter are considered in the lower one as loads.

In order to proceed with the model some assumptions are made about three scenarios and three models are executed correspondingly. The first assumption corresponds to the original state before the concrete slab and the strengthening was installed. In these type of trusses, typically there is a tie beam at the bottom which takes the horizontal thrust. To model this beam, the support on the software is given axial

stiffness in the direction of the beam. Assuming that the beam has a cross-section of (30x30) cm, the axial stiffness is calculated to be 150000 [kN/m]. The model can be seen in the Figure 5.12 (a). In the second scenario is assumed that during the process of strengthening the tie beam was removed or at least its effect on the truss. The model in Figure 5.12 (b) represents this scenario where the support on the truncated rafter has no reaction on the horizontal direction. The support on the main rafter is assumed to have two reactions in the vertical and horizontal due to the external wall. The third scenario, shown in Figure 5.12 (c), represents the current state with the column placed as a strengthening manner. The lower horizontal tie beam is displaced vertically for 5 cm to represent the actual state.

a)

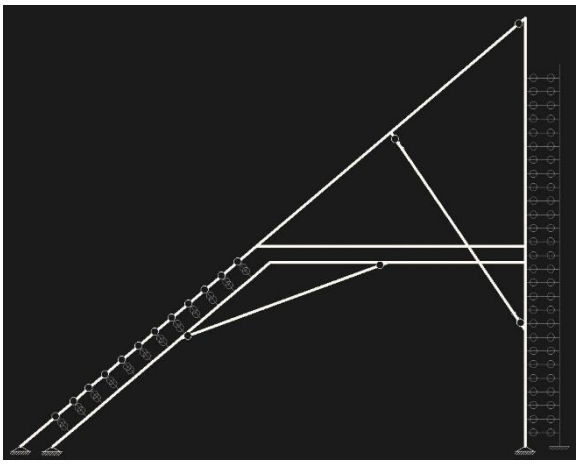

b)

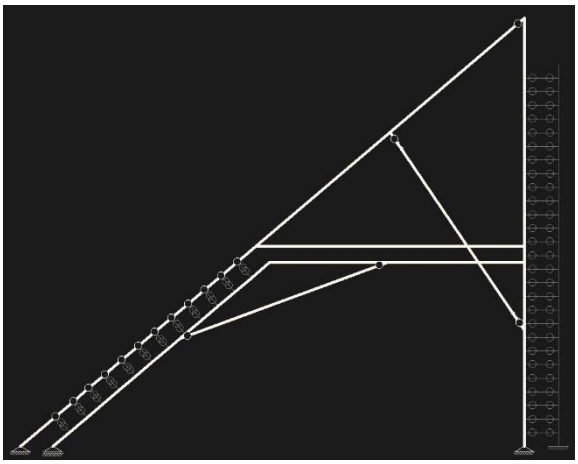

c)

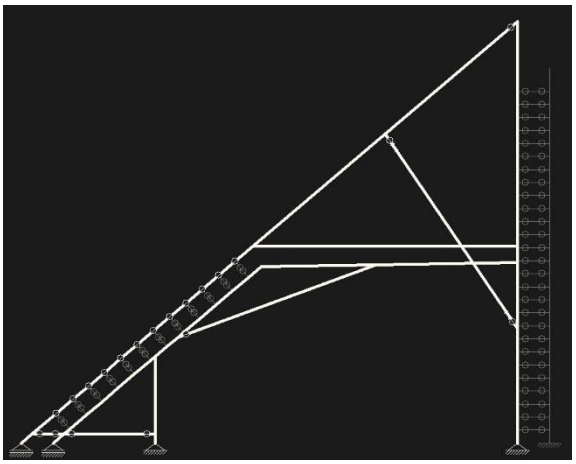

Figure 5.12 – Modelling of Frame 1; a) first scenario with the tie beam; b) second scenario without the tie beam; c) third scenario representing the actual state;

As can be seen from the illustrations above, between the main rafter and the truncated rafter are set the weightless rigid links which work only under compression. Similarly, on the right side are set the same rigid links connected to a member with rigid stiffness, which represents the attic wall. The diagonal strut is set to work only under compression for the first and second model (Figure 5.12-a and -b). In the third

model the diagonal strut works under tension and compression and has a rotational stiffness. The rotational stiffness has been added because of the metallic strengthening element in the strut.

5.3.3 Results

The local axis are also presented in the results in order to have a clear understanding of the results in terms of direction and value. The diagonal strut, due to the configuration of the frame, should work under compression because of the carpentry joint type. That is why in the assumed first scenario, the diagonal strut is set to work only under compression. From the diagram of normal forces (Figure 5.13-left) it can be seen that from all the loading combinations, the diagonal exhibits only compression. This confirms the structural behavior of the frame.

a)

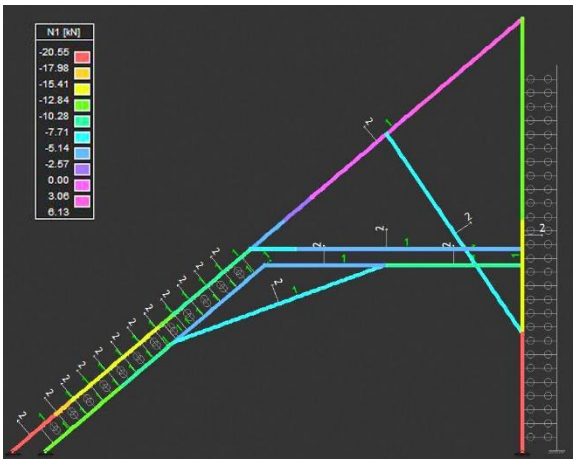

b)

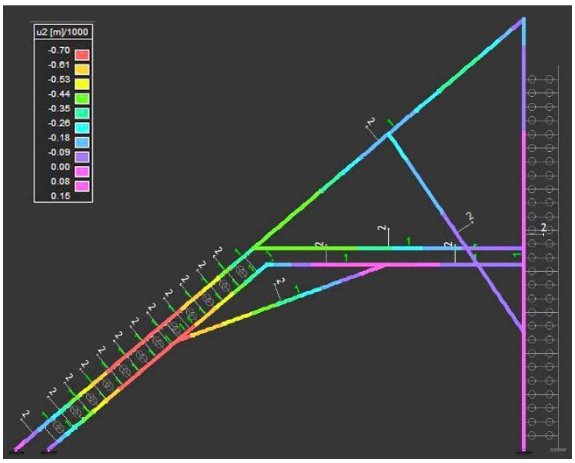

c)

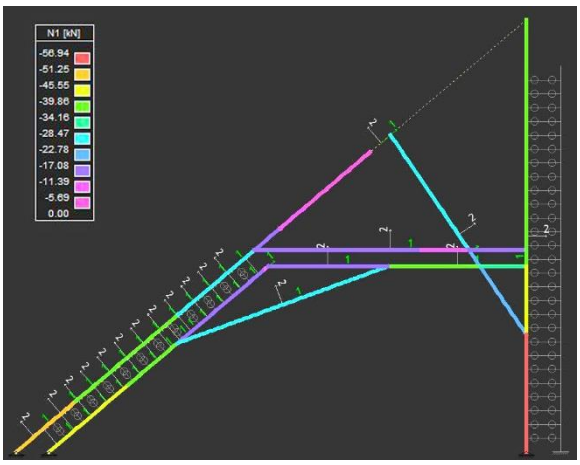

d)

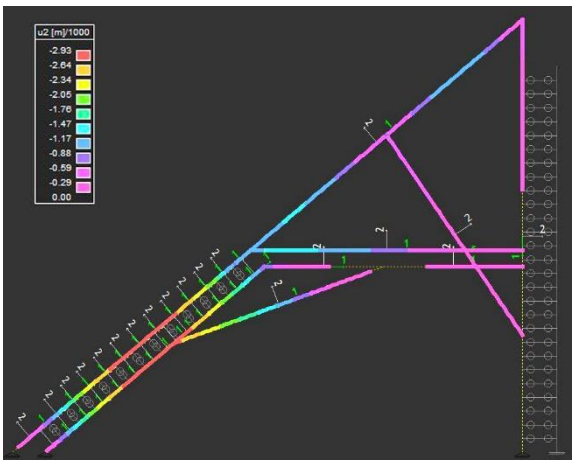

e)

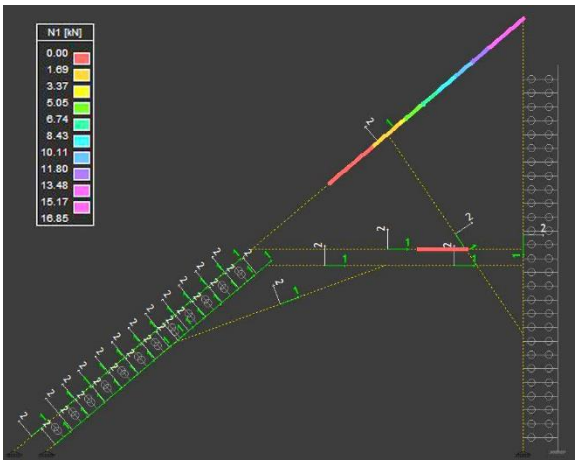

f)

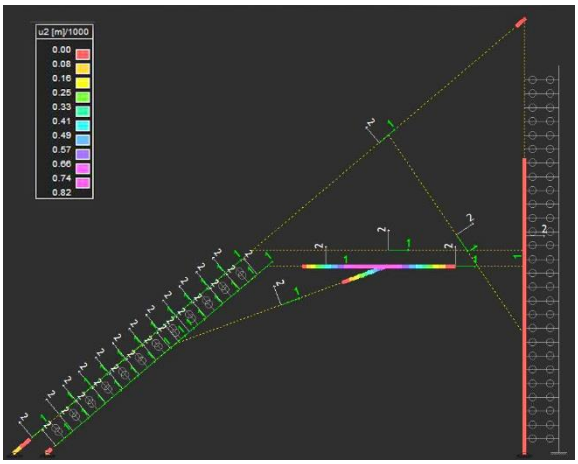

Figure 5.13 – First scenario results; a) dead load axial forces (N_G); b) dead load local axis deflections ($U_{2,G}$); c) envelope of compression axial forces (N_{ENV-}); d) envelope of local axis negative deflections ($U_{2,ENV-}$); e) envelope of tension axial forces (N_{ENV+}); f) envelope of local axis positive deflections ($U_{2,ENV+}$);

Since the loading conditions on the period before and after strengthening are not exactly known the results can be evaluated as relative values. Nevertheless, the results from the dead load present consistent results for all the scenarios. The envelope of the results with the all contributing loads is also shown for comparative values. The deflections range from almost zero for the dead load to about 3 mm for the envelope. The biggest deflection is seen in the middle part of the truncated rafter, which comes from the transmission of the deflection from the main rafter.

The second scenario results are presented in the Figure 5.14 below. With the sliding of the truncated rafter on the bottom part, the diagonal strut starts to work under tension. This behavior can be explained as a common rafter roof with a collar tie. The rafter of this hypothetic truss are the truncated rafter and the lower horizontal beam, whereas the diagonal strut works as a collar tie under tension. This can be seen also from the results where the diagonal does not take tension.

a)

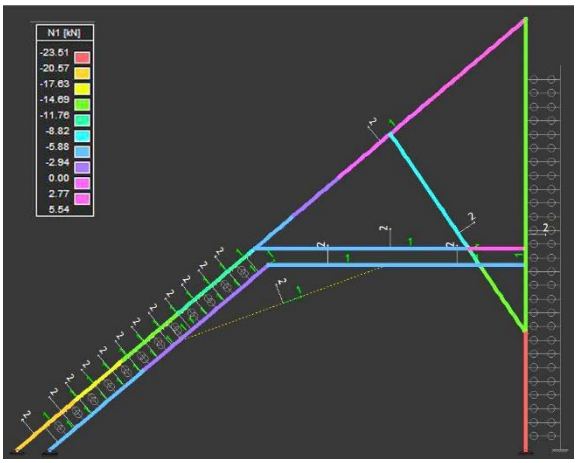

b)

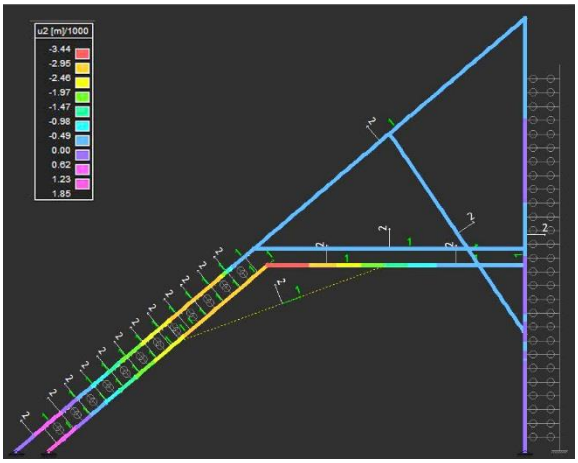

c)

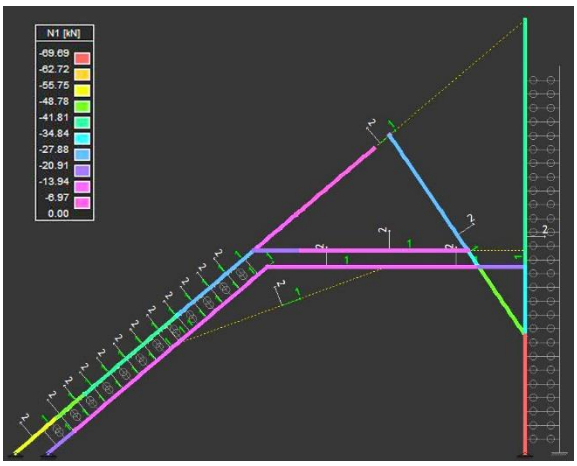

d)

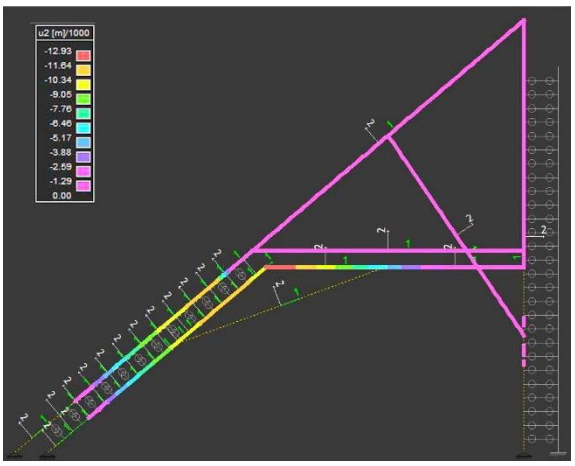

e)

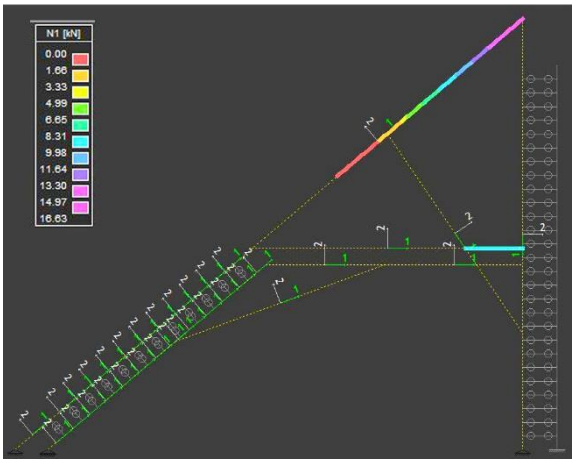

f)

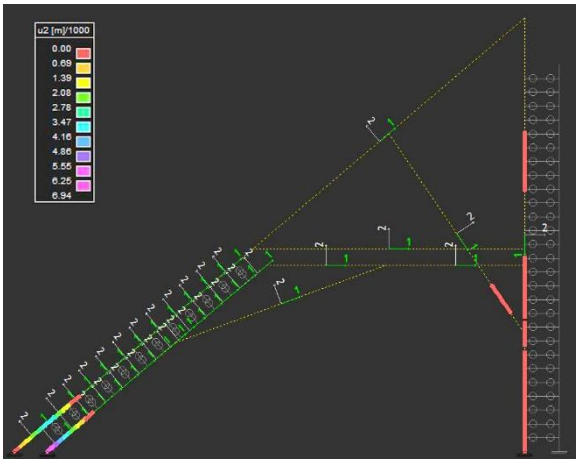

Figure 5.14 - Second scenario results; a) dead load axial forces (N_G); b) dead load local axis deflections ($U_{2,G}$); c) envelope of compression axial forces (N_{ENV-}); d) envelope of local axis negative deflections ($U_{2,ENV-}$); e) envelope of tension axial forces (N_{ENV+}); f) envelope of local axis positive deflections ($U_{2,ENV+}$);

In the Figure 5.14 (b) the deflections from the dead load are excessively higher. The left end of the lower horizontal beam, which suffers from the deformation in the actual state, shows the highest deflection. This can be seen both from the dead load and the envelope, where the deflections for both load cases are around fifteen times higher than in the first scenario. This proves one of the hypothesis of the current deformation seen on site.

For the last scenario which represents the actual deformed shape the results are shown in Figure 5.15. The diagonal strut in this model was set to work in tension and in compression and from the axial forces, both the dead load and the envelope (Figure 5.15-e and -i), the strut works under tension. The assumption explained previously, where the strut works as a collar tie, still stands for the actual state.

a)

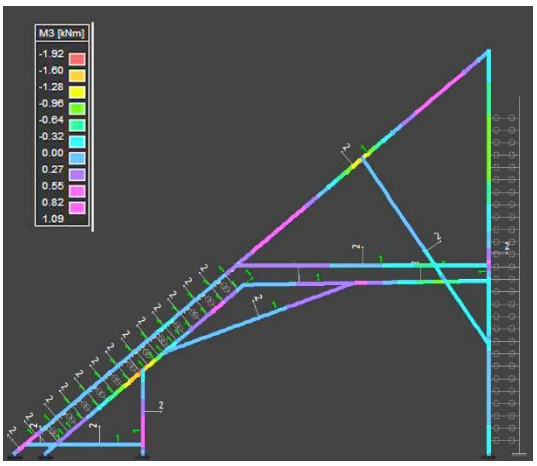
M3 [kNm]
-1.92
-1.60
-1.28
-0.96
-0.64
-0.32
0.00
0.27
0.55
0.82
1.09

b)

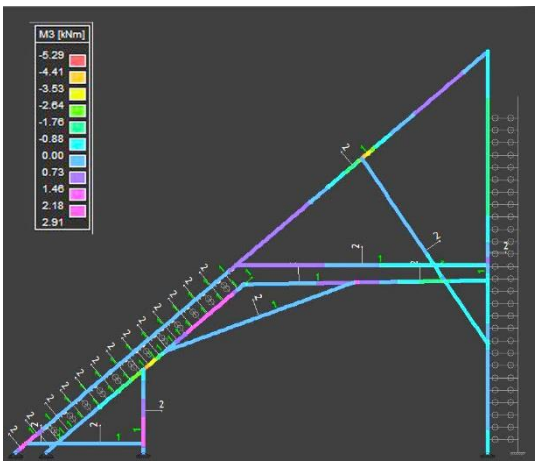
M3 [kNm]
-5.29
-4.41
-3.53
-2.64
-1.76
-0.88
0.00
0.73
1.46
2.18
2.91

c)

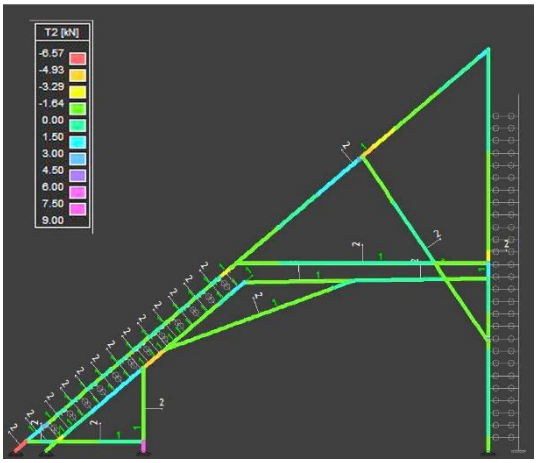
T2 [kN]
-6.57
-4.93
-3.29
-1.64
0.00
1.50
3.00
4.50
6.00
7.50
9.00

d)

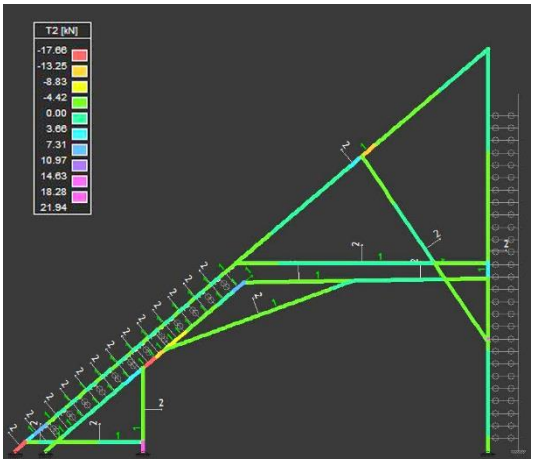
T2 [kN]
-17.66
-13.25
-8.83
-4.42
0.00
3.66
7.31
10.97
14.63
18.28
21.94

e)

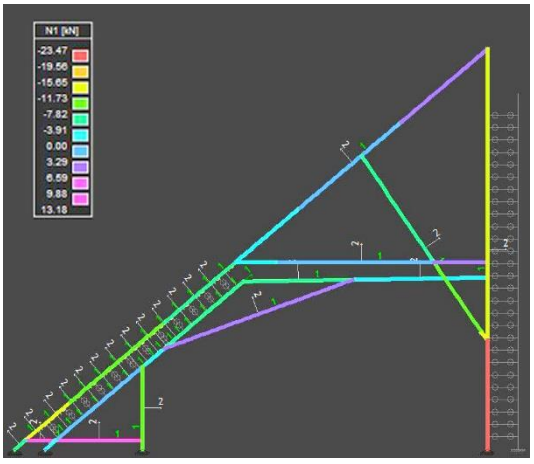
N1 [kN]
-23.47
-19.56
-15.65
-11.73
-7.82
-3.91
0.00
3.29
6.59
9.88
13.18

f)

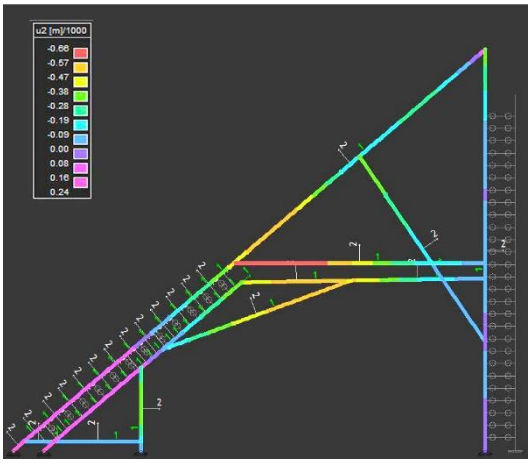
u2 [m]/1000
-0.66
-0.57
-0.47
-0.38
-0.28
-0.19
-0.09
0.00
0.08
0.16
0.24

g)

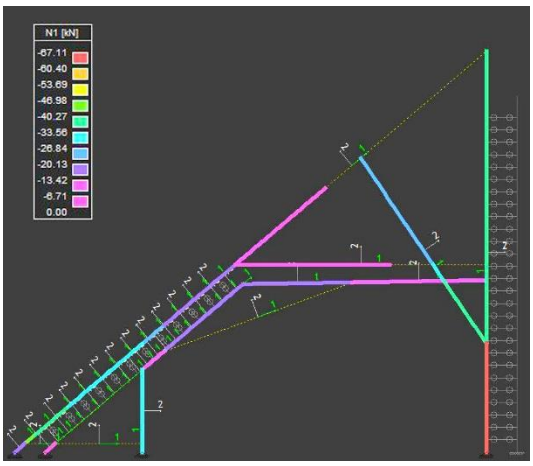

h)

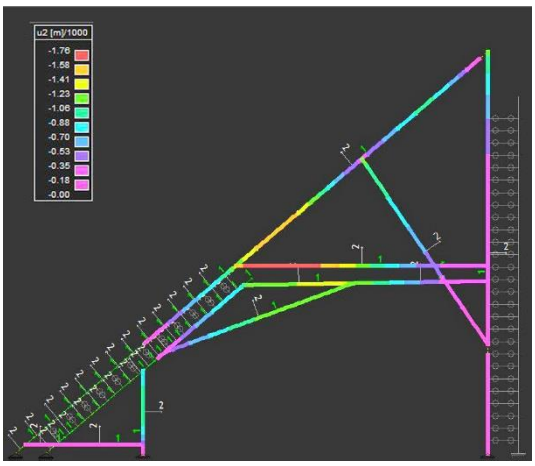

i)

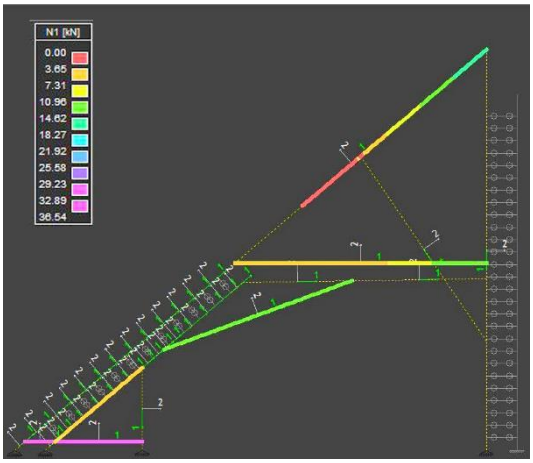

j)

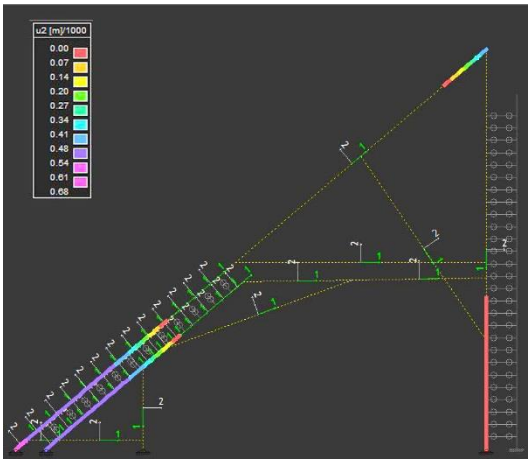

Figure 5.15 - Third scenario results; a) dead load bending moment (M_G); b) envelope bending moment (M_{ENV}); c) dead load shear forces (T_G); d) envelope shear forces (T_{ENV}); e) dead load axial forces (N_G); f) dead load local axis deflections ($U_{2,G}$); g) envelope of compression axial forces (N_{ENV-}); h) envelope of local axis negative deflections ($U_{2,ENV-}$); i) envelope of tension axial forces (N_{ENV+}); j) envelope of local axis positive deflections ($U_{2,ENV+}$);

As can be observed from the results, the bending moments and the shear forces are low on the overall structure. The big deflections seen in the first scenario in the middle of the truncated rafter, are reduced drastically with the addition of the column. The deflections for the dead load from the actual state are three times smaller than those from the first scenario. For the envelope the deflections in the current state are six times smaller than the first scenario. Furthermore, concerning the overall deflections the addition of the column reduces the deflection for around 10% for the dead load and around 50% for the envelope. This certifies the addition of the column in the reduction of deflections for the structure.

For a static frame deformed in the current condition, a stability check is shown in the Figure 5.16 below. Through the stability check process the joint connections are assumed to be perfectly stable. The stability control is done in accordance with the EN 1995-1-1:2004. As can be seen from the results the frame is stable for the loads given by the code.

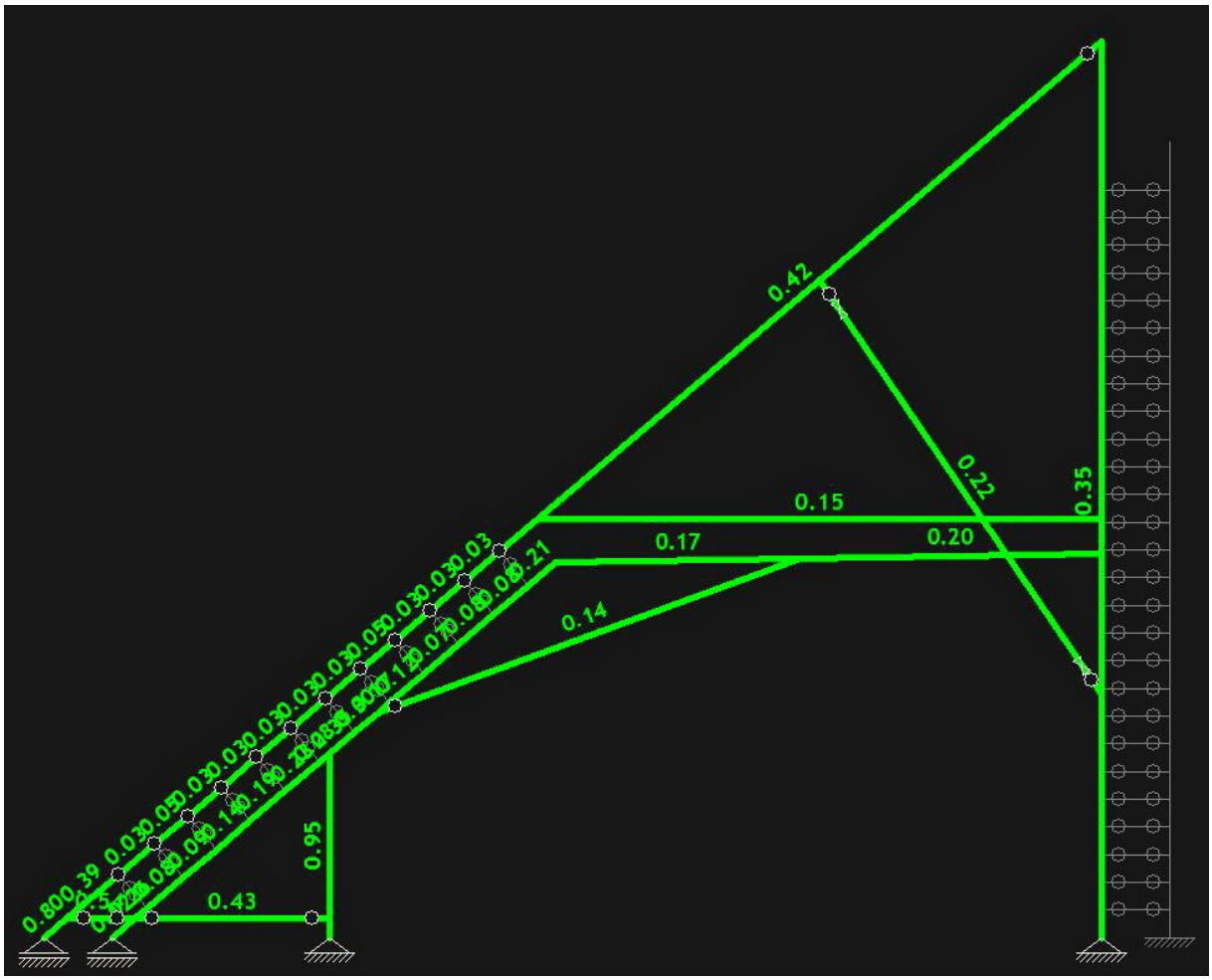

Figure 5.16 – Stability check for the third scenario of Frame 1

5.3.4 Strengthening Proposal

The frame stability check shows a stable frame, assuming by the software that the joints are perfect. Nevertheless, from the observations on site some of the connections are not in perfect condition and in some parts are only some rusted metallic elements. From the structural analysis the diagonal strut works under tension and it can confirm its behavior as a collar tie. Nevertheless, to assess the behavior of the joint is often challenging and presents many difficulties. The main difficulties in assessing old timber carpentry joints are (Meisel, Moosbrugger, & Schickhofer, 2010):

- The stiffness of the joint depends on the loading condition and that defines its mechanical behavior

- The standards do not present any rules on the design of carpentry joints according to the combined stresses
- The assessment of timber joints also requires the design of the contact pressure between the materials. The contact pressure is dependent on the contact surface and the stress distribution and these factors usually are not easily known due to the non-uniform elastic support.
- Furthermore, the big difference of the compressive strength parallel and perpendicular to the grains of timber elements presents another difficulty. This is directly related to the angle of the force and the type of carpentry joint.

In order to simplify joints in structural models, they are considered as ideally pinned or ideally rigid and both cases present either conservative or overestimated designs (Branco & Descamps, 2015). In the model have been used both cases according to the modelling scenario. In the joints are not considered the different values of rotational or axial stiffness, as this is not possible by the capacity of the software. Therefore, due to the short time to finish this thesis and the strengthening of timber frames is not its scope, only strengthening proposals will be given.

As it was seen from the first scenario, the diagonal strut works under compression if there is a tie beam on the bottom of the frame. That is why one of the possible solutions for the strut is to put a tie beam on top of the concrete slab and connect the bottom part of the rafters to the bottom part of the column. Since the short column which was added later consists of two timber planks, a good solution would be to put bigger dimensions of the planks and extend them to reach the column. The illustrated solution is presented in Figure 5.17.

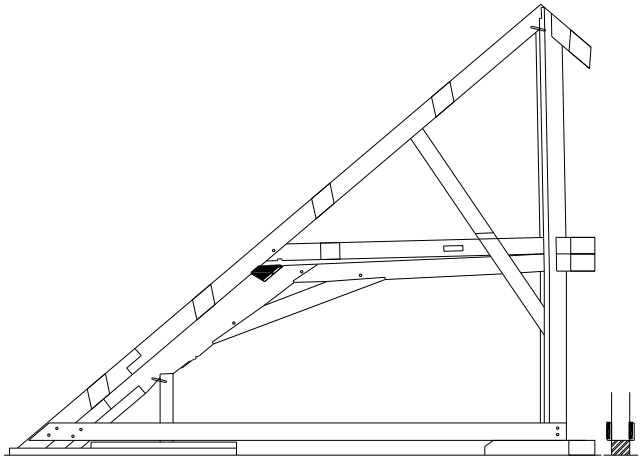

Figure 5.17 – Tie beam strengthening of Frame 1

The other possible solution can be the strengthening of the diagonal strut. The strengthening of the diagonal strut can help the strut receive the axial force and keep the frame stable. Some of the strengthening methods can be by using the metal elements to tie the notched joints of the strut presented

in Figure 5.18 (top and center). Another strengthening method proposed by Branco & Descamps (2015), is to use a steel wire to help the strut work under tension (Figure 5.18-bottom).

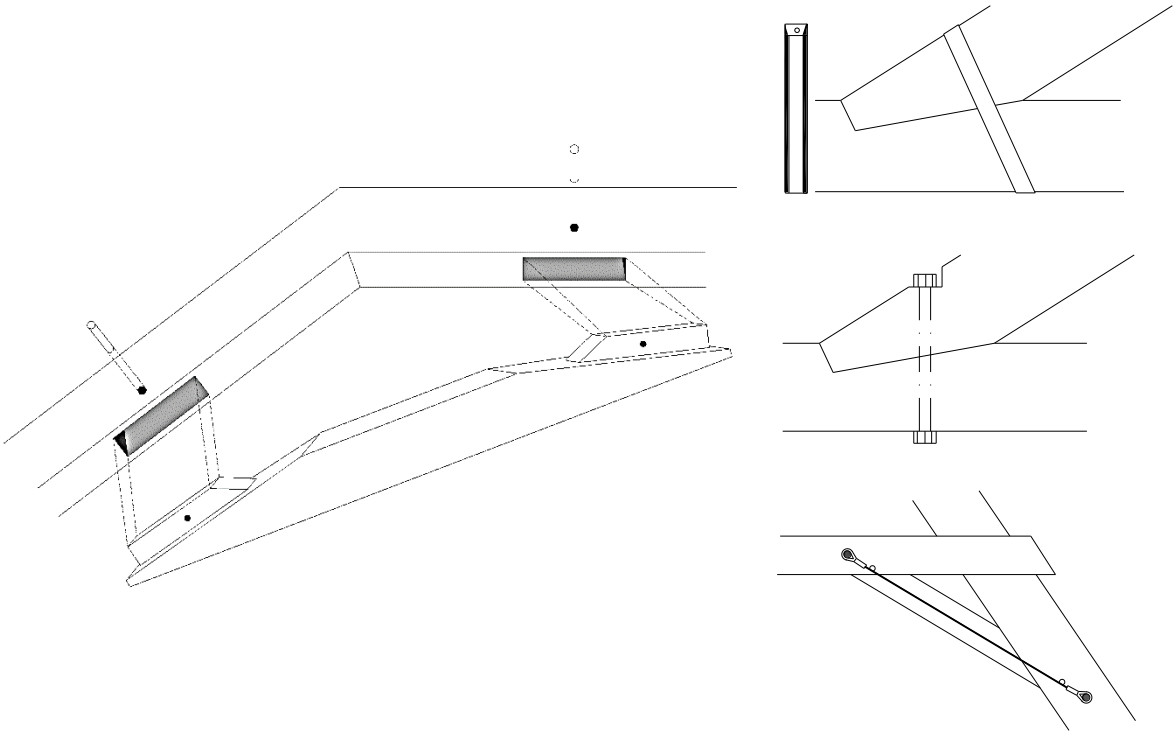

Figure 5.18 – The diagonal strut (left); binding strip (top) (Branco & Descamps, 2015); internal bolt (center) (Branco & Descamps, 2015); steel wire (bottom) (Branco & Descamps, 2015)

The first strengthening solution (Figure 5.17), provides minimum intrusiveness, compatibility and removability. The second solution (Figure 5.18), provides strengthening with more intrusive measures but still compatibility and removability are accomplished.

This page is left blank on purpose.

Chapter 6

6. CONCLUSION

In the Czech Republic are seen many roof typologies and the common rafter roofs with collars are the more common ones. The roofs in Loreta consist mainly of this type of frames made out of timber. As timber material is very susceptible to damage and to deformation the roofs suffered these phenomena. The main causes were observed to be the alterations during the different construction phases.

With the development of the chronological timeline of the monument it was able to distinguish the main eras of construction. The first situation presents the monument with single story cloisters, no chapels and no church in the back. Furthermore, the front building's roof presents the state without the hipped ends and a rectangular tower in the middle. In the second situation, the four corner chapels were added and also the hipped ends of the roof in the front building. The main tower was changed to an octagonal base. The third situation shows the monument with two more chapels, an attic wall in front and a treasury. The actual situation presents Loreta with two story cloisters, a unified façade and the church with two extensions in both directions.

The chronological timeline is utilized, and the location of the tests were performed in different frames which represent different construction periods. The non-destructiveness tests show good results for all the frames tested. Microdrilling shows similar results for both the new and the original member.
was able to observe that for both the original member and the new one. Furthermore, the loading jack results shows a similarity in the conventional strength and modulus of deformability, between the original old frame of the hipped roof and the frame of the elevated cloister. The results compared to the frames in the church show also similarities. The correlation between the conventional strength from the loading jack and the compressive strength provide the same class of timber for the both roof areas. The moisture content results show no decay in the timber elements and no risk of fungus attack.

The obtained timber class according to the codes is used for the mechanical parameters in the structural analysis. The loads from the actual code are computed and the values are relatively low. Different scenarios of the frame according to the construction phases show different results. The first scenario is the hypothetical configuration of the frame before the interventions. From this scenario are seen bigger

deflections in the middle of the truncated rafter and the main rafter. The second scenario is the hypothetical configuration of when the bottom tie beam is removed, and a sliding occurs which is represented with the corresponding boundary conditions. From this scenario the biggest deflections are observed in the same part as seen on the actual frame. This proves the assumption of a possible cause of the current deformation observed in site. The third scenario represents the actual configuration of the roof. The results show a considerable reduction of the deflections in the structure and especially in the middle of the truncated rafter. With these scenarios it can be concluded that the possible cause of the deformation are the construction alterations. Due to the short period of time other assumptions are not done. Moreover, the frame in the current configuration is stable as for the stability check. The strengthening is given as a proposal since it is outside the scope of this thesis. A solution which provides compatibility and removability is the addition of the tie beam and the change of structural behavior of the diagonal strut to compression. The other solution is to enforce the strut to work under tension and receive the axial force.

The Loreta complex is a large monument and the time available to conclude this thesis is short. To analyze the whole monument is required more work and more analysis. Therefore, future works are recommended to be carried out in different parts of the complex. Reinforcement works are ongoing in the center roof of Church of the Nativity of Our Lord. Efficiency of the strengthening of the timber frames can be analyzed. Moreover, the effect of these works on the overall structure of the roof should be evaluated.

BIBLIOGRAPHY

Bláha, J. (2006). The Evolution of Roof Timber Frames in the Southern Part of the Bohemian-Moravian Uplands from the 14th Century to the 19th Century. In M. Drdácký, *European Research on Cultural Heritage: State of the Art Studies Vol.4* (pp. 345-363). Prague: ARCCHIP.

Bláha, J. (2017). The Roofs of the Loreto in Prague. In P. Bašta, & M. Baštová, *Dientzenhofers and Loreto: The story of Loreto Façade* (pp. 27-35). Prague: Czech Capuchin Province.

Branco, J., & Descamps, T. (2015). Analysis and strengthening of carpentry joints. *Construction and Building Materials*.

CEN. (2002). *EN 1991:2002: Eurocode 0 - Basis of structural design.* European Comittee for Standardization.

CEN. (2002). *EN 1991-1-1:2002: Eurocode 1: Actions on structures - Part 1-1: General actions - Densities, self-weight, imposed loads for buildings.* European Comittee for Standardization.

CEN. (2003). *EN 1991-1-3:2003: Eurocode 1: Actions on structures - Part 1-3: General actions - Snow loads.* European Comittee for Standardization.

CEN. (2004). *EN 1995-1-1:2004: Eurocode 5: Design of timber structures - Part 1-1: General - Common rules and rules for buildings.* European Comittee for Standardization.

CEN. (2005). *EN 1991-1-4:2005: Eurocode 1: Actions on structures - Part 1-4: General actions - Wind actions.* European Comittee for Standardization.

ČNI. (2003). *ČSN EN 338: Konstrukční dřevo - Třídy pevnosti .* Český normalizačni institut.

ČNI. (2005). *ČSN EN 1991-1-3: Eurokód 1: Zatížení konstrukcí - Část 1-3: Obecná zatížení - Zatížení sněhem.* Český normalizačni institut.

ČNI. (2007). *ČSN EN 1991-1-4: Eurokód 1: Zatížení konstrukcí - Část 1-4: Obecná zatížení - Zatížení větrem.* Český normalizačni institut.

Drdácký, M., & Kloiber, M. (2013). In-situ compression stress-deformation measurements along the timber depth profile. *Advanced Materials Research*, pp. Vol. 778 pp 209-216.

Ferguson, C. (1970). Concepts and techniques of dendrochronology. In R. Berger, *Scientific Methods in Medieval Archaelogy* (pp. Chap.VII 183-200). Arizona: Laboratory of Tree-Ring Research, University of Arizona.

Hirai, T., Meng, Q., Sawata, K., Koizumi, A., Sasaki, Y., & Uematsu, T. (n.d.). *Some Aspects of Frictional Resistance in Timber Construction.* Sapporo.

Kloiber, K., Tippner, J., Heřmánková, V., & Štainbruch, J. (2012). Comparison of results of measuring by current NDT methods with results obtained through a new device for wood mechanical resistance measuring. *SAHC - 8th International Conference on Structural Analysis of Historical Constructions.* Wroclaw: SAHC.

Kloiber, M., Bláha, J., Václavík, F., Ružička, P., & Kunecký, J. (2015). Modern diagnostic methods and traditional carpentry techniques used for the renovation of the White Tower belfry in Hradec Kralove. *SHATIS - 3rd International Conference on Structural Health Assessment of Timber Structures.* Wroclaw: SHATIS.

Kloiber, M., Drdácký, M., Kunecký, J., Tippner, J., & Sebera, V. (2016). Mini-Jack based direct determination of wood mechanical characteristics in situ. *ICEM 17 - 17th International Conference on Experimental Mechanics.* Rhodes: ICEM.

Kloiber, M., Drdácký, M., Tippner, J., & Hrivnák, J. (2014). Conventional compressive strength parallel to the grain and mechanical resistance of wood against pin penetration and microdrilling established by in-situ semidestructive devices. *Materials and Structures*, pp. 3217-3229.

Kloiber, M., Drdácký, M., Tippner, J., & Sebera, V. (2013). *New construction NDT device for in situ evaluation of wood using compression stress-deformation measurement parallel to grain.*

Kloiber, M., Kunecký, J., Tippner, J., & Sebera, V. (2014). A new diagnostic device for in-situ determination of strength and modulus of deformability in compression of wood parallel to fiber. *SAHC - 9th International Conference on Structural Analysis of Historical Constructions.* Mexico City: SAHC.

Kloiber, M., Tippner, J., & Hrivnák, J. (2014). Mechanical properties of wood examined by semi-destructive devices. *Materials and Structures*, pp. 199-212.

Kloiber, M., Tippner, J., Praus, L., & Hrivnák, J. (2012). Experimental verification of a new tool for wood mechanical resitance measurement. *Wood Research*, pp. 383-398.

Kuklík, P. (2008). History of Timber Structures. In *Handbook 1 - Timber Structures* (pp. Chap.1 pp. 1-14). Leonardo da Vinci and TEMTIS.

Kyncl, T. (2016). *The Loreto in Prague, Report of dendrochronological dating.* Brno: DendroLab.

Líčeníková, M. (2017). Outline of Construction Development of the Prague Loreto. In P. Bašta, & M. Baštová, *Dientzenhofers and Loreto: The Story of Loreto Façade* (pp. 13-25). Prague: Czech Capuchin Province.

Loreto Prague. (2015). *The Loreto cult: Santa Casa*. Retrieved from Loreto Prague: http://stara.loreta.cz

Maddox, J., Drdácký, M., & Kloiber, M. (2014). In situ assessment of strength of historic wood. *SAHC - 9th International Conference on Structural Analysis of Historical Constructions.* Mexico City: SAHC.

Meier, E. (2018). *White Fir*. Retrieved from The Wood Database: http://www.wood-database.com

Meisel, A., Moosbrugger, T., & Schickhofer, G. (2010). Survey and Realistic Modelling of Ancient Austrian Roof Structures. *Conservation of Heritage Structure (CSHM-3).* Otawa.

Tannert, T., Anthony, R., Kasal, B., Kloiber, M., Piazza, M., Riggio, M., . . . Yamaguchi, N. (2013). In situ assessment of structural timber using semi-destructive techniques. *Materials and Structures*.

UNI - LEGNO. (2003). *UNI 11035-1:2003: Legno strutturale - Classificazione a vista di legnami italiani secondo la resistenza meccanica: terminologia e misurazione delle caratteristiche.* Milano: Ente Nazionale Italiano di Unificazione.

UNI - LEGNO. (2003). *UNI 11035-2:2003: Legno strutturale - Regole per la classificazione a vista secondo la resistenza e i valori caratteristici per tipi di legname strutturale italiani.* Milano: Ente Nazionale Italiano di Unifica.

This page is left blank on purpose.

APPENDIX A - GEOMETRY

This page is left blank on purpose.

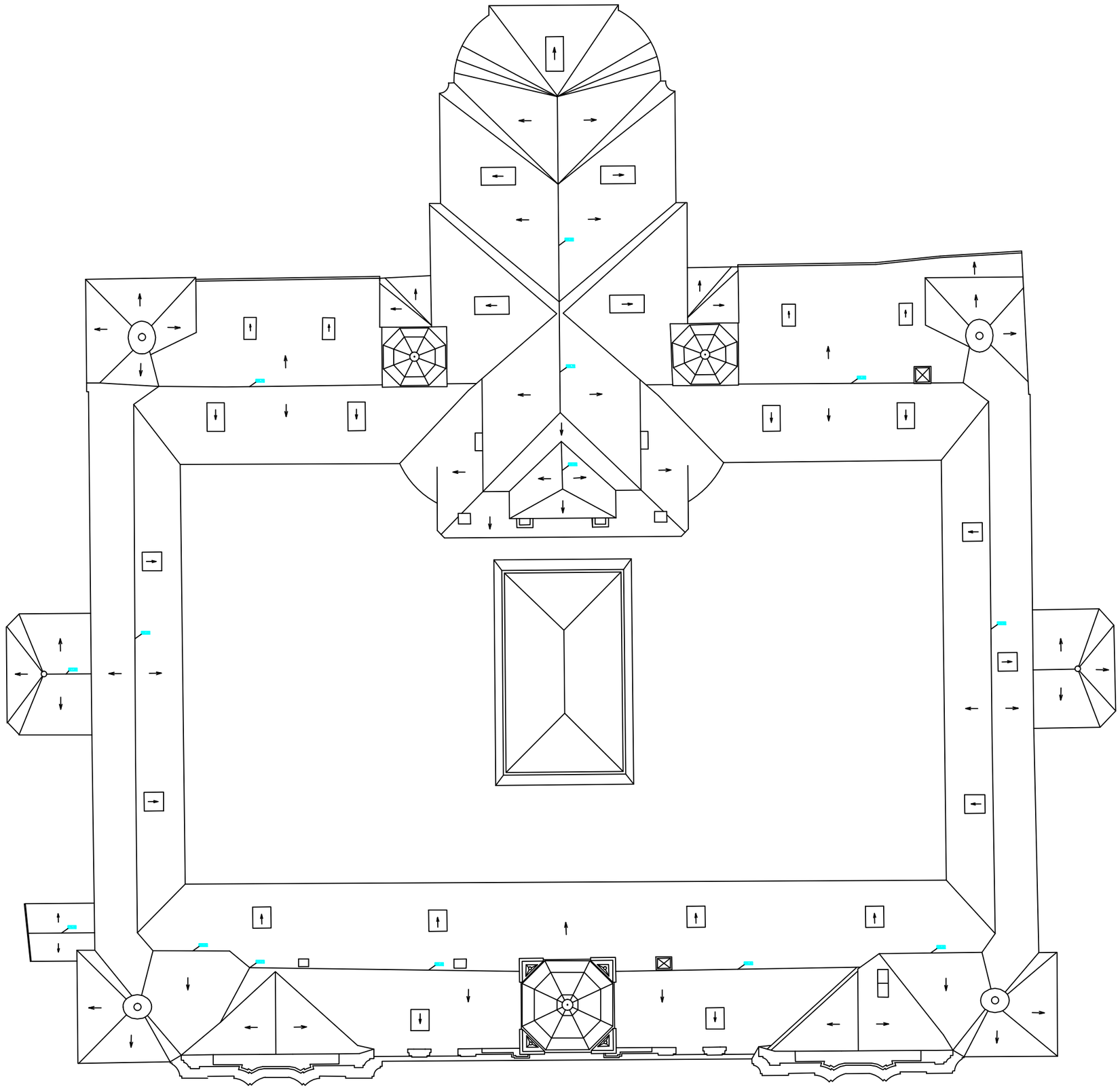

LORETA ROOFS	1:350	
TOP VIEW	BLEDIAN NELA	SAHC

0 5 m

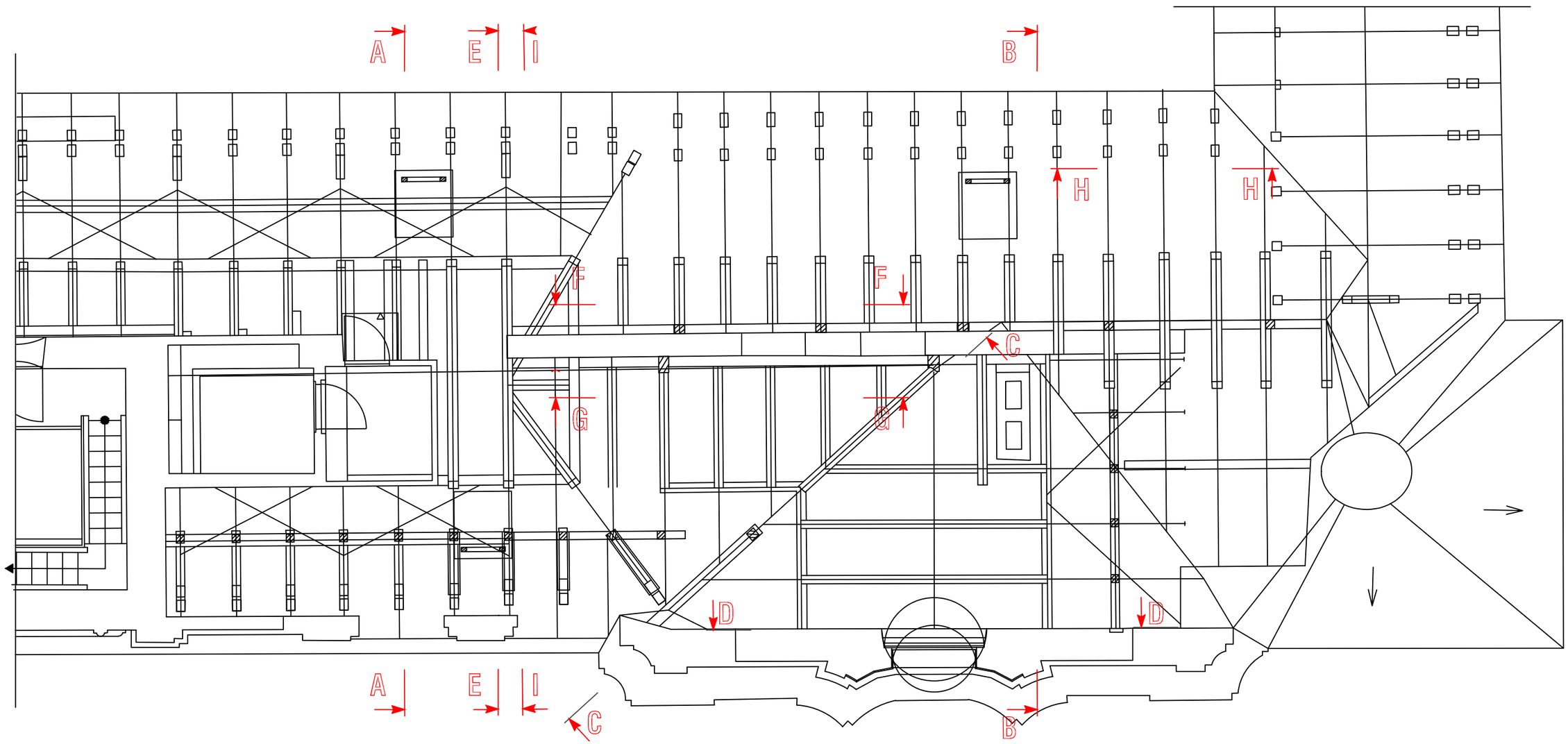

0 5 m

SOUTH PART OF WEST WING - BASE PLAN	1:100	BLEDIAN NELA

C-C

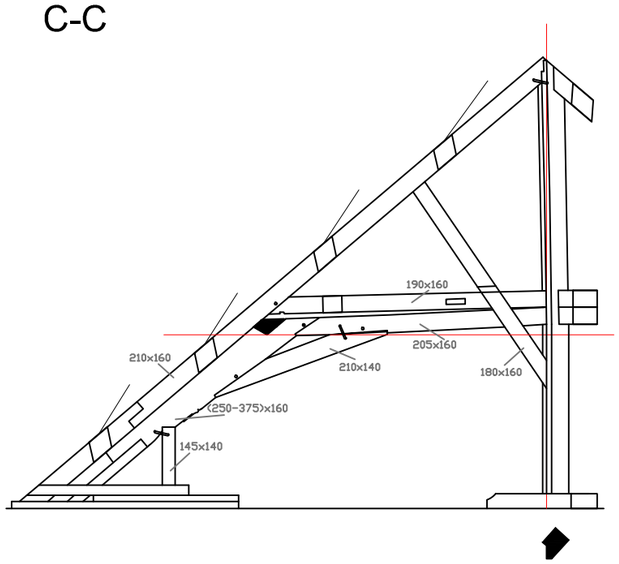

A-A

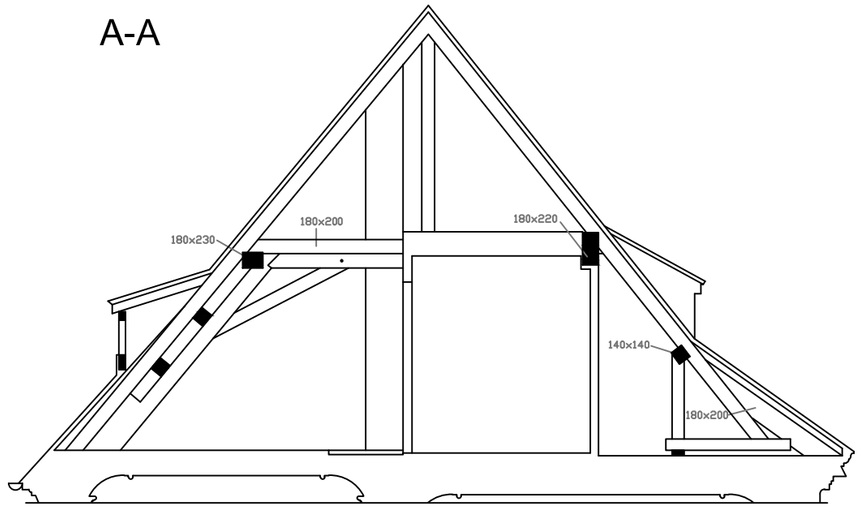

0 5 m

SOUTH PART OF WEST WING - C-C & A-A	1:100 BLEDIAN NELA		SAHC

D-D

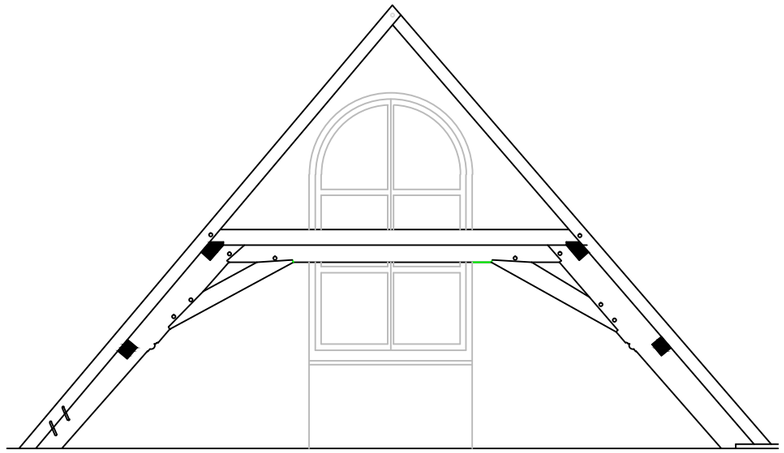

B-B

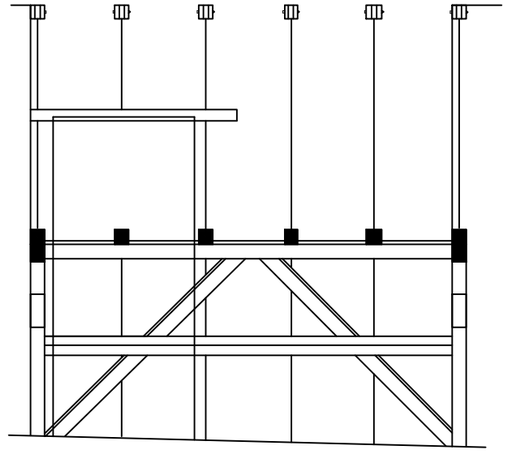

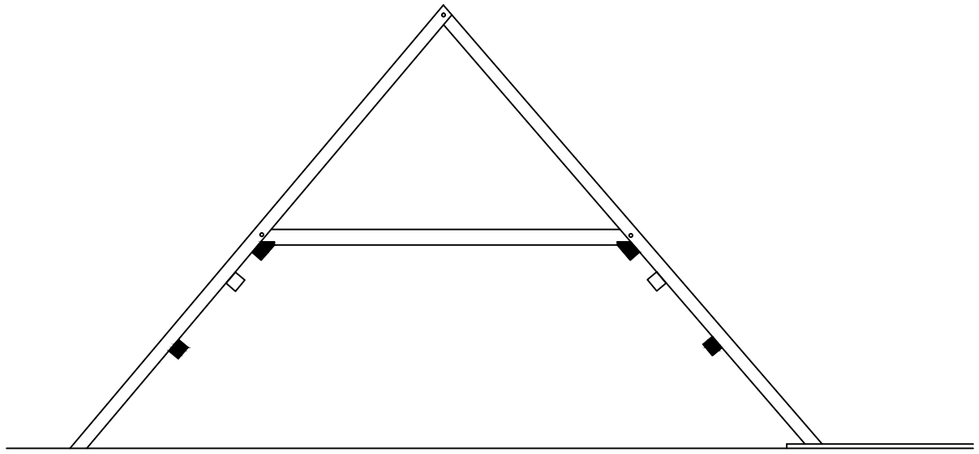

0 5 m

SOUTH PART OF WEST WING - D-D & B-B	1:100		SAHC
	BLEDIAN NELA		

E-E

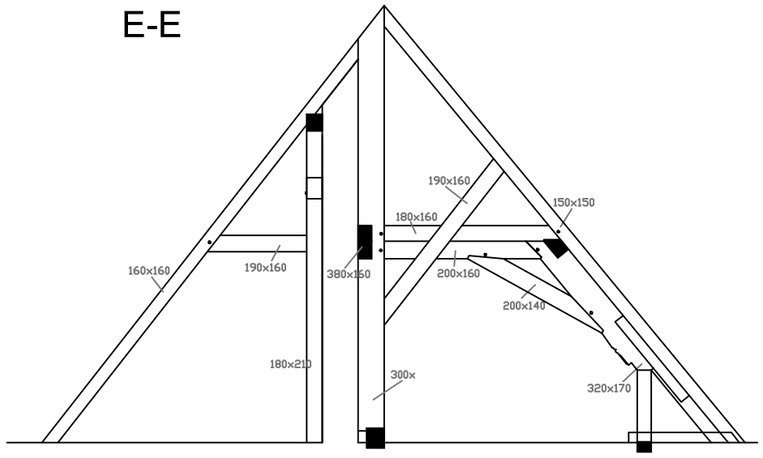

G-G

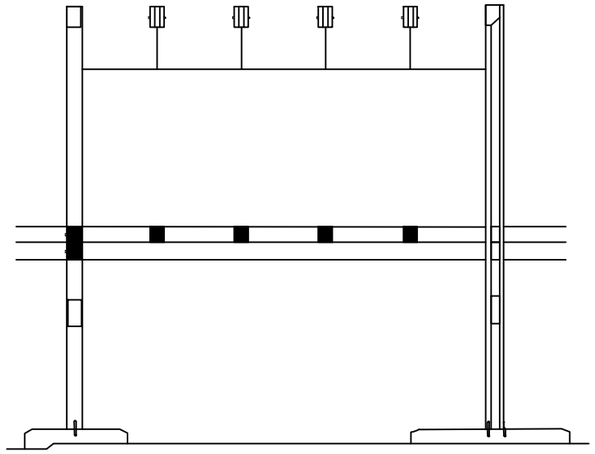

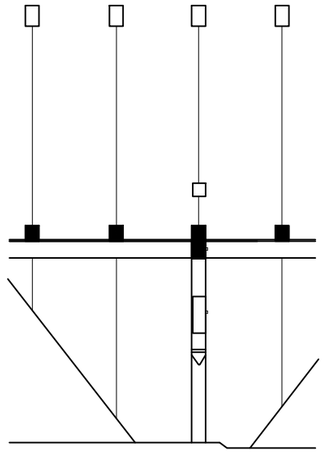

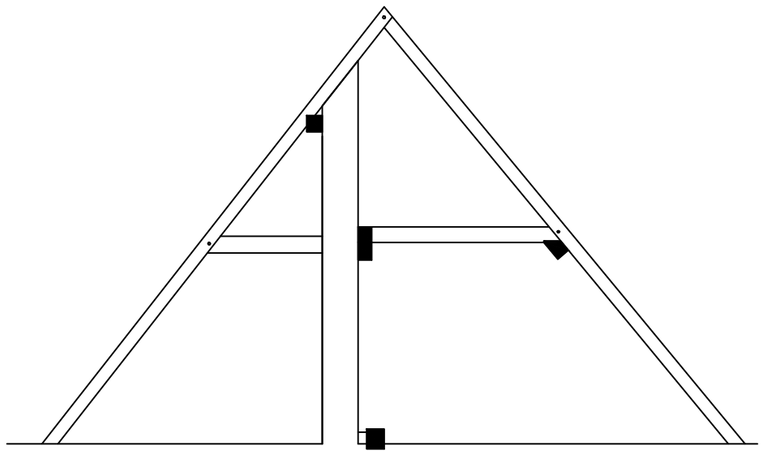

F-F

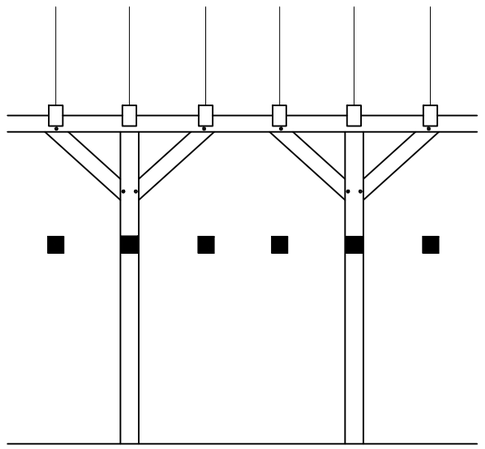

0 5 m

SOUTH PART OF WEST WING - E-E, G-G & F-F	1:100		SAHC
	BLEDIAN NELA		

I-I

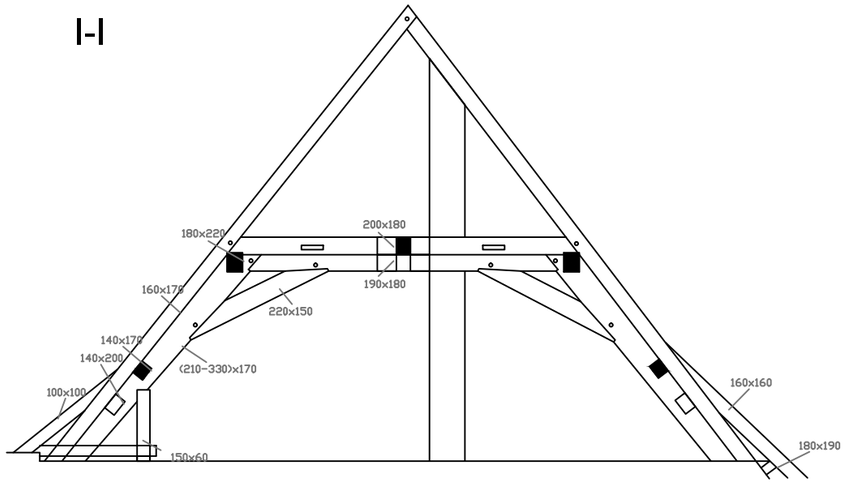

H-H

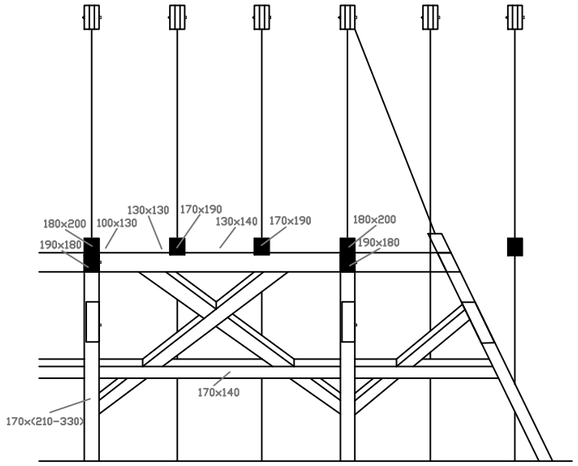

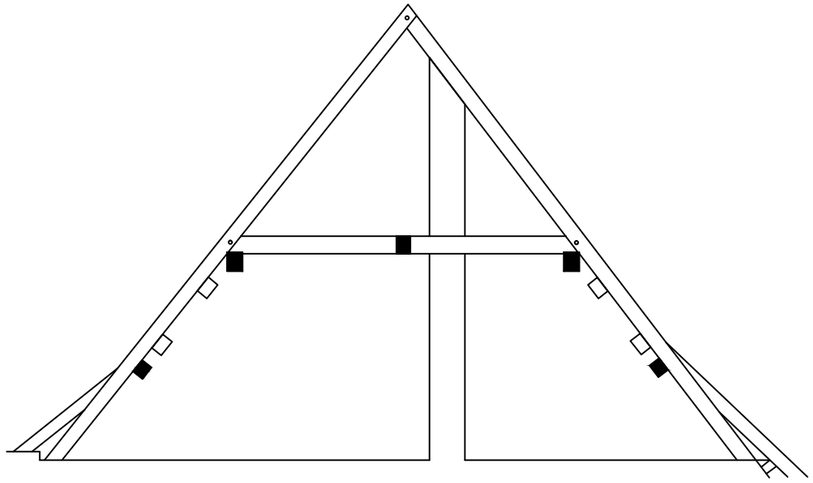

0 5 m

SOUTH PART OF WEST WING - I-I & H-H	1:100 BLEDIAN NELA		SAHC

APPENDIX B – MICRODRILLING MEASUREMENTS

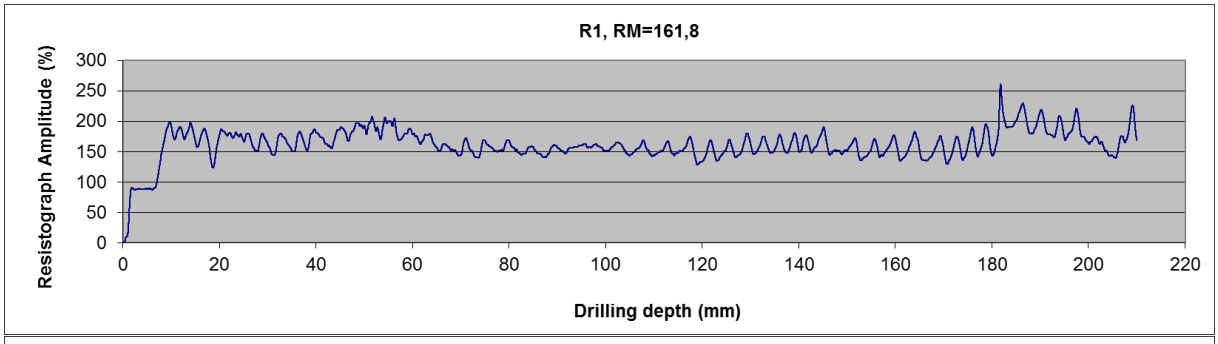

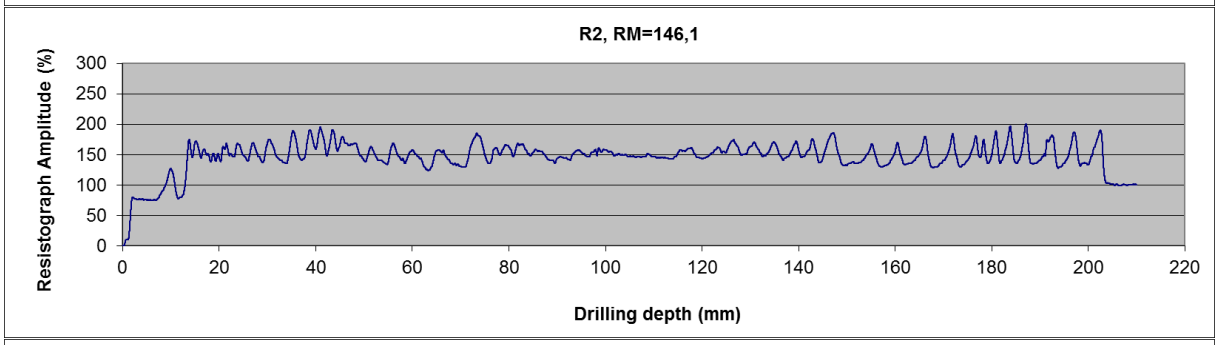

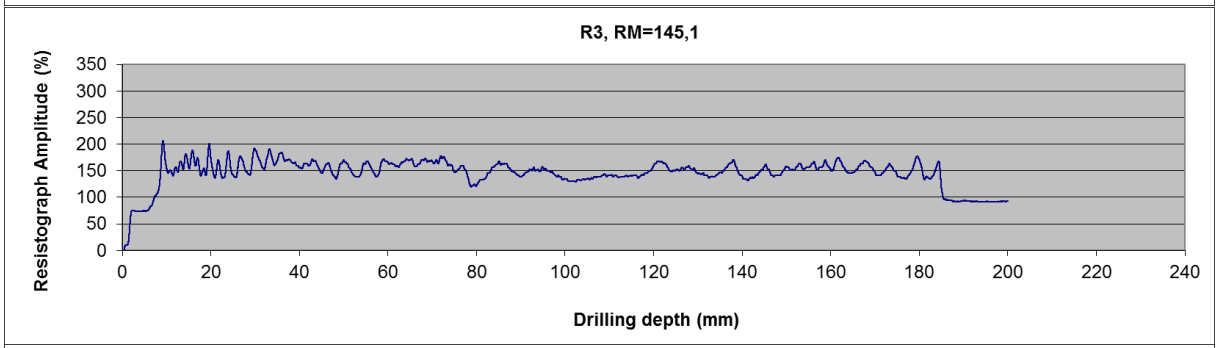

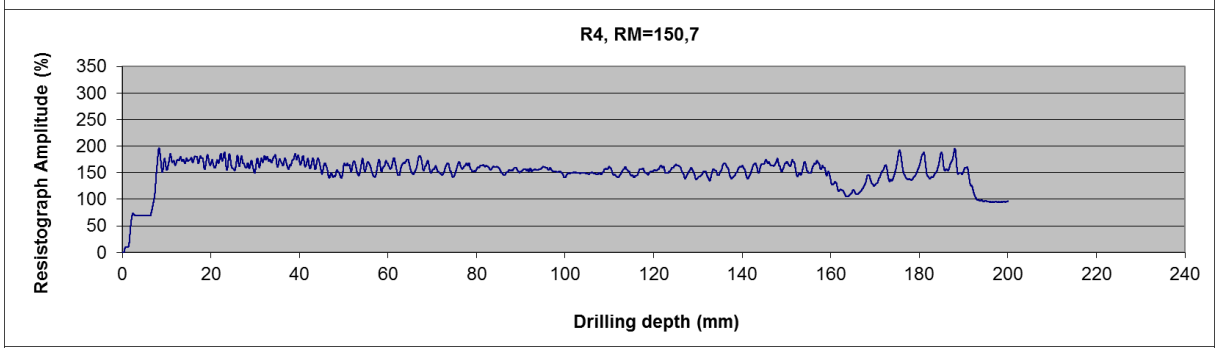

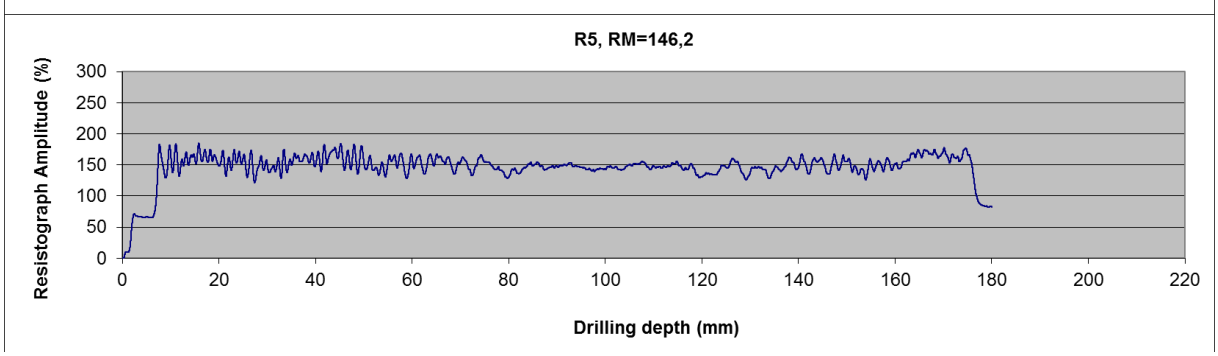

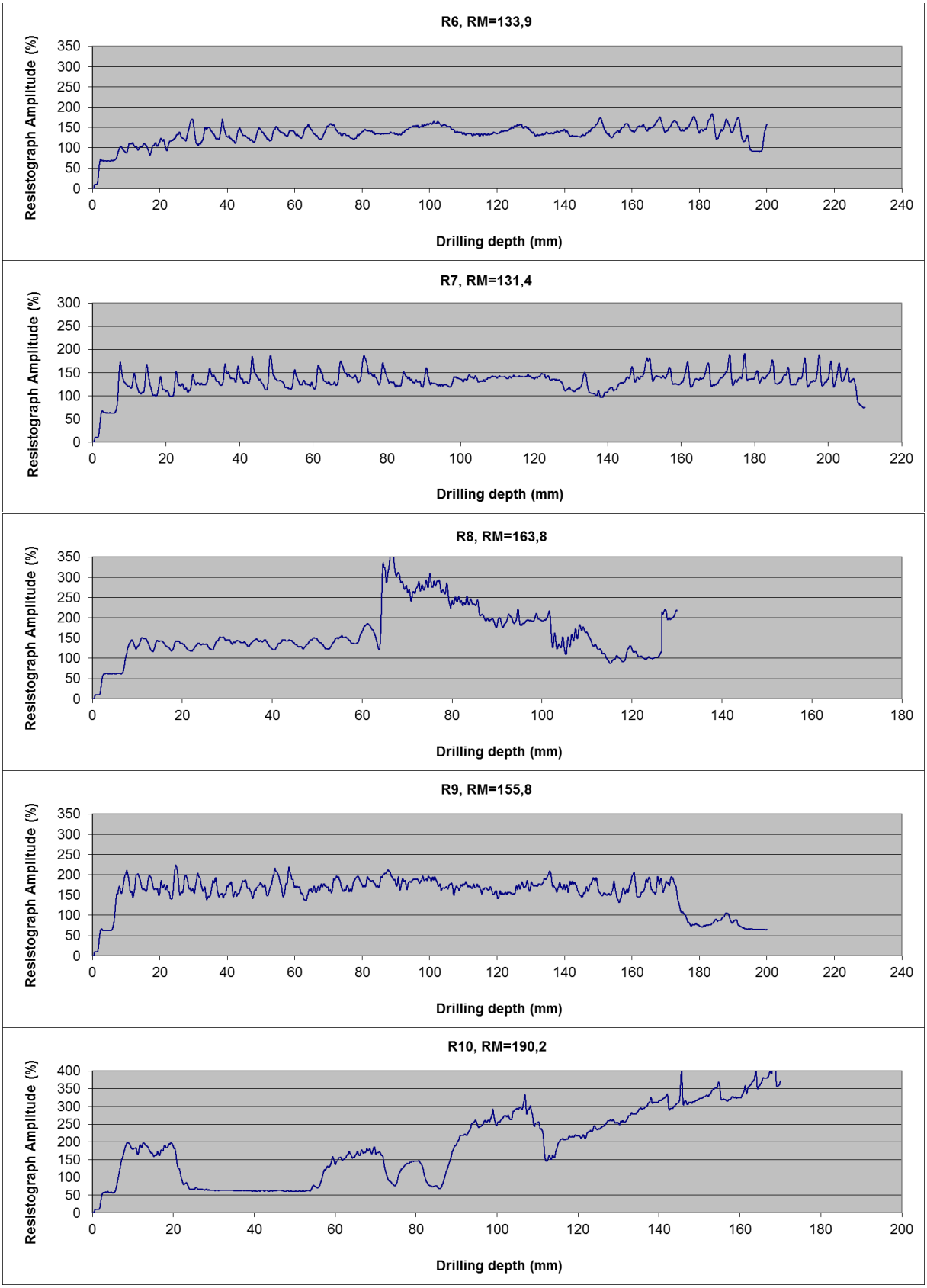
R6, RM=133,9
Resistograph Amplitude (%)
Drilling depth (mm)
R7, RM=131,4
Resistograph Amplitude (%)
Drilling depth (mm)
R8, RM=163,8
Resistograph Amplitude (%)
Drilling depth (mm)
R9, RM=155,8
Resistograph Amplitude (%)
Drilling depth (mm)
R10, RM=190,2
Resistograph Amplitude (%)
Drilling depth (mm)

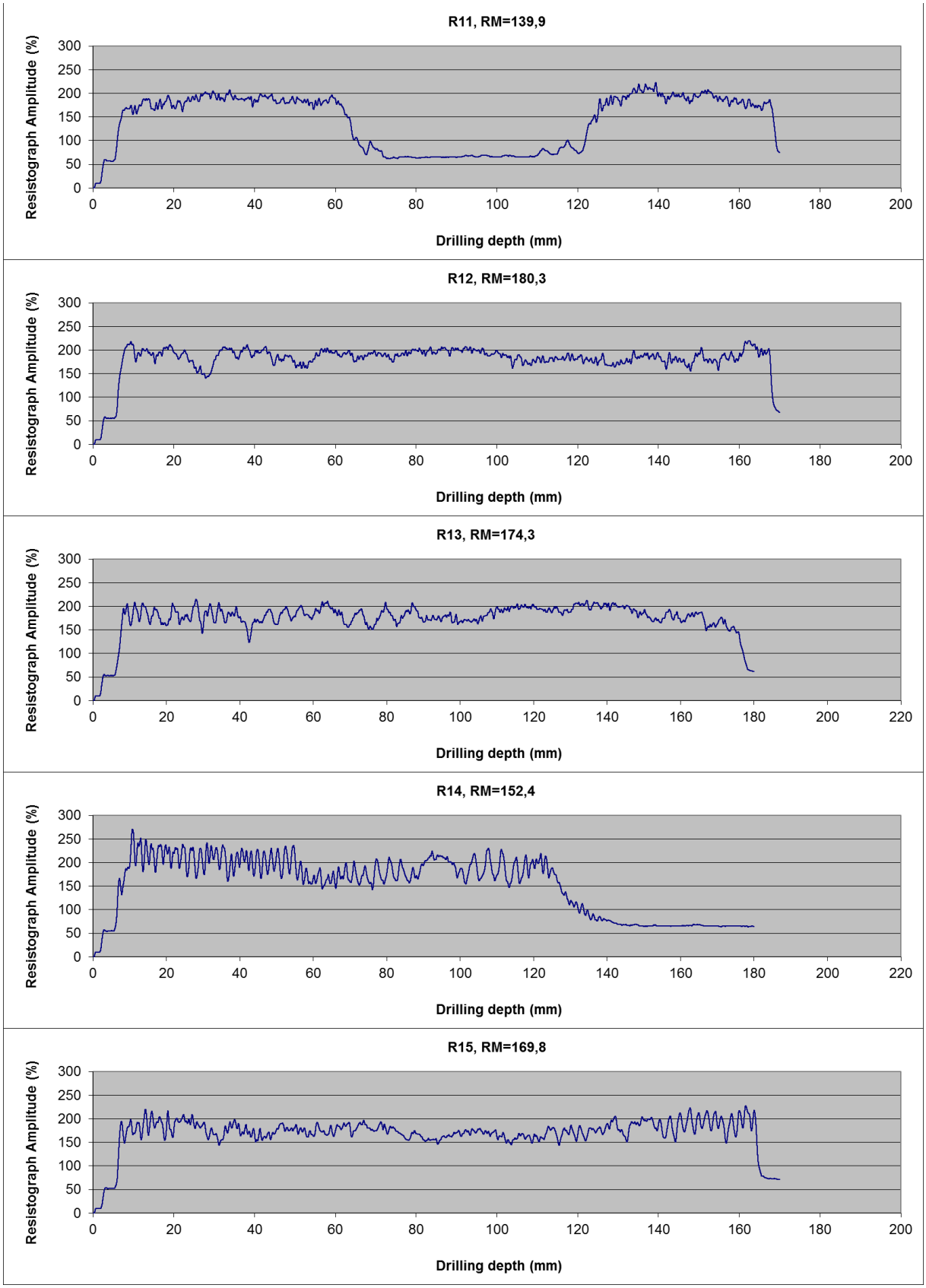
R11, RM=139,9
Resistograph Amplitude (%)
Drilling depth (mm)
R12, RM=180,3
Resistograph Amplitude (%)
Drilling depth (mm)
R13, RM=174,3
Resistograph Amplitude (%)
Drilling depth (mm)
R14, RM=152,4
Resistograph Amplitude (%)
Drilling depth (mm)
R15, RM=169,8
Resistograph Amplitude (%)
Drilling depth (mm)

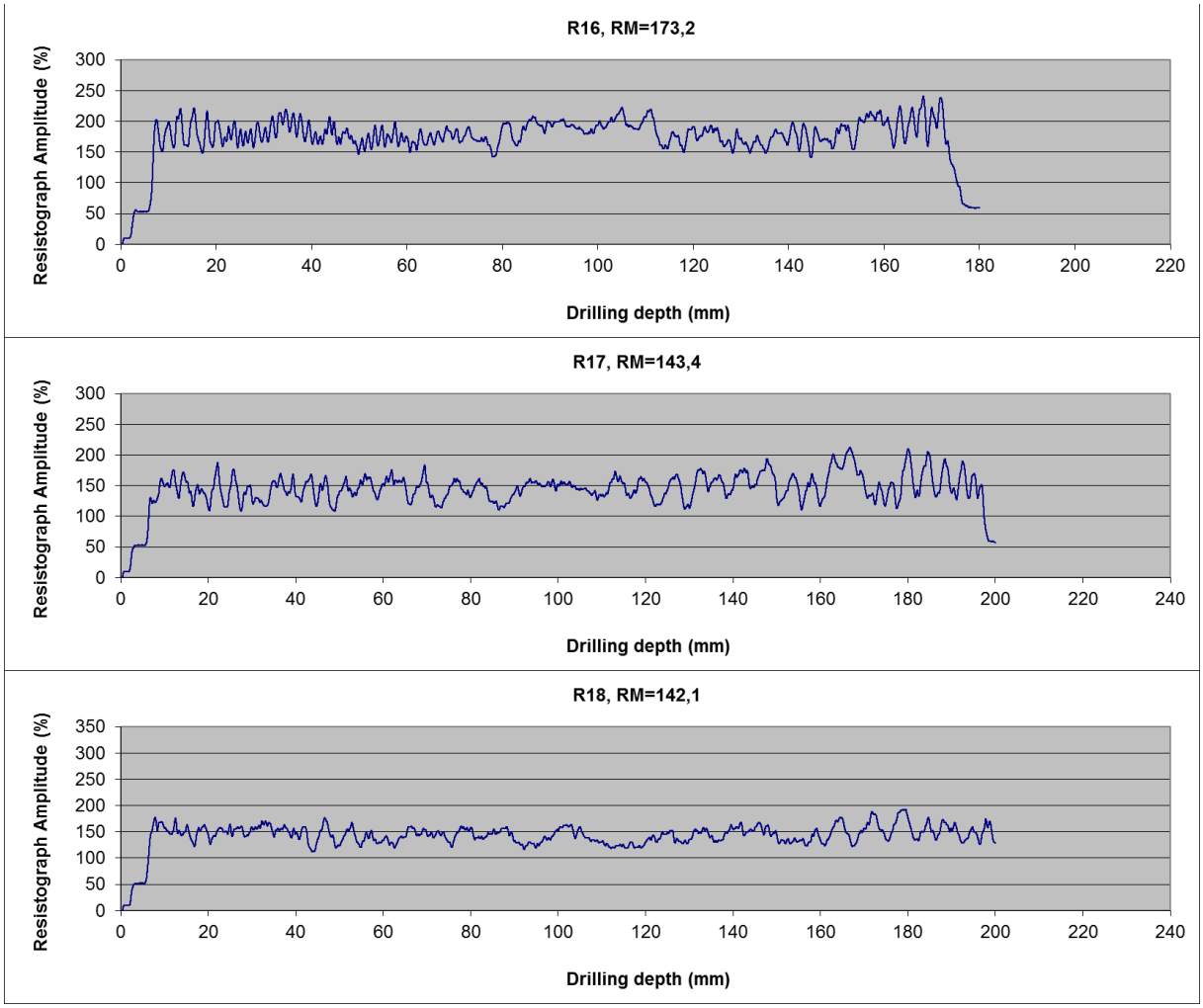

Figure B1.1 – Microdrilling Measurements

APPENDIX C – LOADING JACK RESULTS

LJ 1-1

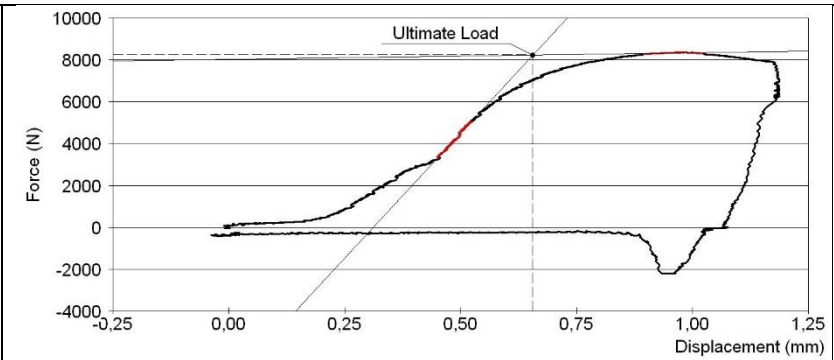

Conventional Strength = 82,309 N/mm^2 Modulus of Deformability = 23924,030 N/mm

LJ 1-2

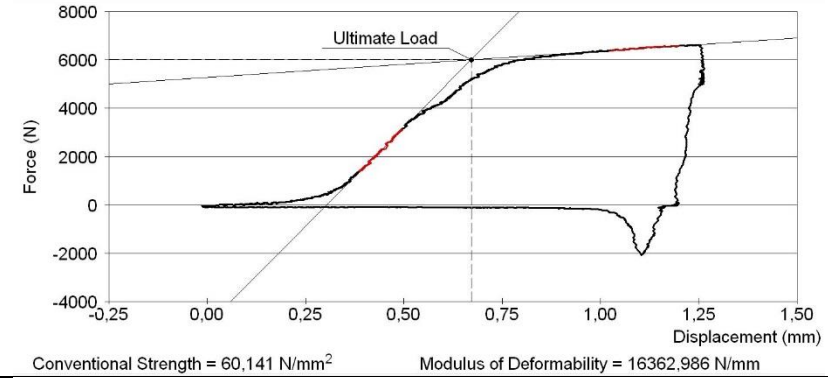

Conventional Strength = 60,141 N/mm^2 Modulus of Deformability = 16362,986 N/mm

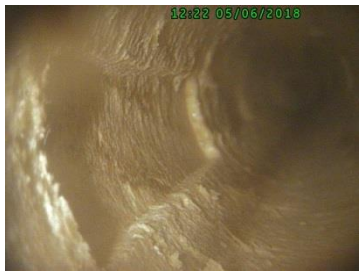

LJ 1-3

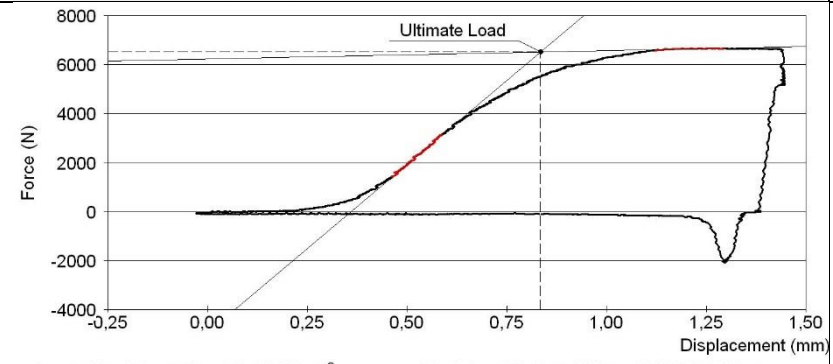

Conventional Strength = 65,161 N/mm^2 Modulus of Deformability = 13712,649 N/mm

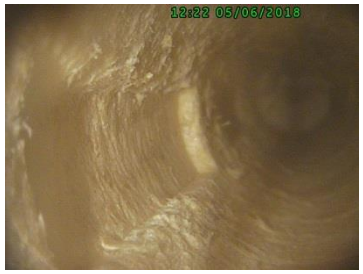

LJ 1-4

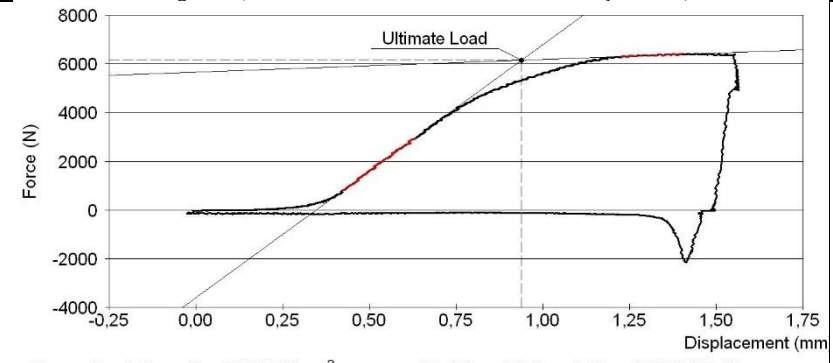

Conventional Strength = 61,531 N/mm^2 Modulus of Deformability = 10396,432 N/mm

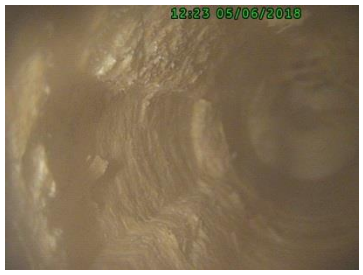

LJ 2-1	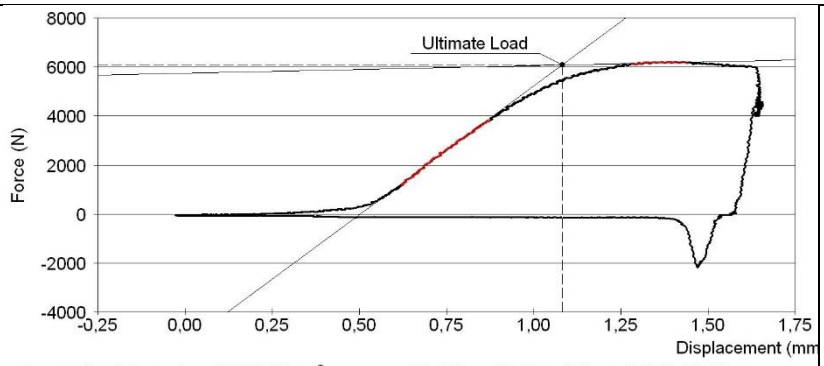 Conventional Strength = 60,901 N/mm^2 Modulus of Deformability = 10508,492 N/mm	
LJ 2-2	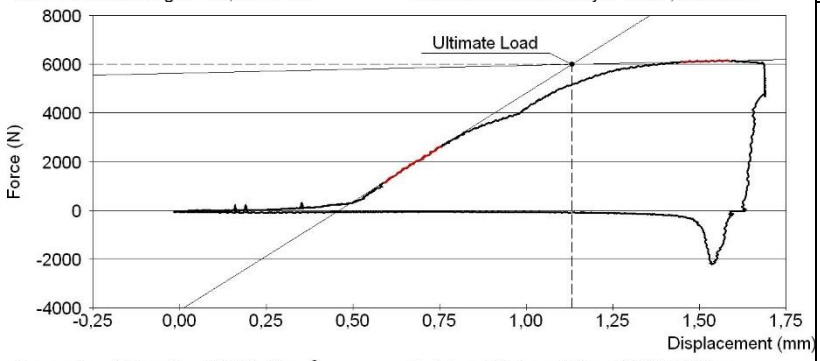 Conventional Strength = 59,984 N/mm^2 Modulus of Deformability = 8917,230 N/mm	
LJ 2-3	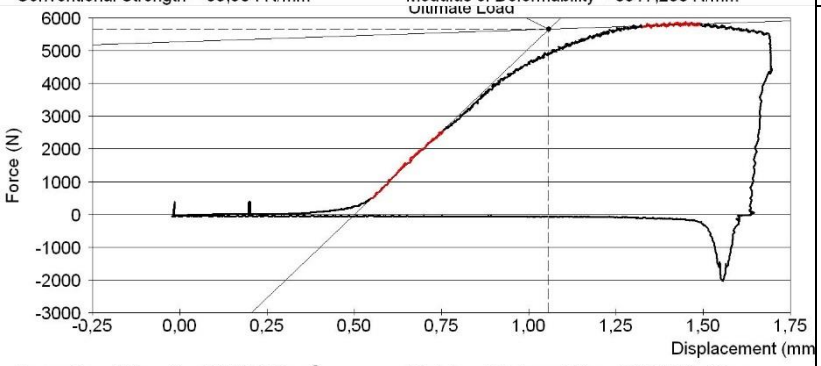 Conventional Strength = 56,587 N/mm^2 Modulus of Deformability = 10150,958 N/mm	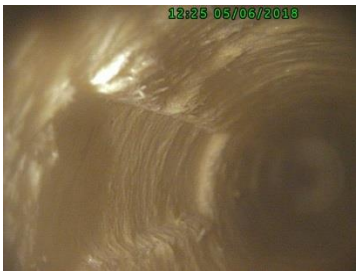
LJ 2-4	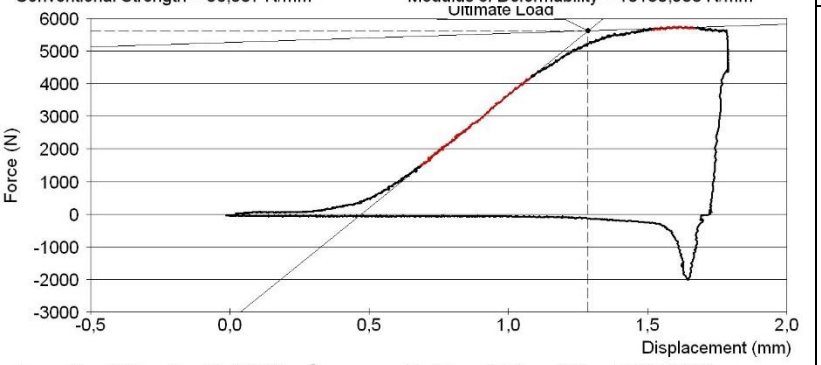 Conventional Strength = 56,191 N/mm^2 Modulus of Deformability = 6903,813 N/mm	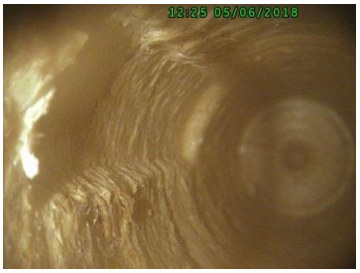

LJ 3-1	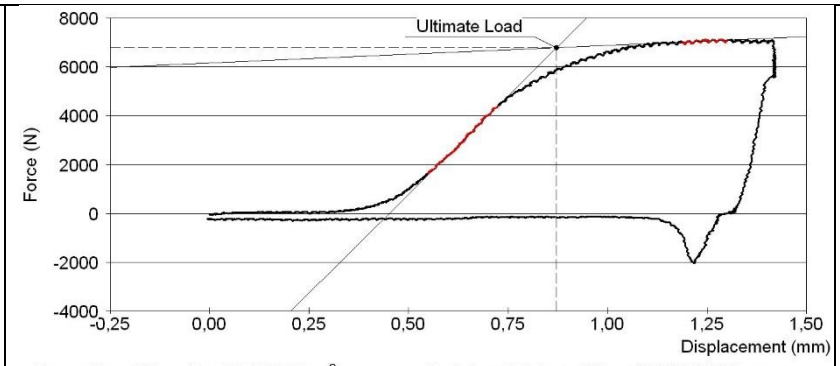 Conventional Strength = 67,873 N/mm^2 Modulus of Deformability = 16125,309 N/mm	
LJ 3-2	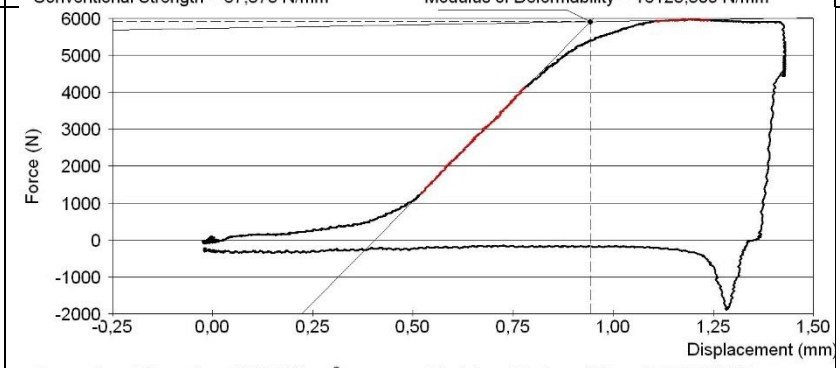 Conventional Strength = 59,056 N/mm^2 Modulus of Deformability = 10958,515 N/mm	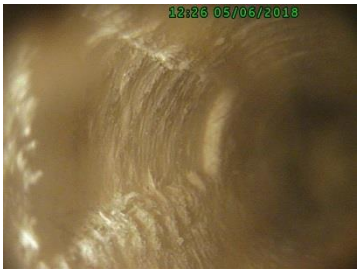
LJ 3-3	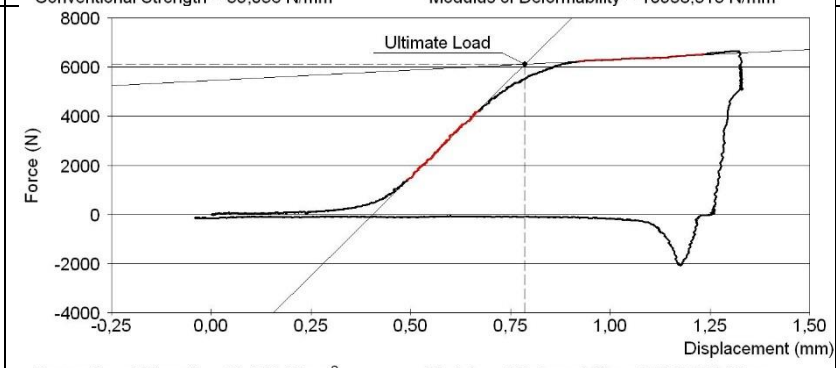 Conventional Strength = 61,159 N/mm^2 Modulus of Deformability = 16052,951 N/mm	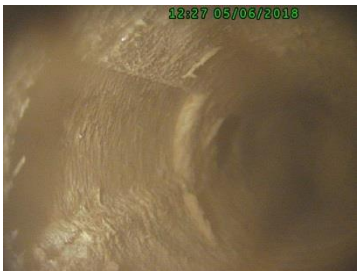
LJ 3-4	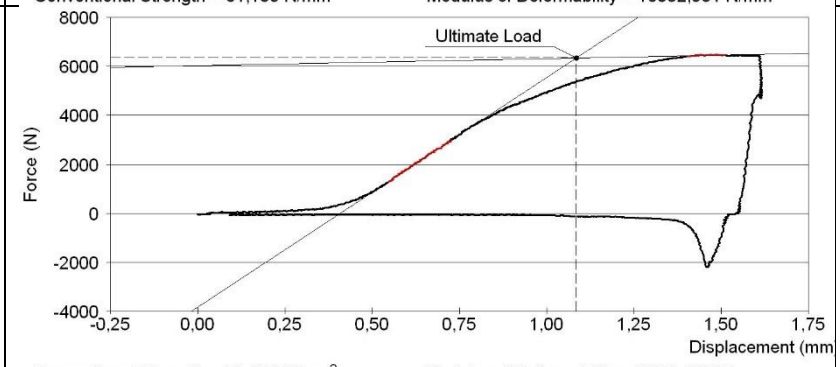 Conventional Strength = 63,404 N/mm^2 Modulus of Deformability = 9374,489 N/mm	

LJ 4-1	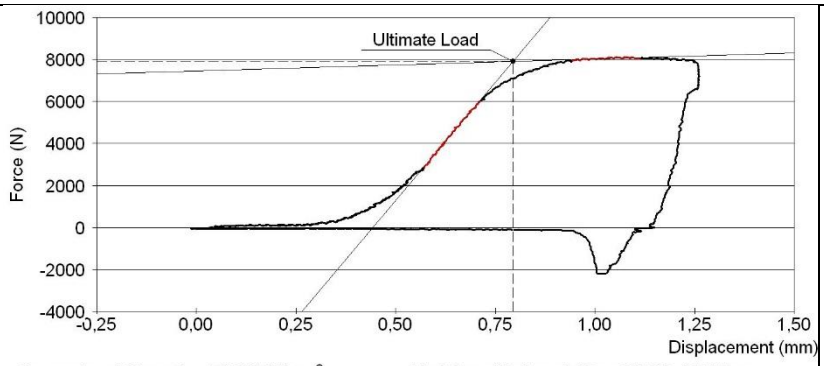 Conventional Strength = 79,097 N/mm^2 Modulus of Deformability = 22508,407 N/mm	
LJ 4-2	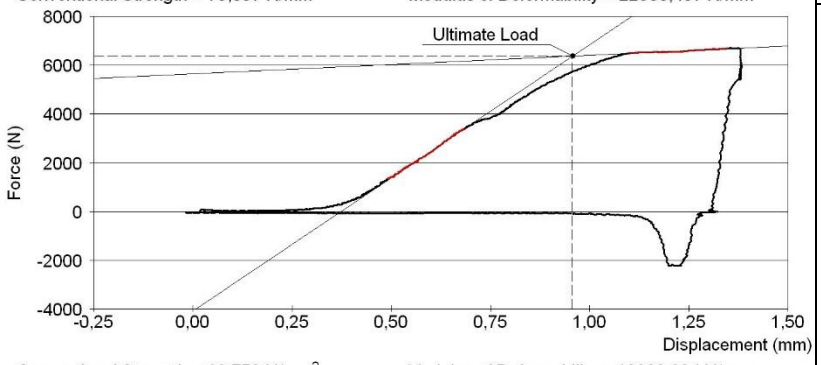 Conventional Strength = 63,753 N/mm^2 Modulus of Deformability = 10908,834 N/mm	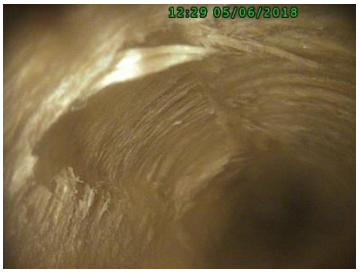
LJ 4-3	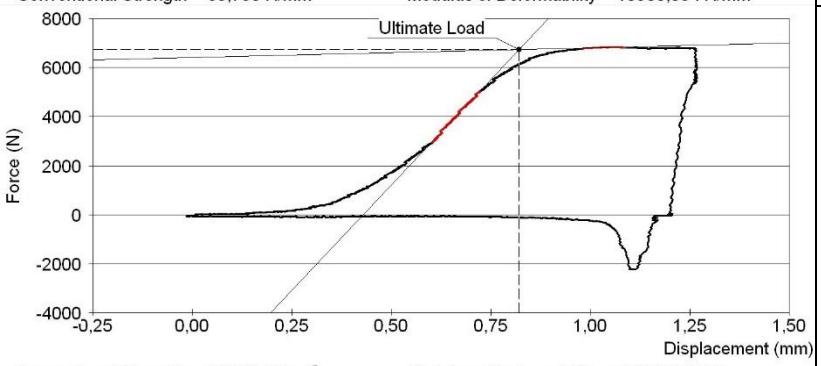 Conventional Strength = 67,312 N/mm^2 Modulus of Deformability = 17179,166 N/mm	
LJ 4-4	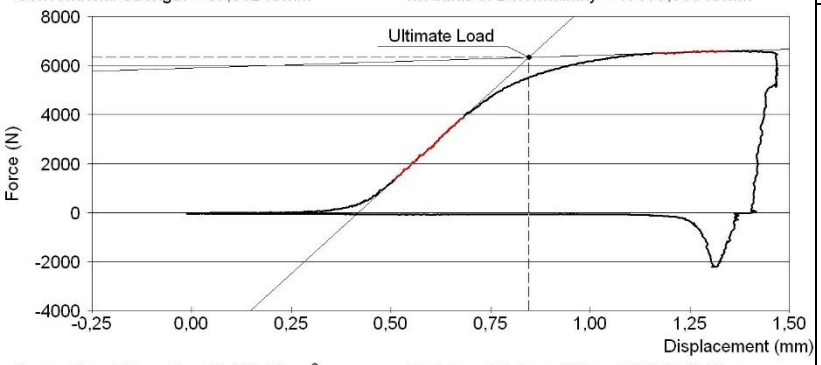 Conventional Strength = 63,289 N/mm^2 Modulus of Deformability = 14795,848 N/mm	

LJ 5-1	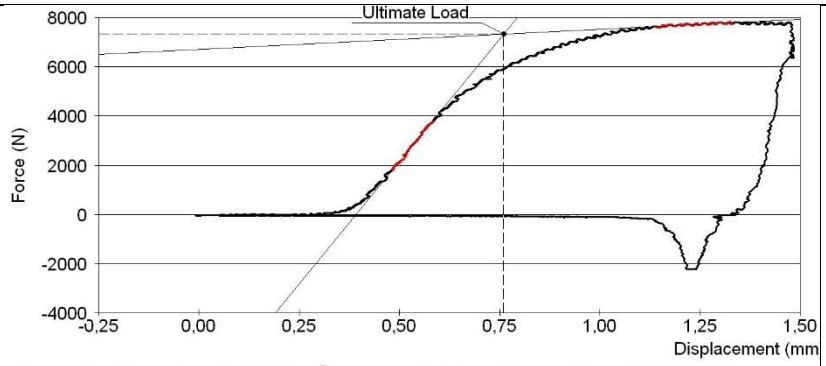	
LJ 5-2	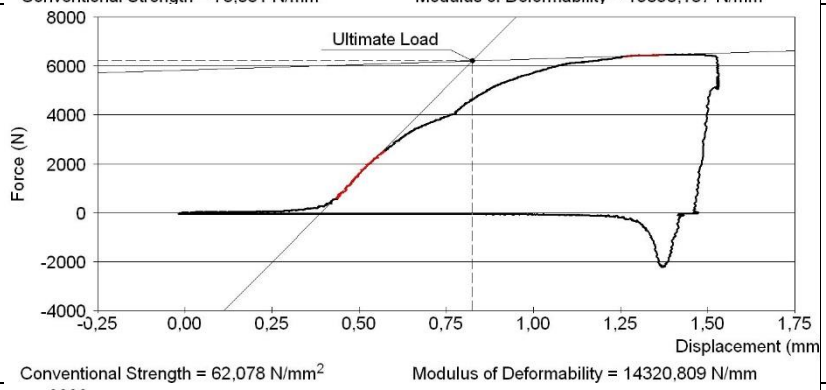	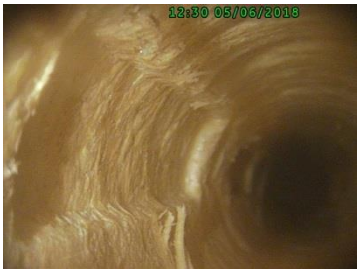
LJ 5-3	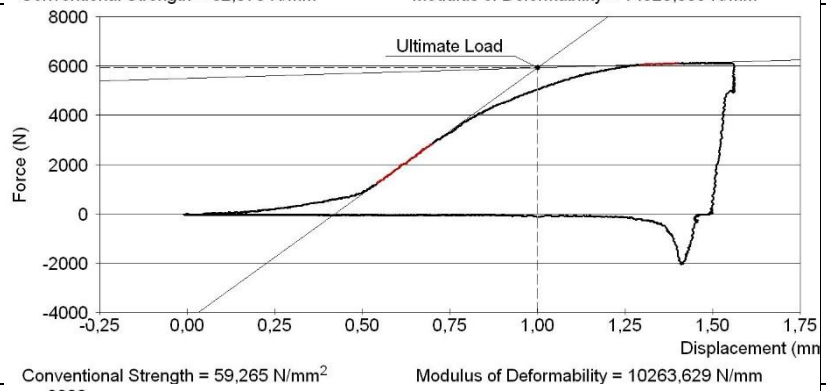	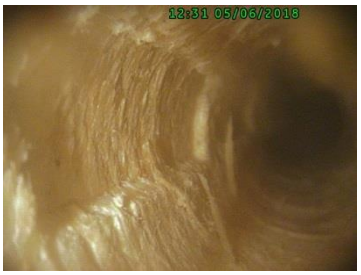
LJ 5-4	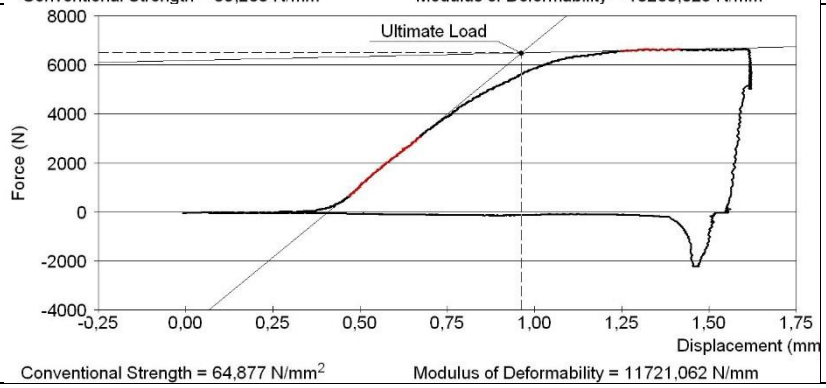	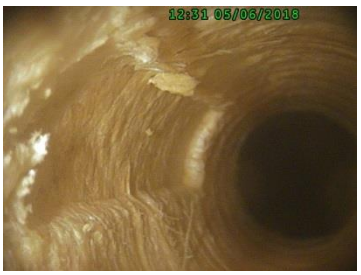

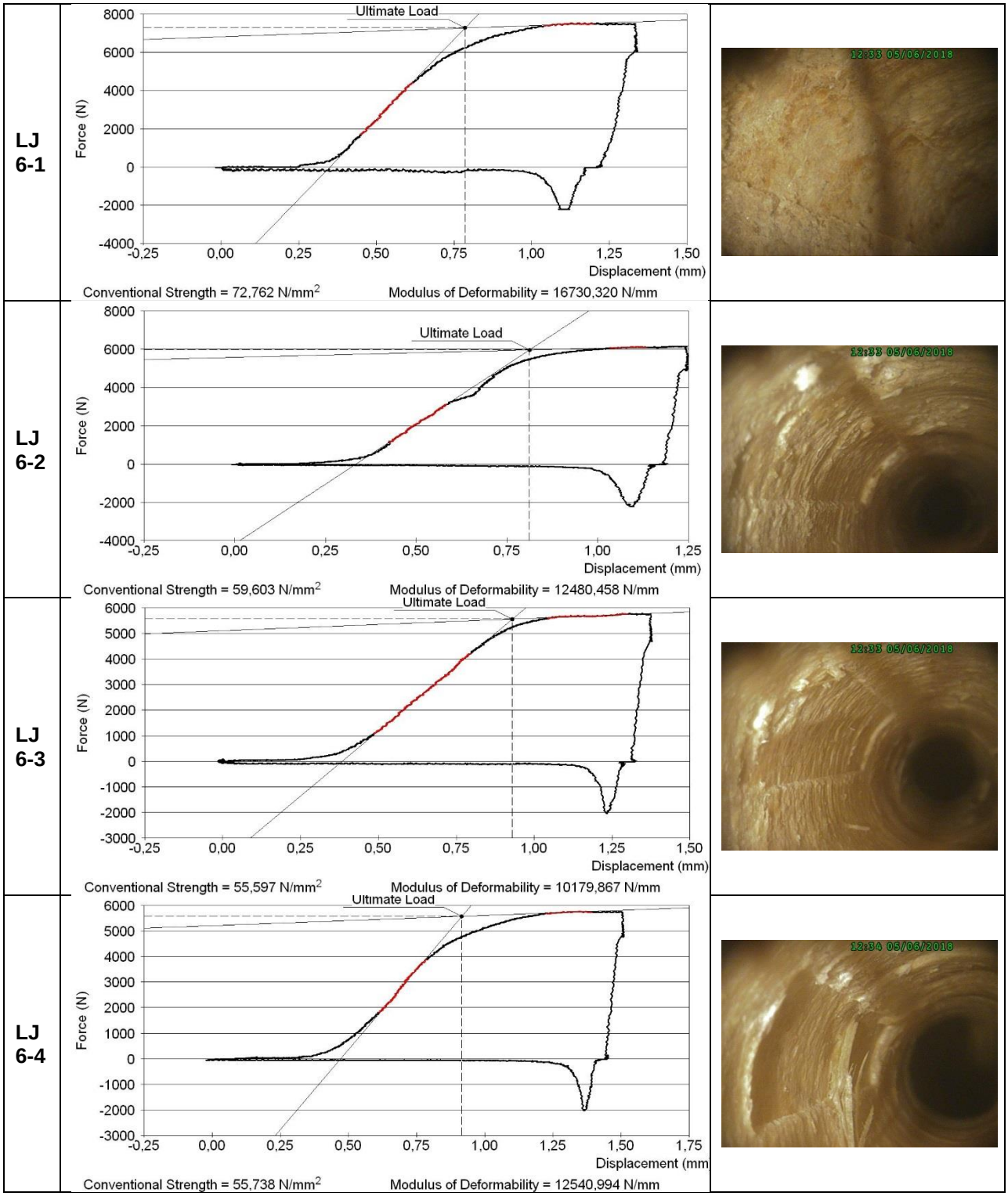

Fig A3.1 – Loading jack results on west wing roof and the endoscopic pictures respectively